# Engineering Journal

American Institute of Steel Construction

Fourth Quarter 2014 Volume 51, No. 4



www.aisc.org

# ENGINEERING JOURNAL

AMERICAN INSTITUTE OF STEEL CONSTRUCTION

*Dedicated to the development and improvement of steel construction, through the interchange of ideas, experiences and data.*





ENGINEERING JOURNAL (ISSN 0013-8029) is published quarterly. Subscriptions: Members: one subscription, $40 per year, included in dues; Additional Member Subscriptions: $40 per year. Non-Members U.S.: $160 per year. Foreign (Canada and Mexico): Members $80 per year. Non-Members $160 per year. Published by the American Institute of Steel Construction at One East Wacker Drive, Suite 700, Chicago, IL 60601.

Periodicals postage paid at Chicago, IL and additional mailing offices. **Postmaster:** Send address changes to ENGINEERING JOURNAL in care of the American Institute of Steel Construction, One East Wacker Drive, Suite 700, Chicago, IL 60601.

# Message from the Editor

As I was preparing this issue for print, a press release landed in my inbox announcing that our very own research editor, Reidar Bjorhovde, was named a Distinguished Member of the American Society of Civil Engineers (ASCE).

The timing of this award coincided with another achievement: this issue of *Engineering Journal* marks Bjorhovde's 36th—and last—"Current Steel Structures Research" column. Bjorhovde, our inaugural research editor, has served for 10 years. He may be retired from our journal but I have no doubt he will continue to travel the globe interacting with the steel design community. And given his penchant for international travel, it's quite fitting that the ASCE award will be presented in Panama this fall.

Fortunately, we have found a capable successor in Dr. Judy Liu, an associate professor of civil engineering at Purdue University. Liu is a graduate of the Penn State architectural engineering program, and she received her doctorate at the University of California at Berkeley. She is a past recipient AISC's Faculty Fellowship Award (now called the Milek Fellowship Award) and is active in AISC's university relations efforts.

We are pleased that Dr. Liu will be contributing to our journal. Watch for her columns in the second and fourth quarter issues in 2015!

Sincerely,

Keith A. Grubb, P.E., S.E.
Editor

P.S. I would also like to thank our valued reviewers for their contributions to the success of our journal. A list of our 2014 reviewers is posted on our website at www.aisc.org/ej.

# Evaluation and Repair of Bridge Truss Gusset Plates

HOWARD HILL, JONATHAN C. McGORMLEY, JONATHAN LEWIS, WADE CLARKE
and THOMAS NAGLE

## Abstract

Gusset plates used to connect members in large steel trusses are important elements in many existing bridge structures. As such, their capacities can influence bridge structural load ratings, especially when the effects of deterioration and/or damage have become significant. In order to provide accurate load ratings, avoid unnecessary repairs and, when necessary, design appropriate repairs, gusset plate conditions and characteristics must be properly incorporated in the responsible engineer's evaluation. Because the cost of being conservative is far greater for existing structures than for new designs, engineers evaluating existing gusset plates should not rely too heavily on design-based methods when making final load rating and repair decisions. The purpose of this paper is to provide some practical guidance to the process of gusset plate evaluation and repair in order to promote efficient use of limited bridge maintenance resources.

**Keywords:** gusset plates, shear, compression, deterioration, and repairs.

In February 2009, the Federal Highway Administration (FHWA) published the document *Load Rating Guidance and Examples for Bolted and Riveted Gusset Plates in Truss Bridges*, Publication No. FHWA-IF-09-014 (Ibrahim, 2009), hereinafter referred to as the *Guide*. Its purpose is to provide engineering guidance in the structural evaluation of existing steel gusset plates. The *Guide* presents a straightforward methodology for evaluating the strengths of gusset plates and gusset plate fasteners that is based on current American Association of State Highway and Transportation Officials (AASHTO) design and load rating methods. Because they are relatively simple and based on provisions that are familiar to practicing engineers, the *Guide* provisions are easy to implement, and gusset plates that satisfy them are expected to provide reliable service.

Like most design-based provisions that must be relatively simple and yet applicable to a wide variety of cases, the *Guide* methods can be quite conservative under certain circumstances. Therefore, gusset plate elements that do not satisfy the basic *Guide* evaluation provisions should not be considered inadequate on this basis alone. The author of the *Guide* clearly recognized this fact, as demonstrated by the occasional reference to performing "more rigorous analysis" (e.g., in Sections 3.2 and 3.3). Given the cost of implementing modifications to in-service structures, it is usually worthwhile to take a more rigorous look at structural elements that do not satisfy basic design provisions. As an example, consider the situation in which a conservative design procedure indicates a 1-in.-thick gusset plate is needed for a new truss joint (i.e., one that is still on paper), while a more rigorous approach would have shown a ¾-in.-thick plate to be sufficient. The cost to the project is limited to an extra ¼ in. thickness of plate material, which would likely be less than the cost of pursuing the more rigorous design approach. In contrast, if a ¾-in.-thick gusset plate on an in-service bridge is deemed inadequate using a conservative evaluation approach, when a more rigorous approach would have shown it to be adequate, the cost to the project is far more than the price of a little extra plate material.

To put the cost of conservatism in perspective, consider a load rating process for a bridge where 70% of the service load is dead load and 30% of the service load is live load. In this case, underestimating actual gusset plate strength by only 10% can lower the live load rating by 33%. If the conservative approach suggests a 15% deficiency (while a more rigorous analysis approach would indicate that the bridge is actually sufficient), the cost of the conservatism would include unnecessary restrictions on bridge use—and unnecessary repairs to remove those restrictions.

Where significant deterioration has occurred, design-based evaluation procedures are typically unable to accurately estimate member capacities. This is due to the fact that such procedures have no way of reasonably quantifying the effects of localized or generally nonuniform degradation or damage. As a result, attempts to evaluate deteriorated or

Howard Hill, Ph.D., P.E., S.E., Director of Project Operations and Principal, Wiss, Janney, Elstner Associates Inc., Northbrook, IL. E-mail: hhill@wje.com

Jonathan C. McGormley, P.E., S.E., Principal, Wiss, Janney, Elstner Associates Inc., Northbrook, IL (corresponding). E-mail: jmcgormley@wje.com

Jonathan Lewis, S.E., Associate Principal, Wiss, Janney, Elstner Associates Inc., Northbrook, IL. E-mail: jlewis@wje.com

Wade Clarke, P.E., S.E., Senior Associate, Wiss, Janney, Elstner Associates Inc., Northbrook, IL. E-mail: wclarke@wje.com

Thomas Nagle, P.E., S.E., Operations Director, Nagle Signs Inc., Waterloo, IA. E-mail: tjnagle@naglesigns.com

damaged elements using standard design procedures often lead to extremely conservative conclusions. Again, the cost of conservatism when dealing with in-service structures can be very high.

When a deteriorated plate requires repair or reinforcing, it is important to give proper credit to its existing capacity. If this is not done, repair/retrofit efforts can become excessive and unnecessarily costly. In many cases, localized deterioration can be effectively addressed with localized repairs. It is also important to note that, unless the bridge in question has been shored or otherwise externally supported for some time, even its most heavily deteriorated plates have proven capable of carrying full dead load demands and heavy trucks (albeit with unacceptable factors of safety, thus necessitating repair).

The purpose of this paper is to provide some practical guidance in the application of additional evaluation rigor that can help increase the efficiency and effectiveness of our limited bridge maintenance resources. Rational methods to account for and properly address common forms of gusset plate deterioration are also explored.

## CONSERVATISM IN FHWA GUIDE STRENGTH PROVISIONS

### Global Shear Strength

The *Guide* procedures for evaluating gusset plate shear yield strength are especially prone to excessive conservatism. This is due to the fact that the shear yield strength equation [*Guide* Equation 6: $V_r = \phi_{vy} V_n = \phi_{vy} (0.58) F_y A_g \Omega$] includes a factor ($\Omega$) that is either 0.74 or 1.0 per the *Guide*, while little guidance is provided for making the appropriate selection in any particular case. In our opinion, given this lack of guidance, engineers will tend to take the conservative approach and use 0.74, even though most situations would warrant a much higher factor.

The current AASHTO (2007) design specifications for truss gusset plates (Section 6.14.2.8) include a strength reduction factor of 0.74 for situations involving *flexural shear.* Unfortunately, the term *flexural shear* is not defined. Because the presence of normal stress (e.g., stress created by flexure) reduces shear strength, it may well be prudent to reduce shear strength where significant normal stress exists. Many potentially critical sections in common gusset plates must carry both shear and normal stresses. However, rare are the cases where normal stresses would be high enough to warrant a 0.74 reduction factor on shear strength. In most practical situations, applying the 0.74 reduction factor will lead to substantial underestimation of actual shear strength. According to Drucker (1956), the interaction of shear and moment acting on a rectangular cross-section can be represented as follows:

$$\frac{M}{M_0} = 1 - \left(\frac{V}{V_0}\right)^4$$

where

$M_0$ = plastic moment strength
$V_0$ = plastic shear strength

Rearranging this equation to solve for $V$ gives the following:

$$V = V_0 \left[1 - \left(\frac{M}{M_0}\right)\right]^{0.25}$$

where

$\left[1 - \left(M/M_0\right)\right]^{0.25}$ = plastic strength reduction factor

For a rectangular plate with $M$ equal to the moment at first yield, according to Drucker (1956), the reduction factor becomes 0.76. Therefore, the AASHTO and *Guide* 0.74 value appears to be a reasonable reduction factor for a steel plate cross-section that is also carrying normal stresses resulting from yield-level moments. Also apparent is that lesser normal stresses will have less effect on shear strength. While the universal application of a lower bound strength reduction factor is suitable for new designs—where the cost of the associated conservatism is small—it is not appropriate in situations where the cost of being conservative can be very high. When evaluating existing, in-service gusset plates, it is appropriate to use a moment/shear interaction relationship to establish shear strength estimates based on actual conditions, rather than a single reduction value for all cases.

Consider the gusset plate shown in Figure 1. Section A-A comprises a potentially critical shear plane that represents the only load path for horizontal forces in the web members to be resolved in the chord. Section A-A also carries substantial normal stresses resulting from the vertical components of the web member forces. In order for the gusset plate to be in equilibrium and for the connected members to carry only axial loads as likely assumed, the free-body diagram shown in Figure 2 must be satisfied. As shown, the moment acting on Section A-A must equal the horizontal force in the chord multiplied by the distance, $e$. This moment can be used in conjunction with the interaction equation shown previously to establish a corresponding shear strength.

Figure 3 provides a schematic representation of the node U10 gusset plates whose failure led to the 2007 collapse of the I-35W Bridge in Minneapolis, Minnesota. At the time

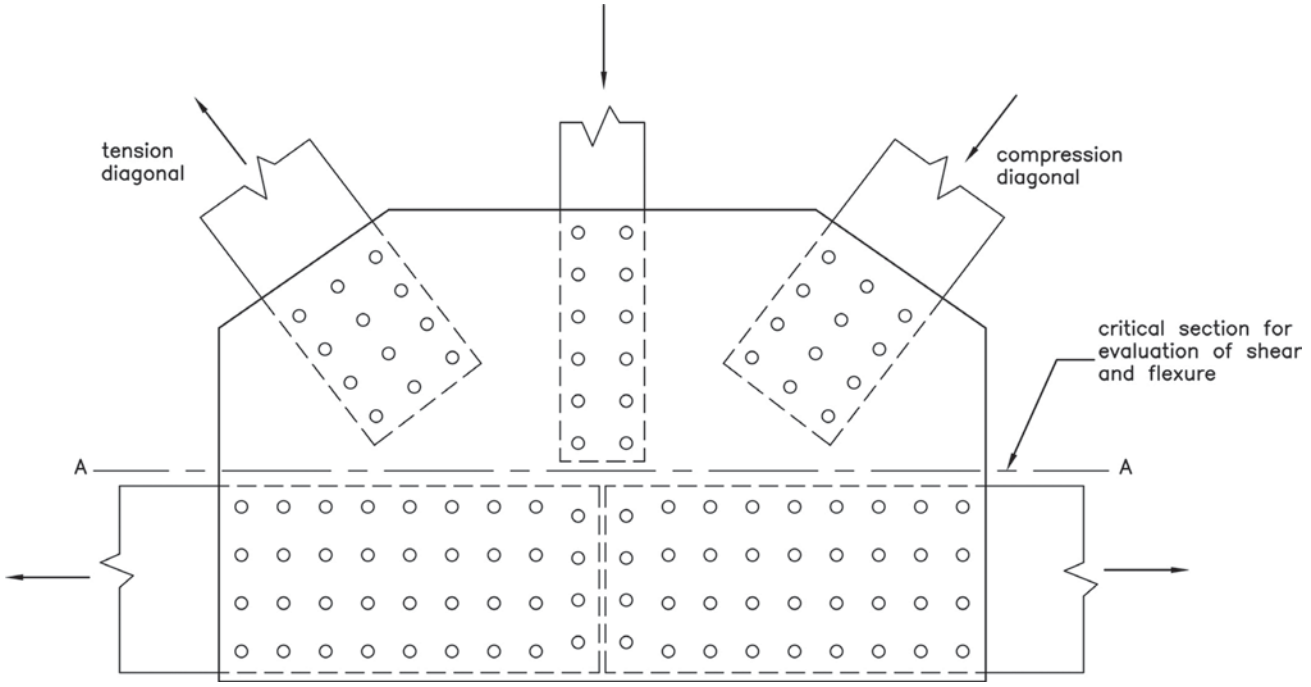


*Fig 1. Typical gusset plate high-stress section.*

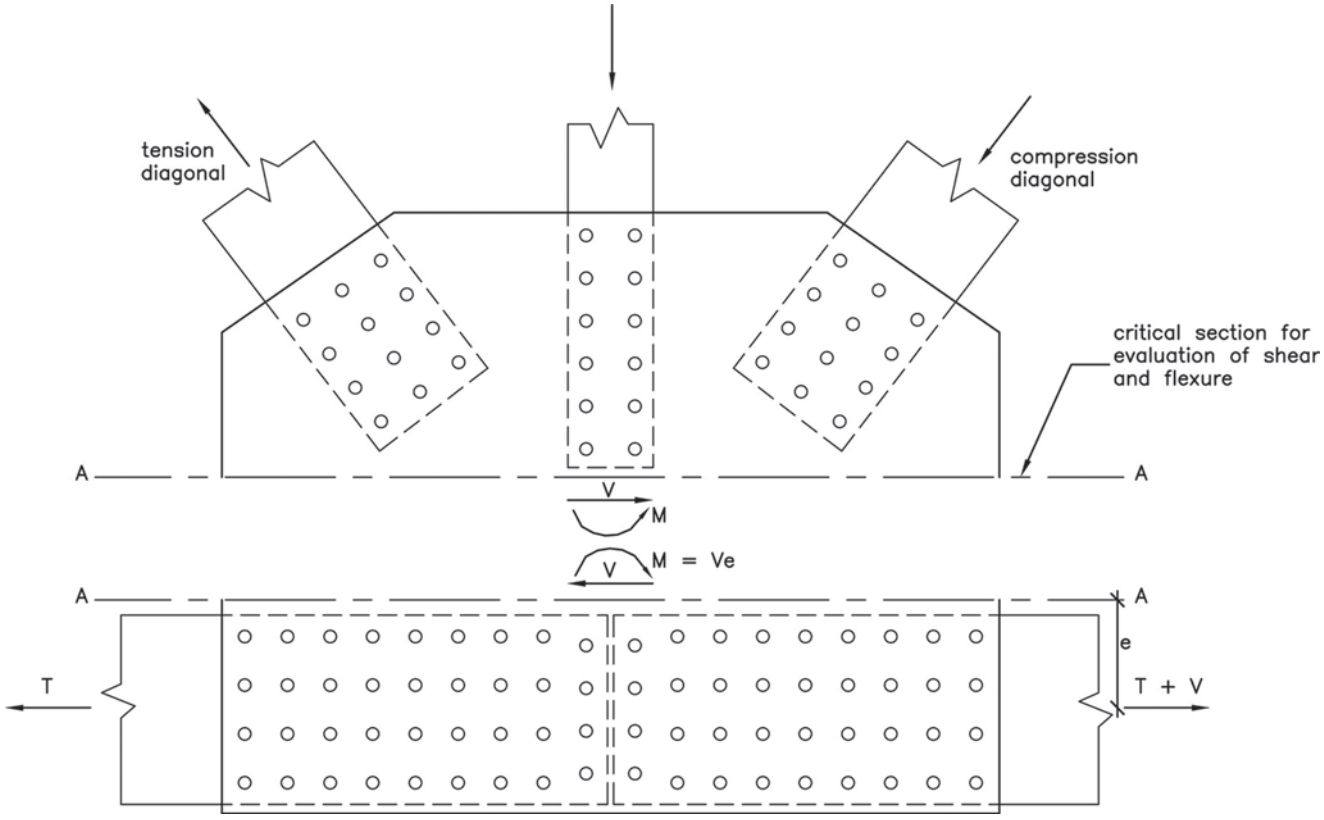


*Fig 2. Horizontal section free-body diagram.*

of their failure, the most critical of the U10 gusset plates were carrying about 92% of their respective plastic shear strengths (about 0.92 × 0.6 × tensile yield strength × area) along Section A-A. Using the moment acting on Section A-A at the time of collapse, Drucker's (1956) interaction equation predicts a shear strength reduction factor of 0.89. While this appears slightly conservative based upon the evidence, it provides a far better estimate than the AASHTO factor of 0.74, which would underestimate shear strength by an additional 17%. As indicated earlier, the cost of such a discrepancy can be substantial.

The *Guide* text accompanying Equation 6, which is used to calculate the factored shear yield resistance, mentions "stiffness to prevent buckling and develop the plastic shear force of the plates." There should be little concern of shear buckling affecting gusset plate strength in most practical situations. If we apply standard AASHTO plate girder shear buckling provisions to a range of gusset plate dimensions, where the gusset plate width is analogous to plate girder height, we would find that the transverse stiffener spacing needed to develop full plastic shear strength would typically be measured in feet. Because the horizontal sections of high shear in most gusset plates are bounded by stiffening elements that are separated by inches rather than feet, shear buckling is rarely a controlling limit state.

**Gusset Plate Compression**

The *Guide* provisions for evaluating gusset plate compression suggest idealizing the plate as a column with a width equal to the Whitmore section and determining the capacity by selecting an appropriate effective length. The process outlined in the *Guide* is similar to that which has been proposed by Dowswell (2006). However, the *Guide*'s application of the process, most notably in the selection of an effective length factor ($K$), appears much more conservative. For example, Dowswell recommends use of full yield strength in situations where the *Guide* sample problems use a $K$ value of 1.2. In fact, $K$ values greater than 1.0 are not recommended in any of the situations covered by Dowswell.

The treatment of gusset plate compression in the *Guide* sample problem is quite conservative. When a gusset plate joint is detailed so that the edges of the compression diagonal fall within a few inches of the edges of the adjoining chord and web elements, sidesway buckling of the type envisioned in the *Guide* samples is effectively restrained. To put it another way, for sidesway buckling to occur in such a situation, essentially all of the plate material surrounding the end of the compression member would have to reach yield-level principal stresses. Even where buckling may preclude development of full yield strength, the *Guide* procedures may be overly conservative.

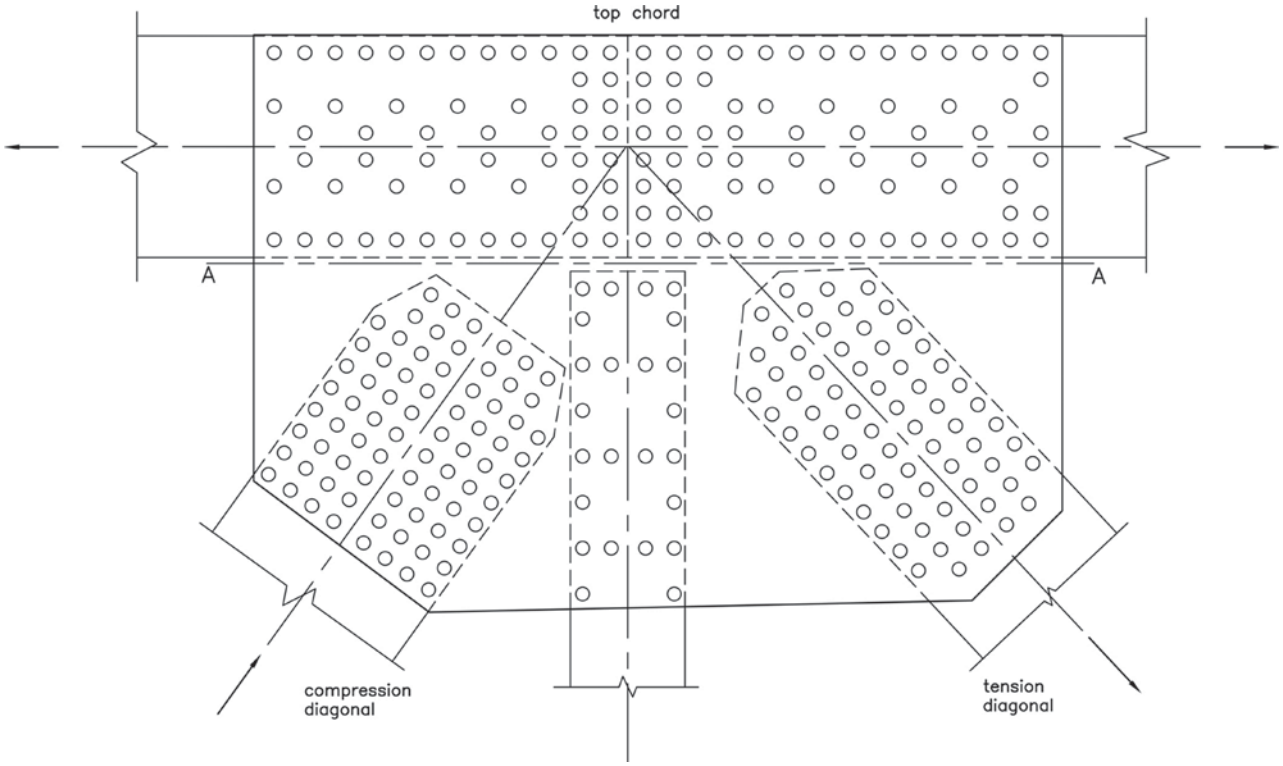


*Fig. 3. I-35W U10 gusset plate detail.*

In most common situations, the approach used to assess compression capacity in the *Guide* examples may not have a significant impact. This is due to the fact that even when using very conservative *K* factors, effective lengths often remain so small that the calculated critical compressive stress is not much less than the corresponding yield strength of the plate material. However, the *Guide* procedure, and most forms of equivalent column procedures can be very conservative under certain circumstances. For example, consider the situation shown in Figure 4 where the sloped bottom chord segment and vertical member form a relatively small angle in which the compression diagonal fits. In this case, the compression diagonal must terminate a considerable distance from the work point, even though the edges of this member nearly contact the edges of the neighboring members. As a result, the length of the compression region measured along the compression member centerline is quite long, leading to a significant average-length value as defined by the *Guide*. When used in conjunction with the *Guide* compression zone evaluation procedure, this average length leads to a significant reduction in strength. However, because this compression zone is stiffened along both sides by the adjoining web and chord elements, the equivalent column approach does not represent actual behavior. For the case shown in Figure 4, the compression zone acts more like the compression flange of a box beam (i.e., it does not act like a column). If we look at the compression flange of a box beam in a region of constant moment (i.e., where it is under the equivalent of a constant axial load), its buckling strength is unrelated to its length. This is because column-type buckling is restrained by the webs that are located along each of its edges. In this case, local buckling is the only buckling of concern, and local buckling depends on the width of the element, its thickness and the degree of restraint along each edge.

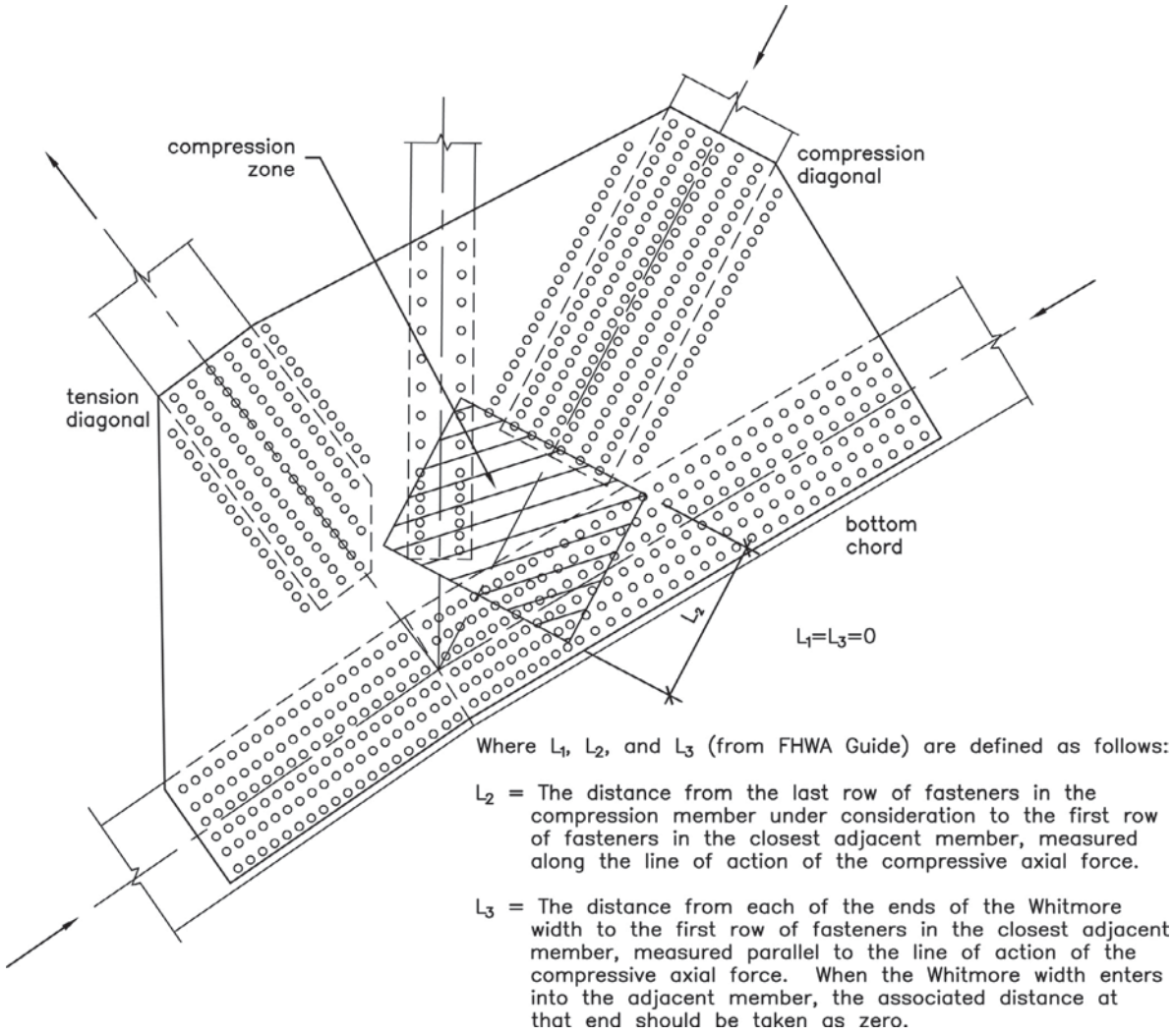


*Fig. 4. Long "compression zone" example.*

Figure 5 shows the compression zone from Figure 4 with some equivalent plate boundaries and associated dimensions. These dimensions and the associated edge conditions can be used with standard plate buckling references (Galambos, 1998; Salmon and Johnson, 1996) to determine critical buckling stress. In cases such as that shown in Figure 4, the plate buckling approach can be used to mitigate the conservatism associated with the equivalent column approach.

## EVALUATING GUSSET PLATE DETERIORATION

Properly accounting for section loss or other forms of damage is of prime importance in gusset plate evaluation. Because the effects of deterioration (e.g., corrosion) are highly variable and often highly localized, a general, formulaic evaluation approach will rarely be able to accurately capture their effect on strength. The evaluator must resist the temptation to make broad, overly conservative assumptions in an attempt to keep the evaluation simple. For example, if a portion of a gusset plate has sustained up to 50% section loss in one area, applying the basic *Guide* formulas using half of the original plate thickness would likely lead to erroneous conclusions and unnecessary repairs. Instead, analytical methods that account for the degree of deterioration and its location should be employed.

### Documenting Existing Conditions

A proper evaluation requires good documentation of the gusset plate condition. Simply knowing the maximum depth of pitting or the total area of perforation is not sufficient. A reasonable estimate of plate strength needs to be based on reasonable estimates of both the magnitude and location of significant section loss. The gusset plate shown in Figure 6 has sustained significant section loss at and around the perforation. At a minimum, documentation of such deterioration should include an outline of the hole perimeter and an outline of the surrounding, full thickness perimeter (i.e., the line around the hole where measureable section loss begins).

If the area of section loss around a hole is large or if the degree of section loss does not vary in a consistent fashion between the edge of the hole and the full thickness perimeter, then intermediate thickness measurements may be necessary to describe the loss.

Figure 6 also shows an area of linear pitting. In this context, linear pitting is section loss that occurs along a generally straight path that is much narrower than it is long. Linear pitting is one of the most common forms of significant gusset plate deterioration. It often occurs where debris accumulates along the intersections of gusset plates with horizontal and low sloping surfaces of chord and web members and is the result of moisture retention on abutting steel surfaces. The fact that areas of debris accumulation often coincide with areas of high gusset plate stress (e.g., in the critical block shear perimeter of a web member or in the critical web/chord shear transfer zone) can make linear pitting especially significant.

When documenting linear pitting, it is important to measure the maximum depth of pitting at regular and closely

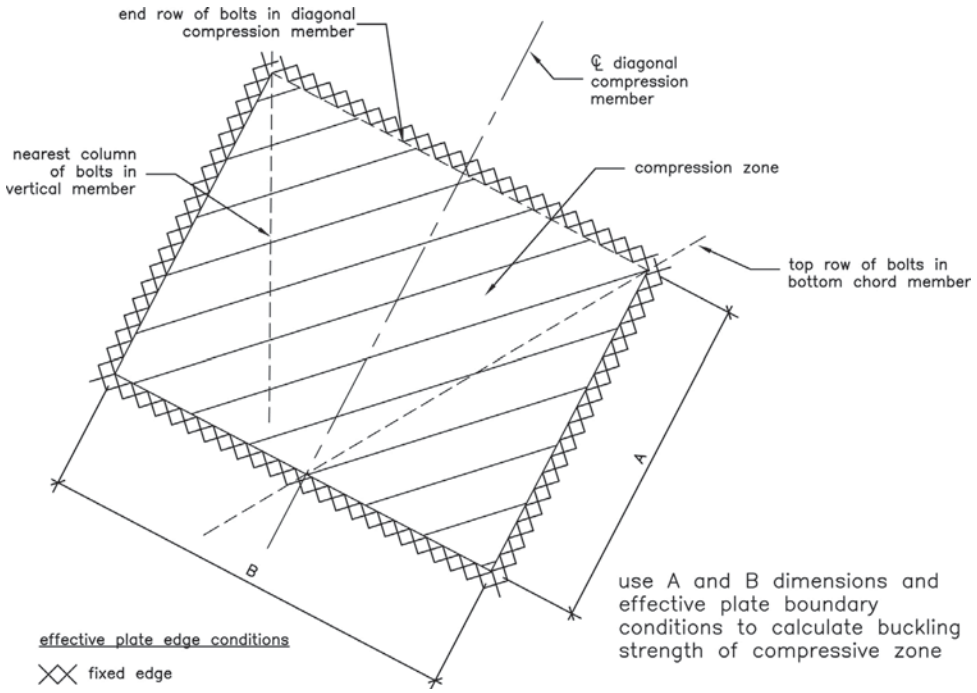


*Fig. 5. Equivalent rectangular plate.*

spaced intervals (say, every few inches) along the pitted zone and record the total width of measureable pitting at each location. This will enable the engineer to make reasonable estimates of section loss when evaluating potential failure surfaces that include all or just part of a line of pitting. If the width of pitting is generally less than the diameter of a common structural bolt (say, 1½ inches or less), a single measurement approximating the maximum depth usually provides sufficient information at each location along the length of the pitted area. As the width of a zone of linear pitting increases, it becomes increasingly important to document the extent of section loss transverse to the long dimension (e.g., take several measurements in the short direction at each location selected along the long dimension).

**Evaluating Gusset Plates with Linear Pitting**

As is the case with any type of deterioration, linear pitting can occur in an infinite variety of forms, defined by different combinations of severity, extent and orientation. This paper addresses the most common forms of linear pitting, although the principles involved would be applicable to other forms as well.

***Bottom Chord Narrow (BCN) Linear Pitting***

One of the most common forms of significant gusset plate deterioration on bridges is a narrow band of linear pitting located parallel to and slightly above the top of the bottom chord, an example of which is shown in Figure 6. Pitting of this type can reduce the ability of a plate to transfer forces between the chord and the web members.

To be considered narrow, a band of linear pitting should be no wider than the diameter of the largest common structural bolts (say, 1½ inches). In this case, as load builds up in the plate, yielding would likely begin in the thinnest sections of the pitted zone. This initial yielding would occur at a load significantly less than the load required to cause initial yielding in the original, unpitted plate. However, this does not mean the plate shear strength is proportionally reduced. First, local areas of deep pitting (i.e., where the plate is very thin) can experience yield-level stresses under small shear loads and then strain further as needed to allow mobilization of the strength of the rest of the plate. In this case, the ductility of the steel makes it unnecessary to limit the strength to the load that causes first yield, and the actual yield strength through the pitted zone is more accurately represented by the average thickness rather than the minimum thickness.

Strain hardening is another factor that should be taken into consideration when evaluating the effect of highly localized section loss. In the Figure 6 example, the shear yield strength through the pitted zone is clearly less than the shear yield strength through a horizontal plane immediately above or below the pitted zone. Therefore, as shear loading increases, the steel in the pitted zone will yield first. However, as shear strains in the pitted zone increase, this steel will strain harden. If the available rupture strength of the pitted zone exceeds the available yield strength of the

*Fig. 6. Narrow band of section loss in gusset plate just above chord member.*

surrounding unpitted areas, the yielding of the unpitted plate will be mobilized, just as it would in an nondeteriorated plate. In such cases, the localized pitting would not reduce the available strength of the gusset plate.

The mechanism just described is what justifies checking shear or tensile rupture on net sections through rows of bolt holes, while checking shear or tensile yield on gross sections. The strain needed to mobilize strain hardening over the small dimension affected by the bolt holes is achievable without excessive deformation. Because the same can be said for a narrow band of pitting, the same mechanism would develop. In most gusset plates that have pitting of the type shown in Figure 6, there is a horizontal row of chord fasteners (i.e., bolts or rivets) located parallel to and a short distance below the pitted zone. The section loss through this fastener row due to hole drilling is considerable, yet it does not result in a proportional reduction in the available shear strength of the plate and may not affect available strength at all since the shear or tensile yield strength of the gross section may be less than the corresponding rupture strength of the net section. To put it another way, if the section loss due to pitting is less severe than the section loss through an adjacent horizontal plane caused by hole drilling, the pitting will not reduce the shear strength of the plate any more than the holes themselves. Therefore, when evaluating the effects of BCN pitting, one of the first steps should be the calculation of the net area in the pitted zone. If the available rupture strength of the pitted net area is greater than the available yield strength of the gross area of the undeteriorated plate, or if the pitted net area is greater than the net area through a nearby row of fasteners, the pitting will not significantly reduce the shear strength of the plate.

Conversely, if the available rupture strength of the net area of a BCN pitting zone is less than the available yield strength of the adjacent nondeteriorated areas, and if it is also less than the available rupture strength of the net sections at nearby parallel rows of fasteners, the BCN pitting can reduce the strength of the plate. Of primary concern in this regard are (1) the transfer of forces between the web members and the chord at the node and (2) the transfer of forces between a single web member and the rest of the members at the node. Methods for evaluating the effects of critical BCN pitting are discussed later.

The horizontal line shown in Figure 6 goes through a BCN zone of pitting that sustains high horizontal shear stresses and high vertical normal stresses. Therefore, it represents a potential critical gusset plate failure plane. A method for determining the capacity of this area in a nondeteriorated plate was provided earlier. The same method can be used to evaluate a plate with BCN linear pitting. Further, if the net area of the pitted zone is greater than the net area through the adjacent row of fasteners, the pitting can effectively be ignored. Otherwise, the pitted net area should be treated like any other net area. The shear/moment interaction approach outlined earlier—substituting ultimate strength for yield strength of the material—is one possible technique.

In a general sense, forces are transferred between the end of a web member and the rest of the node via the gusset plate material that overlaps and surrounds the end of the member. An example of a web member and the associated areas of gusset plate force transfer are shown in Figure 7. Also shown in Figure 7 are a zone of BCN linear pitting and two gusset plate corner sections. The smaller, yellow corner section represents the smallest corner of the gusset plate that must be capable of transferring the total web member load to/from the node, which means it is the most critical corner section for this member in a nondeteriorated gusset plate. The capacity of the corner could be evaluated by calculating the forces that could be sustained on each leg. However, in nondeteriorated plates, other calculations such as the Whitmore check provide reasonable representations of the plate's ability to transfer forces between a single member and the rest of the node.

In plates exhibiting significant BCN linear pitting, Whitmore and other design-based checks might not capture or otherwise appropriately represent the effects of the critical failure mechanism. For this reason, design-based evaluation methods need to be supplemented with something more rigorous. In this case, corner checks that include the BCN linear pitting zone can be used to determine whether the pitting has created a more critical failure mechanism. The larger red corner section in Figure 7 was drawn so that one side includes the BCN linear pitting zone. A relatively simple, and conservative, corner check of this situation is illustrated in Figure 8. In this check, the vertical leg of the corner is located to create the minimum perimeter that encompasses all fasteners. The sides of the corner are assumed to carry only normal (green arrow) and shear (yellow arrow) forces, which act at the center of each plane. In addition, the overall resultant of the forces on the horizontal and vertical planes is constrained as follows:

1. It must act through the truss node work point (point A).
2. It must be aligned with the centerline of the web member.
3. The resultant moment in the web member must be zero.

Because the various members framing into the node and the member in question typically can sustain some degree of flexure, these constraints are conservative. The maximum combination of normal and shear force acting on the pitted leg of the corner is typically established first. This is done by:

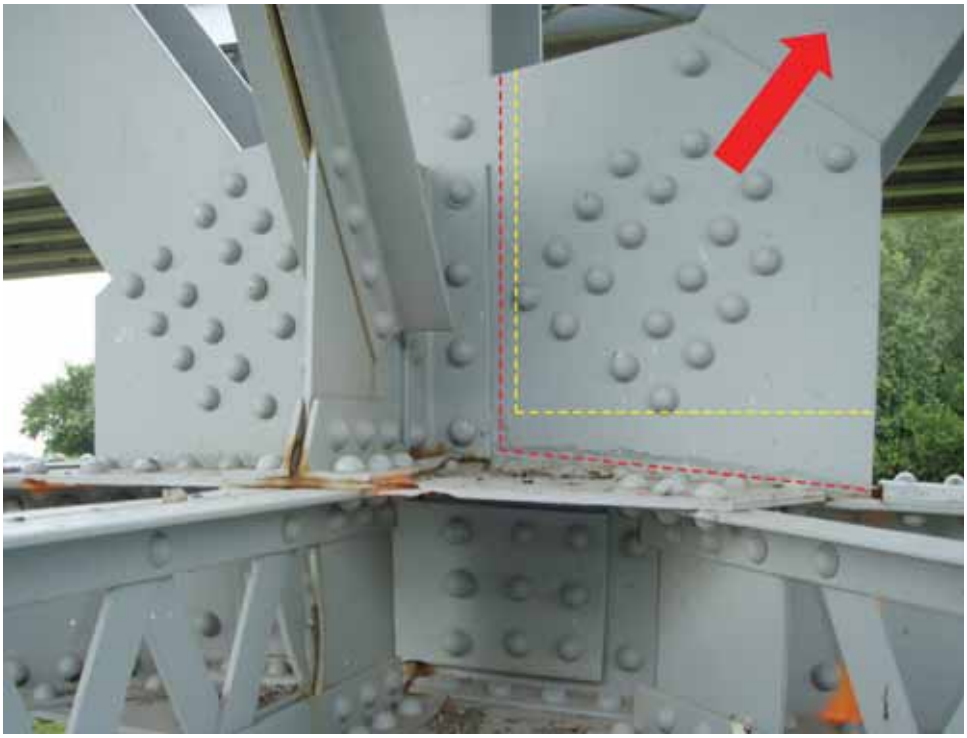

*Fig. 7. Gusset plate corner resisting tension generated by diagonal web member.*

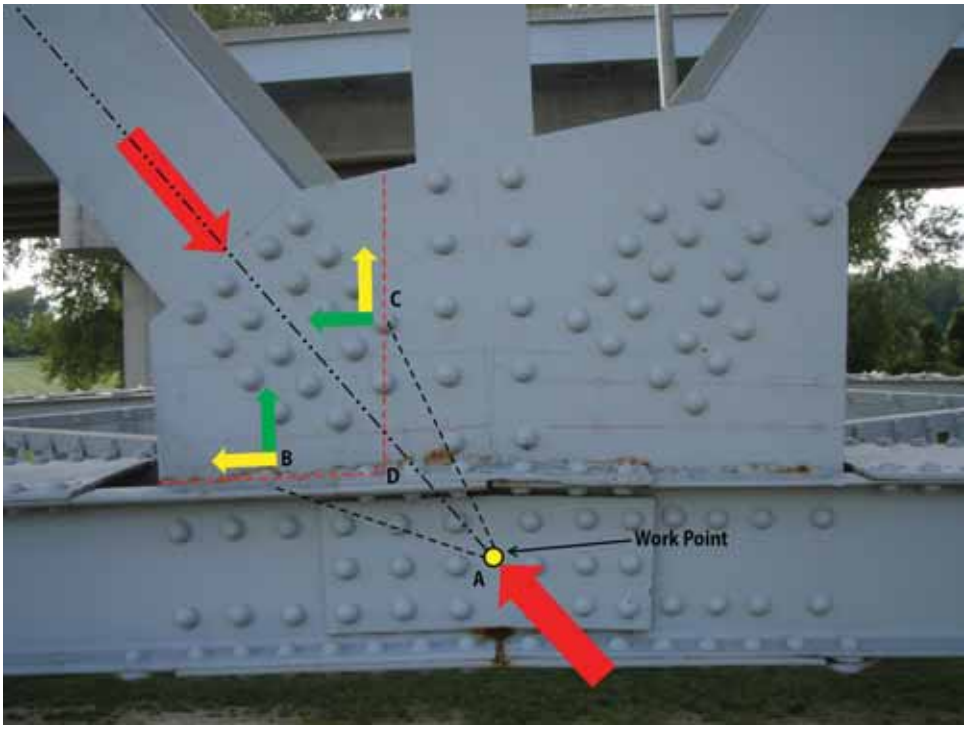


*Fig. 8. Equilibrium check for a representative corner section of a gusset plate.*

1. Assuming the resultant of the two forces follows Line AB, which connects the truss node work point with a point located in the middle of the horizontal leg. This assumption relates the magnitude of the shear force to the normal force or vice versa.

2. Finding the magnitude of the forces that satisfies von Mises yield criteria on the horizontal leg.

Once the axial and shear forces on the horizontal leg are determined, equilibrium is used to determine the corresponding shear and normal forces on the vertical leg. Again, the relationship between the shear and normal forces on the vertical leg is constrained such that their resultant passes through the work point of the gusset plate. Once the forces acting on the vertical leg are determined, the von Mises yield criterion is checked on the vertical surface to verify that it does not control (e.g., the horizontal leg yields before the vertical leg). If the vertical leg is found to control, the forces corresponding to von Mises yielding could be applied to the vertical leg and equilibrium used to determine the corresponding forces on the horizontal leg. However, if the vertical, nondeteriorated leg governs the strength of the corner, then the pitting has not significantly affected the ability of the plate to transfer forces between the member in question and the rest of the node.

With the axial and shear forces on the vertical and horizontal legs known, they are combined to produce an equivalent resultant force that, because of the constraints described earlier, acts along the axis of the member. This resultant force represents the level at which von Mises yielding will initiate on one of the legs of the gusset plate corner and can be treated as a lower bound on the strength of the postulated corner section. It is important to note that significant additional capacity could in most cases be mobilized by considering strain hardening on the pitted section (if appropriate) and/or by taking advantage of the ability of truss members and plate sections to carry flexure. Indeed, if the conservative assumptions outlined in the preceding paragraph result in a calculated overstress condition, they should be relaxed. Sample calculations for a typical, basic corner check are included in the Appendix to this paper.

It should also be noted that if the pitting is not very uniform, the centroid of the remaining material will not necessarily coincide with the midpoint of the horizontal leg (point B). The resulting eccentricity of the normal force on the horizontal section should be considered in these cases.

When determining the resistance of the entire node, it is simple and conservative to use twice the capacity of the most deteriorated gusset plate at the node. Taking the lower capacity of the two plates and multiplying by 2 eliminates the need to consider the out-of-plane eccentricity that would develop from assuming two different capacities for the inside and outside gusset plates. This simplifying assumption can obviously be applied to other gusset plate limit states (e.g., fastener strength and block shear) as well.

Of course, if the members framing into the node have more capacity than the deteriorated gusset plates, they would be able to sustain some flexure before failure of the gusset plates. Therefore, the constraints described earlier related to the concentricity of the forces and the prohibition of moment in the members could be relaxed, resulting in higher capacities.

***Bottom Chord Wide (BCW) Linear Pitting***

Occasionally, bottom chord linear pitting can occur over an area that is much wider than the diameter of common bridge fasteners (see Figure 9). In such cases, treating the minimum net area in the pitted zone like the net area through a row of fasteners may not be appropriate. In situations where wide pitting is also consistently deep, the strains required to mobilize rupture strength across the entire pitted zone may lead to excessive or unrealistic plate deformations. To avoid inappropriate use of rupture strengths in such cases, evaluations that involve BCW linear pitting should include the following:

- A check of the rupture strength based on the thinnest section along the zone of interest (as described earlier for BCN linear pitting).
- A check of the yield strength based on the overall average thickness in the zone of interest. Such a check requires multiple thickness measurements in the transverse direction at each point along the pitted zone.

Figure 9 shows two recommended checks for gusset plates with areas of BCW pitting. The check shown at the left is of the rupture strength through the thinnest section in the plate. If the pitting is deep enough, rupture strength will control over the yield strength on the gross section. However, because the zone of pitting is so wide, it may be unrealistic to assume that the rupture strength can be developed in the thinnest area before strains in the less pitted areas lead to excessive deformations. In this case, using the average thicknesses at the three transverse points ($t_1$, $t_2$ and $t_3$ in Figure 5) at each longitudinal interval along the pitted zone in conjunction with the material yield strength may be more critical than using the minimum thickness/rupture strength check.

In any case, it is important to carefully review the spatial orientation and extent of the deterioration to determine if the rupture strength of the critical section can be mobilized without excessive plate deformation. As mentioned earlier, a good rule of thumb is to compare the narrow dimension of the deteriorated area to the fastener diameter. If the width is less than the fastener diameter, rupture strengths can likely be mobilized with acceptable plate deformation.

***Web Member Narrow (WMN) Linear Pitting***

Another form of linear pitting common to bridge trusses is that which occurs parallel to and just above the top flanges of sloped web members. As is the case with BCN linear pitting, WMN linear pitting is usually associated with accumulated debris that holds moisture against abutting steel surfaces. A case of WMN linear pitting is shown in Figure 10.

WMN linear pitting can be incorporated into an evaluation in much the same way BCN linear pitting is addressed. Typically, the net area should be evaluated to see if there will be any effect on block shear capacity.

***Web Member Wide (WMW) Linear Pitting***

WMW linear pitting is similar to BCW linear pitting and should be addressed in a similar manner.

## GUSSET PLATE STRENGTHENING REPAIRS

Responsible use of available resources demands that repairs be installed only where they are needed or where it is more efficient to install repairs than it is to perform more rigorous analysis that *may* indicate repairs are not needed. Accordingly, conclusions regarding the need for repairs should not be based on overly conservative evaluation procedures. Furthermore, when it is clear that repairs are needed, they should be efficiently designed to address the actual deficiency.

When considering options for addressing localized gusset plate deterioration, the responsible engineer should note that the existing plate has substantial capacity, typically enough to carry all of the service dead load and a significant portion of the design live load without failing. If this were not true, the connection would have failed. Accordingly, most deficient elements only need to be supplemented to restore appropriate safety factors—and not replaced—and often by a relatively small amount.

It is also important for designers of gusset plate repairs to recognize that steel plates and steel structural fasteners are very ductile elements. In fact, plate and fastener ductility are relied on implicitly when standard design methods are employed (e.g., by not superimposing residual stresses with load-induced stresses, by assuming uniform—or nearly so—distribution of shear load in bolt groups, by using plastic shear and flexural strengths). If the benefits of ductility are overlooked, a repair designer may make excessively conservative assumptions that could lead to unnecessarily high repair costs. For example, given the inherent ductility of gusset plate connections, it would rarely be necessary to design repair or strengthening elements to resist the full applied loads. The existing plates can be relied upon to carry their share of the applied loads, even if they must undergo significant plastic deformation in the process. Figure 11 shows an efficient repair addressing the type of BCN deterioration shown previously in Figure 6. In this repair, a new steel angle connected to the bottom chord flange and existing plate/diagonals was added to supplement the reduced strength of the zone affected by substantial BCN deterioration. Such repairs can be proportioned using common splice and connection load transfer mechanics.

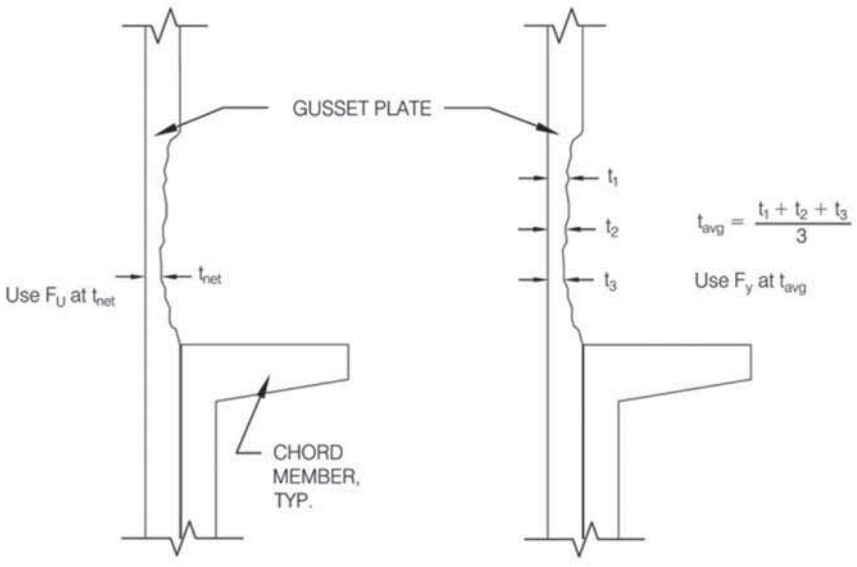


*Fig. 9. Section through gusset plate showing two recommended checks for areas of BCW pitting.*

*Fig. 10. Pitting a long top flange of diagonal member (WMN pitting).*

*Fig. 11. Efficient repair addressing BCN deterioration.*

## SUMMARY

The FHWA *Guide* provides a simple, straightforward, design-based approach for evaluating truss connection gusset plates. As such, it is a useful tool for quickly screening bridge truss connection plates and providing conservative load ratings. However, given its necessarily conservative nature, using it to define when repairs are needed can lead to unnecessary expenditures of limited bridge maintenance resources. In cases where the *Guide* approach indicates deficiencies, more rigorous evaluation methods should usually be employed.

When a gusset plate has experienced significant corrosion or other form of damage, the *Guide* approach is ill-suited to accurately quantify the effects, if any, on plate strength. Such cases should be evaluated using alternative methods. For example, free-body diagrams that incorporate deteriorated areas at their boundaries can be used to supplement the free-body checks that are considered sufficient for undamaged plates. Example free-body diagrams for deteriorated plates are presented herein, and sample calculations are provided in the Appendix. Given the cost of implementing changes to in-service gusset plates, finite-element modeling may also be practical.

When designing repairs to truly deficient plates, efficiency demands that the strength and ductility of the existing plate be taken into consideration. Otherwise, repairs and the associated costs can quickly become excessive. Robust and economical gusset plate repairs need not be mutually exclusive.

## REFERENCES

AASHTO (2007), *AASHTO LRFD Bridge Design Specifications*, 4th edition, American Association of State Highway and Transportation Officials.

Dowswell, B. (2006), "Effective Length Factors for Gusset Plate Buckling," *Engineering Journal*, AISC, Second Quarter, pp. 91–101.

Drucker, D. (1956), "The Effect of Shear on the Plastic Bending of Beams," *Journal of Applied Mechanics,* ASME, Vol. 23, No. 12, pp. 509–514.

Galambos, T. (1998), *Guide to Stability Design Criteria for Metal Structures*, 5th edition, John Wiley & Sons, New York, NY.

Ibrahim, F. (2009), *Load Rating Guidance and Examples for Bolted and Riveted Gusset Plates in Truss Bridges*, Publication No. FHWA-IF-09-014, FHWA, U.S. Department of Transportation.

Salmon, C.G. and Johnson, J.E. (1996), *Steel Structures: Design and Behavior*, 4th edition, Harper Collins, New York, NY.

## APPENDIX

### Example

This check is a simple and conservative way to evaluate equilibrium of the gusset plate corner that resists the force imparted by the diagonal. The diagonal member force is assumed to be resisted by a combination of shear and axial forces acting on the vertical and horizontal legs that bound the corner. For the deteriorated state, the corner is chosen such that the legs extend through the deterioration. See Figure A-1.

Leg 1 is defined as the horizontal leg of the corner, leg 2 is the vertical leg, and $\theta_{member}$ is the angle between the horizontal and vertical planes.

$\theta_{member} = 52.37°$
$t_{gusset} = 7/16$ in.

***Leg 1 properties*** *(horizontal)*

$L_1 = 13.31$ in.
$t_{loss1} = 3/16$ in. (average section loss across 2-in.-wide band)
$A_1 = L_1 (t_{gusset} - t_{loss1}) = 3.33$ in.$^2$
$\theta_1 = 26.55°$

***Leg 2 properties*** *(vertical)*

$L_2 = 17.75$ in.
$t_{loss2} = 0$ in. (no section loss)
$A_2 = L_2 (t_{gusset} - t_{loss2}) = 7.77$ in.$^2$
$\theta_2 = 23.00°$

### Design Steps

1. Assume the horizontal leg controls. Pick $V$ such that the von Mises stress equals $F_y$ on horizontal leg.
2. Determine $V$ (and, by extension, $P$) on vertical leg such that the resultant force acting on the entire corner is along the axis of the diagonal. In other words, the resultant of all forces acts at angle $\theta_{member}$.
3. Compute the resultant axial force. This is the axial force in the diagonal that the gusset can sustain without substantial yielding and without generating any significant moment at the node.
4. If the band of section loss is narrow (e.g., less than 1.5 in. wide), $F_u$ can be used on the reduced section instead of

$F_y$. Section loss considered in this example is assumed to be wide, thus $F_y$ is used.

***Leg 1*** (horizontal)

Trial *V*: $V_1 = 60.9$ kips

*P* is determined such that the resultant force on horizontal leg acts through the gusset work point.

$P_1 = V_1\tan(\theta_1) = 30.4$ kips

Iterate on trial *V* until von Mises yield criteria is met along the leg:

$$\sigma_1 = \frac{P_1/A_1}{2} + \sqrt{\left(\frac{P_1/A_1}{2}\right)^2 + \left(\frac{V_1}{A_1}\right)^2} = 23.4 \text{ ksi}$$

$$\sigma_2 = \frac{P_1/A_1}{2} - \sqrt{\left(\frac{P_1/A_1}{2}\right)^2 + \left(\frac{V_1}{A_1}\right)^2} = -14.3 \text{ ksi}$$

$$\sigma_{vm} = \sqrt{\sigma_1^2 + \sigma_2^2 - \sigma_1\sigma_1} = 33.0 \text{ ksi (onset of von Mises yielding)}$$

***Leg 2*** (vertical)

Trial *V*: $V_2 = 108.1$ kips

*P* is constrained as in leg 1.

$P_2 = V_2\tan(\theta_2) = 45.9$ kips

After determining the trial *V* for leg 1, determine the forces on vertical leg that will result in no net moment acting about the axis of the member. Using iteration or spreadsheet solver functions, the Von Mises stresses may be calculated:

$$\sigma_1 = \frac{P_2/A_2}{2} + \sqrt{\left(\frac{P_2/A_2}{2}\right)^2 + \left(\frac{V_2}{A_2}\right)^2} = 17.2 \text{ ksi}$$

$$\sigma_2 = \frac{P_2/A_2}{2} - \sqrt{\left(\frac{P_2/A_2}{2}\right)^2 + \left(\frac{V_2}{A_2}\right)^2} = -11.3 \text{ ksi}$$

$$\sigma_{vm} = \sqrt{\sigma_1^2 + \sigma_2^2 - \sigma_1\sigma_2} = 24.8 \text{ ksi}$$

This is less than the yield stress, $F_y$, of 33 ksi, so the assumption that the horizontal leg controls is correct.

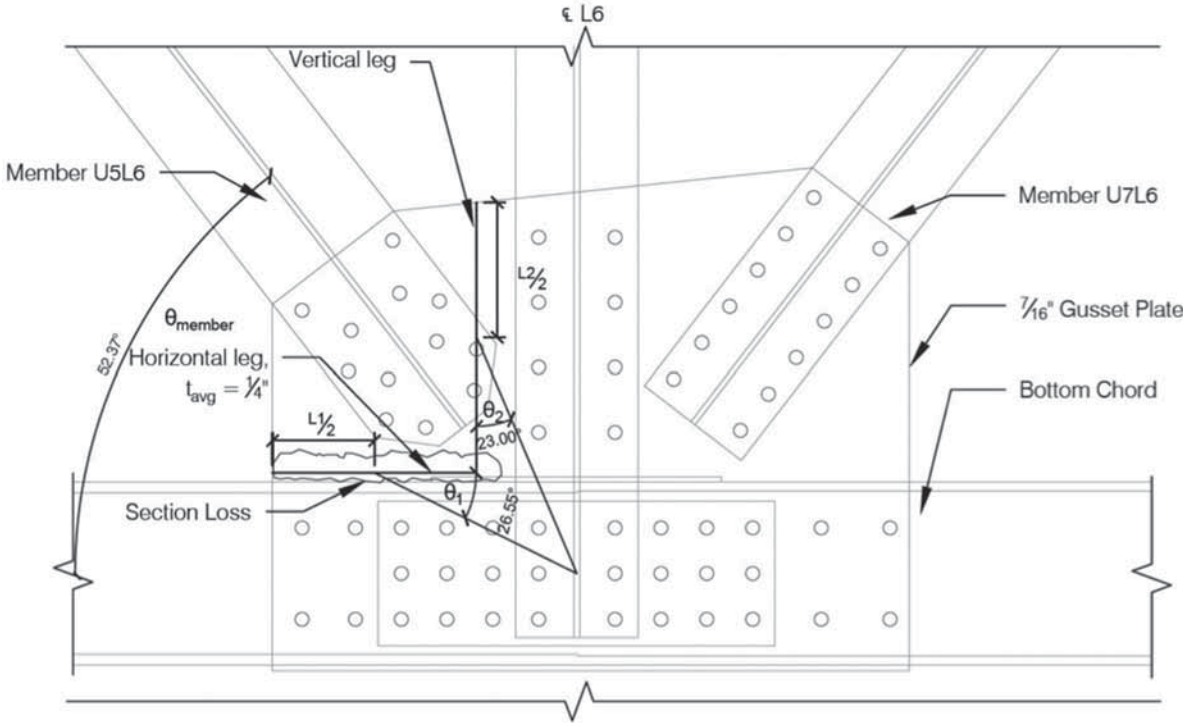


*Fig. A-1. Example configuration.*

Because the trial forces act through gusset work point by definition, we must simply check that they align with the member axis to ensure equilibrium of the corner:

$$\text{atan}\left(\frac{V_2 + P_1}{V_1 + P_2}\right) = 52.37^\circ = \theta_{member} = 52.37^\circ$$

**o.k.**—solution found that meets all established conditions

$\phi_y = 0.9$
$\phi_v = 0.9$

Strength reduction factors vary based on governing code. For simplicity, we assume 0.9 for the yielding limit state.

Compute the total resultant force acting on the corner:

$$\phi R = \sqrt{(\phi_v V_2 + \phi_y P_1)^2 + (\phi_v V_1 + \phi_y P_2)^2} = 157 \text{ kips}$$

Because there are two gusset plates per node, compare this computed capacity to one-half of the design load in the diagonal.

**Notes**

1. The computed capacity is a lower bound in this case. The constraint that only shear and axial forces act on the legs could be relaxed, as could the requirement that resultant member and nodal forces are concentric. Also, if the band of deterioration is narrow, it is conservative to use $F_y$ on the net section. Items like this should be explored if the methods described previously result in insufficent capacity.
2. In cases where the deterioration is not uniform along the leg (e.g., a large hole at one end), it may be necessary to refine the equilibrium check to account for the resulting eccentricty. In such a case, the resultant force will not act through the midpoint of the corner leg as assumed.

TECHNICAL NOTE

# Two-Way Bending of Base Plates under Uniaxial Moment Loading—Alternative Approach

EDWARD R. HANINGER and BRUCE M. TONG

## ABSTRACT

This Technical Note presents an alternate model for two-way bending design of column base plates under uniaxial moment loading and is based on the design premises of AISC Design Guide 1, *Base Plate and Anchor Rod Design* (Fisher and Kloiber, 2006). Two-way bending, in this paper, refers to bending of a column base plate in the direction perpendicular to the primary direction of bending and is also called side bending. When two-way bending governs, which is commonly the case, this procedure results in more efficient base plates that more closely reflect available strengths. A sample calculation is also provided.

**Keywords:** base plate, steel design, column base, two-way bending, side bending.

## INTRODUCTION

Two-way bending will commonly govern the required thickness of column base plates subjected to compressive loads, with or without an applied moment. For the purposes of this paper, the term *two-way bending* refers to bending of a column base plate perpendicular to the primary direction of bending. Two-way bending is particularly important for wide base plates and narrow column flanges. The focus of this paper is the situation where the applied moment dominates the plate stresses. A diagram of a column base plate subject to a uniaxial moment about the column's strong axis is shown in Figure 1.

AISC Design Guide 1, *Base Plate and Anchor Rod Design* (Fisher and Kloiber, 2006), provides a design procedure for determining the required thickness of a base plate. In this guide, hereafter referred to as Design Guide 1, a design procedure is provided for the $m$ and $n$ cantilever lengths, as shown in Figure 1. The cantilever length for two-way bending, $n$, is as defined in the *Manual of Steel Construction*, 14th edition (AISC, 2011) and Design Guide 1. As noted in Figure 1, the cantilever length, $n$, used to determine the two-way bending force is based on 0.8 times the width of a wide flange column. The 0.8 factor would also apply to pipe columns. A factor of 0.95 would be used for rectangular column sections. Wide flanges are commonly used for columns, so this shape will be used to demonstrate the procedure in this paper.

The primary method of analysis used in Design Guide 1 is to assume a rectangular stress block for compression on the concrete as shown in Figure 2. The rectangular compression block is an effective design method and is also used in this paper.

## THE PROBLEM

Design Guide 1 presents a design procedure that considers bending caused by compression at the bearing interface and bending caused by tension on the anchor rods on the tension side. However, Design Guide 1 uses a simple and conservative means of designing the base plate for the common bending case when the cantilever lengths perpendicular to the primary load direction are greater than the cantilever lengths in the direction of load ($n > m$). This failure mechanism is called two-way bending in this paper.

Design Guide 1 provides direction for two-way bending only in notes at the ends of Sections 3.3.2 and 3.4.2, where it is recommended that $n$ be substituted for $m$ in Equations 3.3.14a-1, 3.3.14b-1, 3.3.15a-1 and 3.3.15b-1 when $n$ is larger than $m$. This procedure functionally sets the effective bending width, $b_{eff}$, of the plate equal to the compression length $Y$ ($b_{eff} = Y$). This is reasonable when the base plate is in full compression. However, for cases where the bearing length is small, such as in Figure 2, this can lead to overly conservative results because resistance to bending would utilize a larger effective plate width. Moreover, for the case $Y < n$, the note in these Design Guide 1 sections could lead to inaccurate design results. The objective of this paper is to present an improved procedure for design of the $n$ cantilever length.

Edward Haninger, P.E., S.E., Director I, Design Engineering, Fluor Corporation, Irvine, CA (corresponding). E-mail: ed.haninger@fluor.com

Bruce Tong, P.E., Principal Engineer, Fluor Corporation, Irvine, CA. E-mail: bruce.tong@fluor.com

| Table 1. Roark Values for $K_m$ as a Function of $c/a$ at $z = 0$ | |
|---|---|
| $c/a$ | $K_m$ |
| 1.0 | 0.509 |
| 0.75 | 0.428 |
| 0.5 | 0.370 |
| 0.25 | 0.332 |

This procedure results in an effective plate width, which is then used to determine section properties for the strength of the plate in flexure.

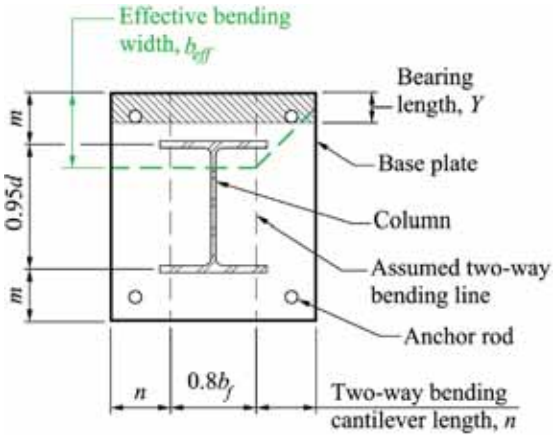


*Fig. 1. Base plate two-way bending terms.*

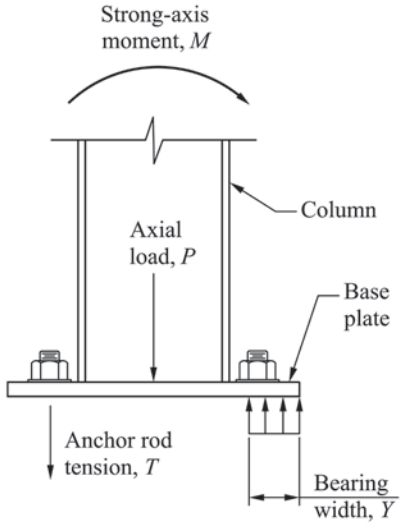


*Fig. 2. Rectangular stress block forces.*

## RESEARCH AND DEVELOPMENT

### Roark

In *Roark's Formulas for Stress and Strain* (Young and Budynas, 2001), Section 8.11, "Beams of Relatively Great Width," a case is presented of a very wide cantilever plate under a concentrated load. The bending stress σ at any point is expressed by the equation

$$\sigma = K_m \left( \frac{6P}{t^2} \right) \tag{1}$$

where $P$ is the concentrated load, $t$ is the plate thickness and $K_m$ is a dimensionless coefficient that depends on the location of the point in question. Values for $K_m$ are presented in a table in which the rows indicate the ratio $c/a$ and the columns indicate the ratio $z/a$ and where $c$ and $a$ are as shown in Figure 3. The dimension $a$ used in Roark's tables corresponds to $n$ in base plate two-way bending design.

Roark presents the bending factor $K_m$ in the context of a single concentrated load. A review of the values of $K_m$ as a function of $c$ for $z = 0$ indicates that the effective factor for a line load along the X-axis for all values of $c$ would average approximately 0.4. A table of Roark's values for $K_m$ for varying values of $c/a$ at $z = 0$ is shown in Table 1, and a diagram showing an equivalent line load is shown in Figure 4.

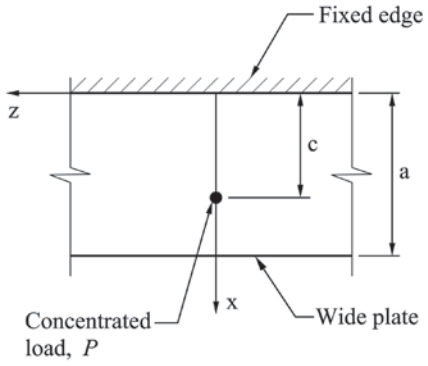


*Fig. 3. Roark case of a concentrated load on a cantilever.*

An average value of $K_m$ = 0.4 implies that the effective width would have been about 2.5$n$, or 1.25$n$ on each side. To account for the unbalanced or twisting forces caused by the asymmetrical load, this coefficient was then reduced to 1.0, leaving a reduced value of 1.0$n$ for the additional width effective for bending. This value was then added to the $z$-direction distance from the centroid of the loaded area to the edge of the loaded area to arrive at the final equation for $b_{eff}$:

$$b_{eff} = \frac{Y}{2} + n \tag{2}$$

For the purposes of establishing an upper limit to this theory, we will mirror the $b_{eff}$ calculation to the opposite side of the X-axis, giving us a total width of 2.0$n$. Therefore, the equation for $b_{eff}$ will be limited to the condition $Y \leq 2n$, beyond which we will revert to Design Guide 1's original $b_{eff} = Y$.

**Finite Element Analyses**

Finite element analyses were performed to provide confirmation of the proposed equation. The analyses included both (linear) elastic and (nonlinear) plastic methods. The base plate was modeled as a simple cantilever plate, fixed at the assumed bending line described earlier, with a constant uniform load. In doing so, two simplifying assumptions are made, which are consistent with current design methods:

1. The effective fixed edge is a straight line at 0.8$b_f$ This simplifies the effect of the flange tips and the off-center loaded area.
2. The loading is uniform over the bearing area. This neglects the interaction effect between the plate and foundation surface.

The base plate used for both the elastic and plastic analysis is a 1-in.-thick base plate under partial compression loading. The plate's plan dimensions and the assumed cantilever length beyond the bending line are shown in Figure 5.

***Elastic Analysis***

A simple analysis, based on Design Guide 1's assumptions, was performed using elastic plate elements in RISA-3D (2012). Uniform loads were applied over various load widths to represent varying lengths of the compression block, $Y$. In each analysis, the effective width, $b_{eff}$, was determined by comparing the results of similar loading on two different RISA-3D models: (1) a cantilever plate of width 22 in. loaded with a uniform load of width $Y$ along one edge and (2) a cantilever plate of width $Y$ loaded with the same uniform load of width $Y$. The two models were created using shell elements 0.5 in. × 0.5 in. × 1.0 in. thick. RISA uses the MITC4 plate element described in K.J. Bathe's self-published book, *Finite Element Procedures*, which includes bending and shear effects. The effective width was determined by comparing the maximum moments found in the two runs, which is equivalent to comparing the results at the point of initial yield. The ratio of the maximum plate moments in the two runs was then used to determine $b_{eff}$ by:

$$b_{eff} = \frac{\text{Maximum moment, 22-in.-wide model}}{\text{Maximum moment, } Y\text{-in.-wide model}} \times Y$$

The results of the elastic analysis are shown in Figure 6: Four data points correspond to the four pairs of analysis runs, and a curve was fitted to the results. The curve connecting these points also passes through the known theoretical point at the upper right corner, where the effective width is equal to the plate width for full compression on the plate.

In addition to the elastic analysis results, Figure 6 also plots the proposed equation for $b_{eff}$, the value of $b_{eff}$ used in Design Guide 1 and the plastic analysis results discussed in the next section.

Figure 6 shows a wider divergence between the elastic and $b_{eff} = Y$ curves at smaller bearing widths. This indicates that two-way action is most significant in this lower range. The values for the elastic curve are lower than for the proposed formula for $b_{eff}$ due to the limitation of elastic analysis

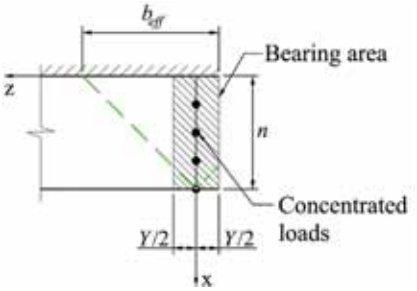


*Fig. 4. Roark case adapted for line load.*

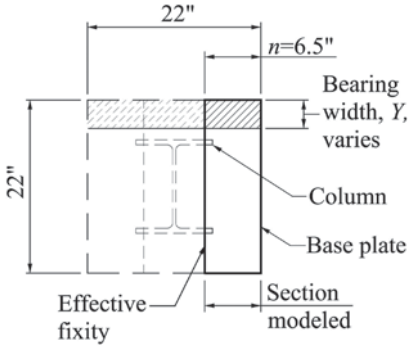


*Fig. 5. Base plate used in analyses.*

and the effects of twisting. As we shall see in the following plastic analysis, the elastic analysis results are based on first yield and are not representative of the true strength of the plate.

***Plastic Analysis***

In order to get a better estimate of the true strength of a base plate in two-way bending, a basic plastic analysis was performed with a nonlinear program. A series of runs was made on two plates in SAP2000 (2011): one 2 in. wide, and the other 22 in. wide, with uniform loading of width 2 in. ($Y$) on each. The two models were created using shell-type layered shell elements 0.5 in. × 0.5 in. × 1.0 in. thick. Layered shell elements in SAP2000 use the thick-plate (Mindlin/Reissner) formulation for bending behavior, which includes the effects of transverse shear deformation. The material stress-strain properties used a common 50-ksi material with an initial elastic portion, then a plateau above yield with strain hardening starting after 1.5% strain. In each run, the uniform load was increased and the resulting deflection at the plate corner was recorded. The progression of plate yield is shown in Figure 7. The force-deflection plot of these runs is shown in Figure 8.

The plastic limit of the 22-in.-wide plate was found to occur at a load of 5.0 ksi, and the plastic limit of the 2-in.-wide plate was found to occur at 0.8 ksi, indicating a $b_{eff}$ of 5.0/0.8 = 6.25 at $Y$ = 2 in. Figure 7 shows that first yielding occurs at the top, loaded edge of the plate. This first yield point is also indicated in Figure 8 and occurs relatively early due to twisting of the plate under load. The twist is caused by the centroid of the load being eccentric from the centroid of the plate resistance.

The curve for two-way bending starts out much steeper and thus stiffer than the one-way bending curve. This leads to the higher overall strength demonstrated with two-way action.

The analysis was then repeated for other values of $Y$. As the width of the loaded area became wider and wider, the yield line migrated lower and lower on the plate until, eventually, the entire length of the base plate was involved in resisting two-way bending moment—in this case, after $Y$ = 12 in. The results of the plastic analysis series are also shown on Figure 6. The results of the plastic analysis demonstrate a significantly higher strength than predicted by elastic methods. The plastic curve is significantly above the proposed method at all points and is considered sufficiently conservative for now.

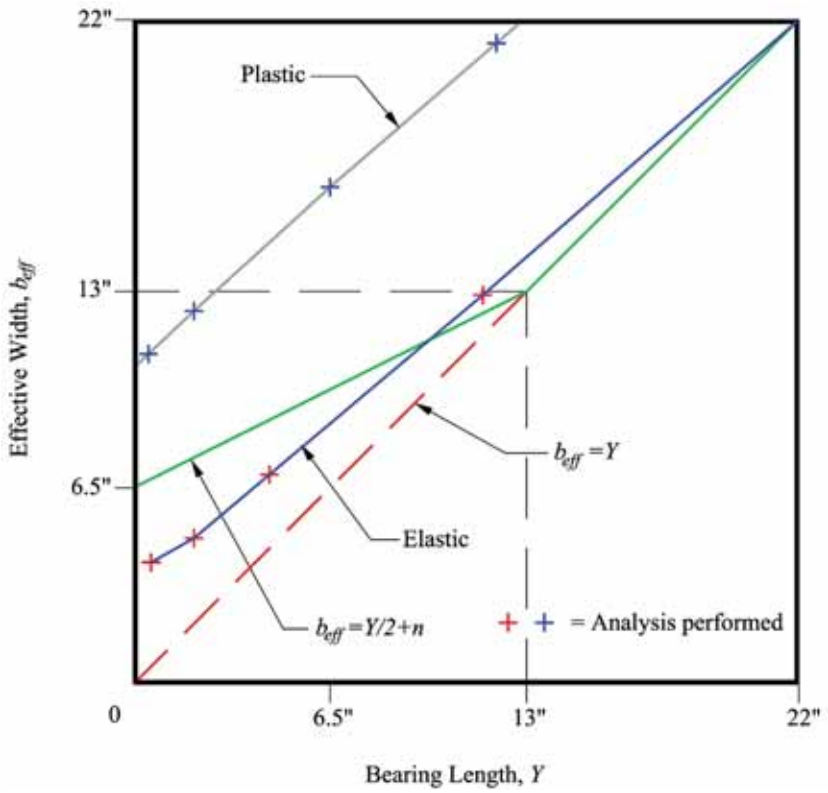


*Fig. 6. Analysis results, effective width vs. bearing length.*

**Comparison to Tests**

Recent full scale tests were reviewed to shed additional light on the above analysis. Gomez, Deierlein and Kanvinde (2010) provided a detailed report on the testing with a summary by Kanvinde and Deierelein (2011). From a review of the test results, two comments can be made. First, tests demonstrated that base plates can continue to provide resistance well beyond the yield point. This indicates that the post-yield behavior seen in the preceding nonlinear analysis can be counted on to take the design loading. The second point concerns the observed plate bending behavior. The theory indicated by Design Guide 1 is that the effective bending width is equal to the rectangular stress block width ($b_{eff} = Y$). Using this theory and the dimensions of the test specimens, calculations indicate that two-way bending should have governed. However, the only compression-related bending reported was bending in the primary direction across the entire width of the plate parallel to the column flange. It should be noted that during actual tests, the bearing pressure is expected to decrease toward the end of the cantilever due to flexibility of the plate. This will tend to make the actual plate moment less than that resulting from the assumed uniform load.

Although two-way bending behavior was not one of the goals of the tests, the observed end bending failure mode lends credence to the proposed model. This indicates that the following recommended design procedure for two-way bending should be considered in design of base plates.

## RECOMMENDED DESIGN PROCEDURE

Based on the preceding analysis and discussion, the authors of this paper recommend the use of an effective width, $b_{eff}$, rather than $Y$ when determining the base plate thickness

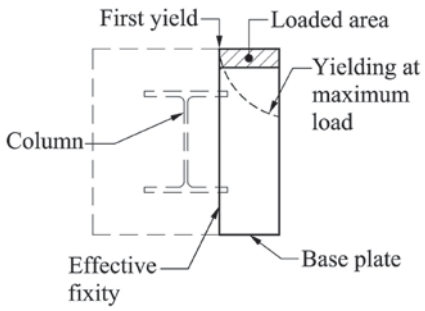


*Fig. 7. Plastic analysis–yield progression for Y = 2 in.*

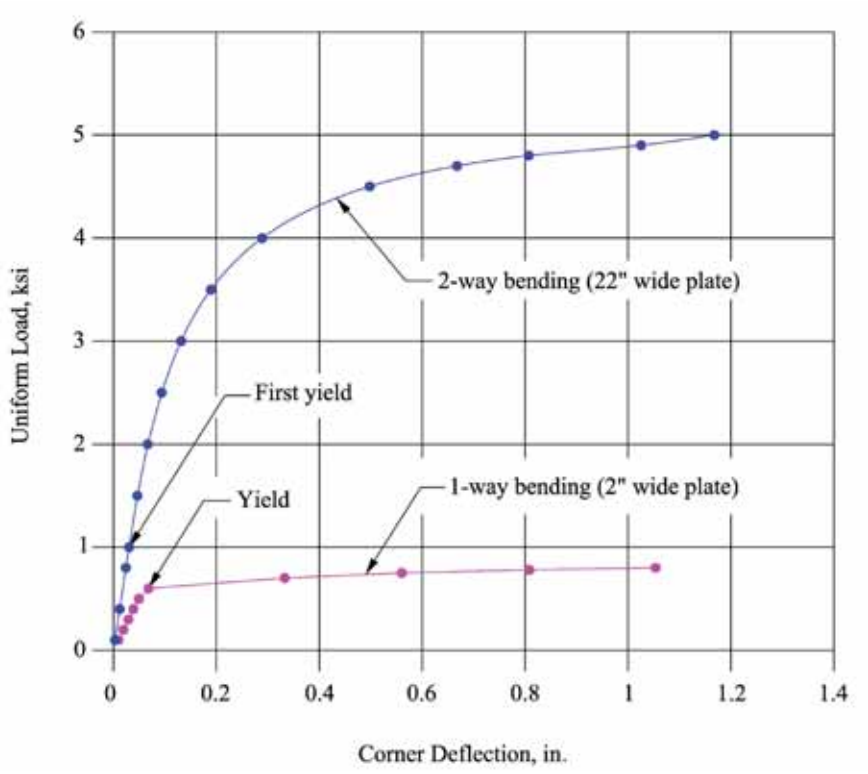


*Fig. 8. Plastic load-deflection diagram of plate at Y = 2 in.*

required for two-way bending. The effective width $b_{eff}$ recommended is:

$$b_{eff} = \frac{Y}{2} + n \qquad \text{for } Y < 2n \tag{3}$$

and

$$b_{eff} = Y \qquad \text{for } Y \geq 2n \tag{4}$$

This is shown graphically in Figure 9 in terms of plate variables. The effective width for two-way bending, $b_{eff}$; the rectangular stress block width, $Y$; the lateral cantilever, $n$; and the length of base plate, $N$, are defined in Figure 10.

Using the earlier $b_{eff}$, the plate thickness required to resist two-way bending is determined from Equation 5:

$$t_{p(req)} = n\sqrt{\frac{2f_{p(max)}Y}{\phi F_y b_{eff}}} \tag{5}$$

where

$f_{p(max)}$ = maximum design bearing stress in concrete using LRFD (strength design)

$\phi$ = resistance factor in bending = 0.9

$F_y$ = specified minimum yield stress of the base plate

Equation 5 combines both loading and plate section properties and can be derived from Equation 3.3.14a-1 in Design Guide 1 by substituting $n$ for $m$, $f_{p(max)}$ for $f_p$ and $\phi$ for 0.9. Then, because the quantity under the radical is related to the applied moment divided by the plate section properties, the quantity under the radical is multiplied by the ratio $Y/b_{eff}$.

## CONCLUSION AND RECOMMENDATIONS

The following points can be drawn from the preceding discussion:

1. Two-way bending of base plates should be considered. Two-way bending will commonly govern the plate thickness required, particularly for narrow columns and/or wide base plates.
2. Two-way action should be considered in determining the plate resistance.
3. Twisting of a base plate under two-way action can become significant; however, first yielding of the plate is not representative of true strength.
4. A recommended design method incorporating two-way bending is given by Equations 3, 4 and 5.

This design method is simple enough to use in everyday design, yet effective. Although only limited analysis was performed, indications are that the method is conservative and is considered appropriate for design purposes at this time.

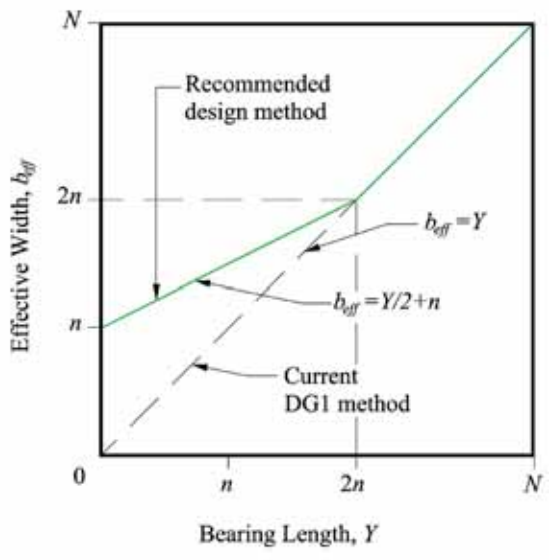


*Fig. 9. Recommended design method for two-way bending.*

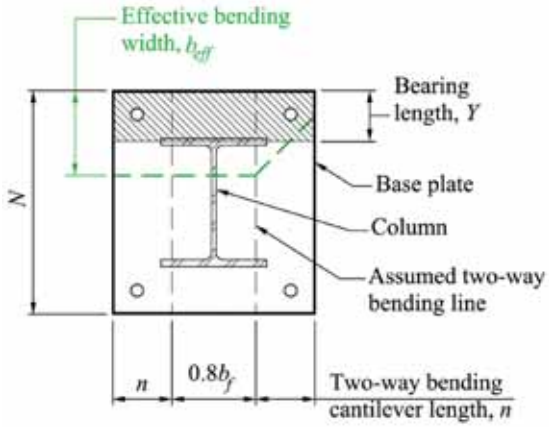


*Fig. 10. Base plate terms.*

## EXAMPLE PROBLEM

Determine the minimum base plate thickness required to resist two-way bending in a base plate with a factored axial load $P_u = 60$ kips and factored moment $M_u = 80$ kip-ft, using LRFD. Bending is about the strong axis of a W12×22 wide flange column with a flange width $b_f = 4.03$ in. Conservatively consider the ratio of the concrete to base plate area is unity, $F_y$ of the base plate is 36 ksi and $f'_c$ of concrete is 4 ksi. For the purposes of this example, assume the bearing value $f_{p(max)}$ and bearing width $Y$ have been found to be 2.21 ksi and 1.91 in, respectively. The base plate is 20 in. wide ($B$) and 20 in. long. (See Figure 11.)

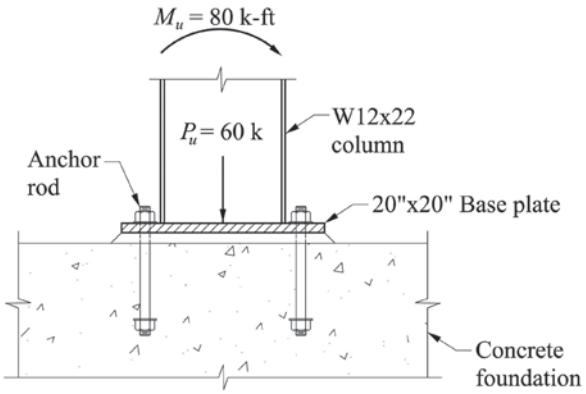


*Fig. 11. Example.*

**Step 1**. Determine the two-way bending cantilever:

$$n = \frac{(B - 0.8b_f)}{2}$$
$$= \frac{20 \text{ in.} - 0.8(4.03 \text{ in.})}{2}$$
$$= 8.39 \text{ in.}$$

**Step 2.** For comparison, determine minimum base plate thickness for two-way bending per Design Guide 1. Use $b_{eff} = Y$:

$$t_{p(req)} = n\sqrt{\frac{2f_{p(max)}Y}{\phi F_y b_{eff}}}$$
$$= 8.39 \text{ in.}\sqrt{\frac{2(2.21 \text{ ksi})(1.91 \text{ in.})}{(0.9)(36 \text{ ksi})(1.91 \text{ in.})}}$$
$$= 3.10 \text{ in.}$$

**Step 3.** Per the new model:

Because $Y < 2n$, use

$$b_{eff} = \frac{Y}{2} + n$$
$$= \frac{1.91 \text{ in.}}{2} + 8.39 \text{ in.}$$
$$= 9.35 \text{ in.}$$

$$t_{p(req)} = n\sqrt{\frac{2f_{p(max)}Y}{\phi F_y b_{eff}}}$$
$$= 8.39 \text{ in.}\sqrt{\frac{2(2.21 \text{ ksi})(1.91 \text{ in.})}{(0.9)(36 \text{ ksi})(9.35 \text{ in.})}}$$
$$= 1.40 \text{ in.}$$

It can be seen from this example that a significant reduction in plate thickness due to two-way bending can be used with the new model.

## REFERENCES


AISC (2011), *Manual of Steel Construction,* 14th edition, American Institute of Steel Construction, Chicago, IL, pp. 14-4 to 14-9.

Fisher, J.M. and Kloiber, L.A. (2006), *Design Guide 1, Base Plate and Anchor Rod Design*, 2nd edition, 2nd printing, American Institute of Steel Construction, Chicago, IL.

Gomez, I.R., Deierlein, G.G. and Kanvinde, A.M. (2010), Exposed Column Base Connections Subjected to Axial Compression and Flexure, https://nees.org/resources/839.

Kanvinde, A.M. and Deierlein, G.G. (2011), "Recent Research on Column Base Plate Connections," *Modern Steel Construction*, Vol. 51, No. 4, pp. 42–44.

RISA-3D (2012), Software, Version 10.0.1, RISA Technologies, Foothill Ranch, CA.

SAP2000 (2011), Software, Version 15.1.0/1, Computers and Structures Inc., Walnut Creek, CA.

Young, W.C. and Budynas, R.G. (2001), *Roark's Formulas for Stress and Strain*, 7th edition, McGraw-Hill, New York, NY.

# A Graphical Design Aid for Selecting Standard W-Shape Steel Beam-Columns with Minimum Weight

MOHAMMAD ALI SA'ADAT and MOHAMMAD REZA BANAN

## ABSTRACT

This paper presents an alternative technique for selecting the lightest W-section for beam-column members. Following the AISC procedure, the number of required steps to find a feasible section highly depends on the initial trial section. A new graphical technique based on the AISC interaction formula for designing steel beam-columns is proposed. By employing the newly developed diagrams, the new approach quickly leads to the lightest feasible section for a member subjected to combined biaxial bending and axial force. The number of computational steps in the proposed method is slightly reduced from the current AISC procedure. Some advantages of the new proposed method are converging to the solution in fewer steps, imposing no limit on $L_b$, considering the effect of $C_b$, considering biaxial bending by simply using a modification factor and covering cases where $L_b$ is not equal to $KL$.

**Keywords:** beam-column, design aid, graphical solutions.

## INTRODUCTION

Prior to the third edition of the AISC *Load and Resistance Factor Manual of Steel Construction* (2001), the procedure for design of steel beam-columns was based on computing an approximate equivalent axial load then selecting a trial shape from the column load tables and finally checking the compliance of the section with those requirements specified by the 1999 AISC LRFD *Specification*.

Aminmansour (2000) rewrote the 1999 AISC LRFD interaction equations for beam-columns and developed design-aid tables in terms of three parameters—*b, m* and *n*—which, after adoption by the third edition AISC LRFD *Manual* (2001) in Part 6, became the parameters $p$, $b_x$ and $b_y$, respectively. Hereinafter, we will refer to this method as either the AISC method or the current method. In the same year, Keil (2000) presented graphical design aids for $C_b = 1$. The curves were developed for a standard case where $KL = L_b = 0$. For other cases, he provided some linear transformation factors such that the same graphs developed for the standard case could be used. Hosur and Augustine (2007) improved Keil's technique to consider the effect of $C_b$ (with a value between 1.0 and 2.3).

Although all these works are referred to as graphical design aids, they all require using some tables during the course of design. In each of these methods, the graphical design aid is used in the last step in place of using interaction equations.

The graphical design aids proposed by Keil (2000) and Hosur and Augustine (2007) could not handle cases with biaxial bending.

## PROPOSED METHOD COMPARED WITH AISC METHOD

The proposed method as an alternative to the current method enjoys some advantages in terms of the following points of view.

- *Visualization:* Graphical design aids provide a visual representation of the design procedure, to some extent.
- *Least weight:* Following the current method, the selected shape may not be the lightest one, which must be verified by trying other shapes (at the expense of additional computation). It is important to remember, however, that the least weight solution may not always be the least expensive solution.
- *Initial depth:* The current method is more like a checking guide because the designer must know the initial depth of the W-shape before starting the design process.
- *Initial trial section independence:* Tables presented in Part 6 of the 14th edition of the AISC *Manual* (2011) are sorted by depth, and shapes with the same depth are sorted by their corresponding weights in descending

Mohammad Ali Sa'adat, Senior Student, Department of Civil and Environmental Engineering, School of Engineering, Shiraz University, Shiraz, Iran. Email: malisaadat92@gmail.com

Mohammad Reza Banan, Associate Professor, Department of Civil and Environmental Engineering, School of Engineering, Shiraz University, Shiraz, Iran (corresponding). Email: banan@shirazu.ac.ir

order. As a general rule, it is understood that between two shapes with the same weight, the deeper one has higher flexural strength. Thus, a good practice is picking a depth for the section—say, W12—and then finding a shape that satisfies the interaction equation. And as a final step, search among deeper and lighter shapes to find the lightest one if desired.

There are some cases, however, that violate this simple rule. For instance, a W8×31 has higher flexural strength than a W16×31 for $L_b > 13.5$ ft and higher axial strength for all $KL$ (considering $C_b = 1$ and $F_y = 50$ ksi). Examples like this could be a source of confusion in selecting the best section. This case will be discussed later in Example 1.

Furthermore, in Part 1 of the 14th edition AISC *Manual* (2011), dimensions and properties, after categorizing shapes by their depth, the first subcategory is based on flange width and then by weight in a descending order. Because, for the same depth, the strength is more dependent on flange width rather than weight (e.g., a W40×372 has higher flexural strength than a W40×392 for $L_b > 10.5$ ft in spite of its lighter weight because of wider flanges), there is the possibility of not selecting the lightest section.

- *Speed:* Some reasons that make the current method relatively lengthy, which increases the possibility of errors, are as follows.
  - There are two interaction equations H1-1a and H1-1b in the 2010 AISC *Specification*, and one has to find out which one to use. Sometimes this step could be forgotten. So, if equation H1-1b must be used, then the user may not follow the appropriate required modifications.
  - Finding the lightest shape involves trying sections of different depths (and not necessarily deeper ones).
  - When $C_b \neq 1$, one has to check extra tables or diagrams to find or compute plastic moment capacity and consequently to recalculate coefficient $b_x$.

In the proposed new method, there is no need to decide which interaction formula is appropriate. The curves are ready to use. When the plotted curve is solid, the W-shape assigned to that curve is the lightest possible shape for the given combination of loads applied to the member. When the curve is represented by a dashed line, a lighter W-shape exists. There are no additional tables or diagrams. In most cases, the calculations can be done easily without using a calculator.

## DEVELOPMENT OF THE PROPOSED DESIGN AIDS

The criterion for checking the adequacy of a member as a beam-column is its compliance with AISC *Specification* equations H1-1a or H1-1b. These interaction equations are based on the required and provided axial compressive and flexural strengths of a member.

$$\text{If } \frac{P_r}{P_c} \geq 0.2$$

$$\frac{P_r}{\phi_c P_c} + \frac{8}{9}\left(\frac{M_{rx}}{\phi_b M_{cx}} + \frac{M_{ry}}{\phi_b M_{cy}}\right) \leq 1.0 \qquad \text{(H1-1a)}$$

$$\text{If } \frac{P_r}{P_c} \leq 0.2$$

$$\frac{P_r}{2\phi_c P_c} + \left(\frac{M_{rx}}{\phi_b M_{cx}} + \frac{M_{ry}}{\phi_b M_{cy}}\right) \leq 1.0 \qquad \text{(H1-1b)}$$

Required strengths $P$, $M_{rx}$ and $M_{ry}$ are determined from analysis. So, the provided strengths will govern the selection process of an appropriate member. A closer look at the AISC equations reveals that for a beam-column subjected to uniaxial bending about major axis ($M_y = 0$), with uniform moment factor ($C_b = 1$) and having unbraced length $L_b$ (for the flexural design strength) the same as effective length $KL$ (for the axial compressive design strength), these two equations can be rewritten as follows. Note that $M_{cx}$ is the flexural capacity about the major axis for $C_b = 1$.

$$\text{If } \frac{P_r}{P_c} \geq 0.2$$

$$P_r = \phi_c P_c \left[1 - \frac{8}{9}\left(\frac{M_{rx}}{\phi_b M_{cx}}\right)\right] \qquad (1)$$

$$\text{If } \frac{P_r}{P_c} \leq 0.2$$

$$P_r = 2\phi_c P_c \left(1 - \frac{M_{rx}}{\phi_b M_{cx}}\right) \qquad (2)$$

These interaction equations can be plotted with two straight lines. Figure 1 shows the interaction curve for a section—in this case, a W44×230. Above and below each curve, additional parameters are included. All curves are developed for $F_y = 50$ ksi.

Remember that $P_c$ is calculated based on buckling about the minor axis. If buckling occurs about the major axis, the effective length, $(KL)_x$, has to be modified as follows:

$$\left(KL\right)' = \frac{(KL)_x}{\left(r_x / r_y\right)} \tag{3}$$

## PROCEDURE FOR USING PROPOSED DESIGN AID

In this section, we explain a unified procedure suitable for designing beam-column members (subjected to either compression or tension) by using the proposed design aid.

### Beam-Column (Compression and Flexure)

While designing a beam-column, six different cases could happen, discussed in detail as follows.

**Case 1.** $M_y = 0$, $C_b = 1$ and $KL = L_b$

In this case, we have a beam column with uniaxial bending about the major axis. The only step that leads to the most economical section for this member is to locate a point with known $P_r$ and $M_{rx}$ on the graph corresponding to the given $L_b$. All sections above that point will be adequate for the given loading.

**Case 2.** $M_y \neq 0$, $C_b = 1$ and $KL = L_b$

In this case with biaxial bending, we can rewrite Equations 1 and 2 as follows.

$$\frac{M'}{\phi_b M_{cx}} = \frac{M_{rx}}{\phi_b M_{cx}} + \frac{M_{ry}}{\phi_b M_{cy}} = \frac{M_{rx}M_{cy} + M_{ry}M_{cx}}{\phi_b M_{cx} M_{cy}} \tag{4}$$

where $M'$ is an equivalent bending moment, defined such that the designer could use the same diagrams as before.

Solving Equation 4 yields:

$$M' = M_{rx} + r_b M_{ry} \tag{5}$$

where

$$r_b = M_{cx}/M_{cy} \tag{6}$$

In this equation, the new variable $r_b$ is the ratio of flexural capacity about the major axis $C_b = 1$ to flexural capacity about the weak axis. The recommended procedure for use of this method is to split the diagram into equal parts. In every step, add $M_{ry}$ to the modified (or original) $M_{rx}$ to compute new $M'$ (Figure 2). For the $n$th step, we have

$$M' = M_{rx} + (n+1)M_{ry} \tag{7}$$

Those sections in the range of $(M_{rx} + M_{ry}, M_{rx} + (n+1)M_{ry})$ that satisfy $1 \leq r_b \leq n+1$ could be the answer. Finally, the equivalent bending moment, $M'$, should be computed using Equation 5. Compliance with AISC interaction equations can be checked by using the developed diagrams.

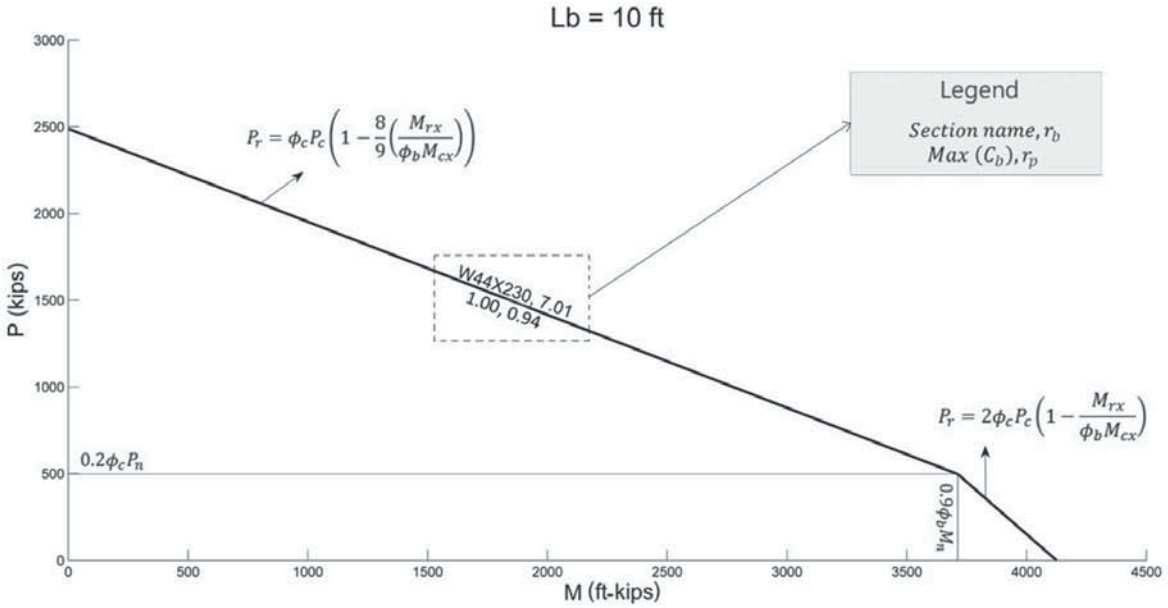


*Fig. 1. Interaction curve for* W44×230 *(*$L_b = KL =$ *10 ft and* $F_y =$ *50 ksi).*

**Case 3.** $M_y = 0$, $C_b \neq 1$ and $KL = L_b$

In the case where $C_b$ assumes values other than 1.0, we just need to calculate the transformed bending moment, $M'$ (Equation 8), and then adjust the diagrams with given $P$ and calculated $M$. Because the bending moment capacity of a member cannot exceed the plastic moment capacity when a shape is compact and when either yielding controls or compression flange yielding governs the strength for a shape with noncompact web, the maximum value that $C_b$ can take is specified for each section on the diagrams.

$$M' = \frac{M}{C_b} \tag{8}$$

**Case 4.** $M_y \neq 0$, $C_b \neq 1$ and $KL = L_b$

In this case, modification will be as given in Equation 9. The procedure to select the lightest cross-section will be the same as the procedure used in case 3.

$$M' = \frac{M_{rx}}{C_b} + r_b M_{ry} \tag{9}$$

**Case 5.** $M_x = 0$ and $M_y \neq 0$

This case is similar to case 2, except $M_{rx} = 0$. The same procedure as defined for case 2 must be followed.

**Case 6.** $KL \neq L_b$

For this case, we have

$$\frac{P_r'}{P_{c\,\text{at}\,L_b}} = \frac{P_r}{P_{c\,\text{at}\,KL}} \tag{10}$$

where $P_r'$ is an equivalent axial load defined such that the same diagrams developed before can be used. Now, Equation 10 will be rearranged as follows:

$$\frac{P_r'}{P_r} = \frac{P_{c\,\text{at}\,L_b}}{P_{c\,\text{at}\,KL}} = \frac{\dfrac{P_{c\,\text{at}\,L_b}}{P_{c\,\text{at}\,KL=0}}}{\dfrac{P_{c\,\text{at}\,KL}}{P_{c\,\text{at}\,KL=0}}} \tag{11}$$

By introducing $r_{p\,\text{at}\,\beta} = \dfrac{P_{c\,\text{at}\,\beta}}{P_{c\,\text{at}\,KL=0}}$, which is the ratio of axial compression capacity at $KL = \beta$ to axial compression capacity at $KL = 0$, the equivalent axial load, $P_r'$, can be computed as given in Equation 12.

$$P_r' = \frac{r_{p\,\text{at}\,L_b}}{r_{p\,\text{at}\,KL}} P_r \tag{12}$$

To select the lightest section, we have to compute equivalent axial load and locate the corresponding point on the proper curve.

**Beam-Column (Tension and Flexure)**

If the beam-column is subjected to tension instead of compression, either of the two limit states of tension yielding and tension rupture might govern.

**Case 1.** Tension yielding governs the tensile capacity of the member: The tension yielding strength, $\phi F_y A_g$, is equal to compression strength for $KL = 0$; therefore, we should follow the same procedure as explained for the case with $KL \neq L_b$. Because $r_{p\ \text{at}\ KL=0} = 1$, the axial load must be modified to $P_r'$ as follows:

$$P_r' = \frac{r_{p\,\text{at}\,L_b}}{r_{p\,\text{at}\,KL=0}} = r_{p\,\text{at}\,L_b} P_r \tag{13}$$

**Case 2.** Tension rupture governs the tensile capacity of the member. By assuming shear lag factor $U = 0.75$, we must simply modify the axial load and compute the equivalent axial force, $P_r'$, as follows:

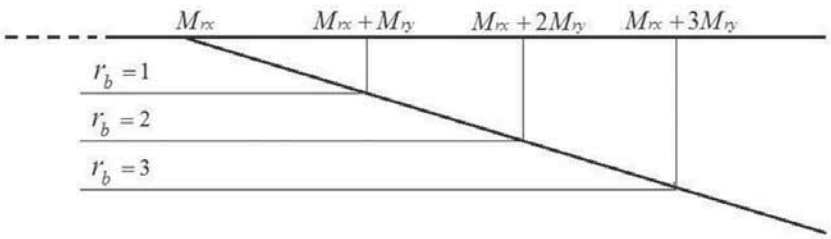


*Fig. 2. Distribution of* $r_b$ *for different values of* $M'$.

| Table 1. Average Relative Errors and Standard Deviation for Interpolation between Diagrams | | |
|---|---|---|
| | **Average Relative Error** | **Standard Deviation** |
| $M_{cx}$ | 0.000957 | 0.00245 |
| $P_c$ | 0.002669 | 0.006418 |
| $M$ for constant value of $P$* | 0.002316 | 0.003973 |

* Error for this case is dependent on value of $P_r$, so for calculating error, the value of $P_r$ has been changed from $0.1P_c$ at $KL = 0$ to $0.9P_c$ at $KL = 0$ for each section, and error has been calculated for different $KL$. The overall average relative error and standard deviation are reported.

$$\frac{\phi_t F_y A_g}{\phi_t F_u A_e} = \frac{(0.9)(50)A_g}{(0.75)(65)(0.75)A_g} = 1.23 \tag{14}$$

which leads to

$$P_r' = (1.23)\left(r_{p \text{ at } L_b}\right)P_r \tag{15}$$

**Beams**

To design a beam subjected to uniaxial or biaxial bending, we can follow the same procedure as that given for a beam-column with $P_r = 0$.

**Columns**

To design a column, the procedure is the same as the one given for a beam-column, except $M_{rx}$ and $M_{ry}$ will be zero.

**Interpolation**

If no diagram for a specific $L_b$ is provided, we can conservatively design the member for a larger $L_b$. But if more accuracy is desired, we can compute $M$ for the given $L_b$ and $P$ by using linear interpolation between two values for $M$ corresponding to a smaller and a larger value for $L_b$. Then the section must be checked for the given loads.

The error and corresponding standard deviation for $M_{cx}$ and $P_c$ from different cases are computed and summarized in Table 1. Because these values are small, we can conclude that interpolation between diagrams with different $L_b$ is permitted.

Because $C_b$, $r_b$ and $r_p$ are explicitly related to $M_{cx}$ and $P_c$, interpolation is permitted for these parameters as well.

## EXAMPLES

To show the validity of the new developed method, some problems will be simultaneously solved by using the AISC and the proposed methods. For each case, it is assumed that all given loads are determined through a second-order analysis. Therefore, no modification on either $P$ or $M$ is required.

**Example 1.** [Variation of Aminmansour (2000) Example 1]

*Given:* $P_u = 179$ kips, $M_{ntx} = 47.6$ ft-kips, $L_b = (KL)_y = 10$ ft. Select the lightest W-shape of ASTM A992 steel.

To follow the proposed method, locate the corresponding point on the appropriate diagram (Figure 4) and move to the right to find the answer.

First section is W80×31, and because the curve is solid, the designer will be assured that it is the most economical section.

**Example 2.** [Aminmansour (2000) Example 2]

*Given:* $P_u = 400$ kips, $M_{ntx} = 250$ ft-kips, $M_{nty} = 80$ ft-kips, $L_b = (KL)_y = 14$ ft. Select the lightest W14 shape of ASTM A992 steel.

In Figure 5, look for W14s.

**Step 1.** $330 \le M' \le 410$ and $r_b \le 2$ ∴ No answer

**Step 2.** $410 \le M' \le 490$ and $r_b \le 3$

W14×99 with $r_b = 2.06 \rightarrow M' = 250 + (2.06)(80) = 415$ kip-ft → Good

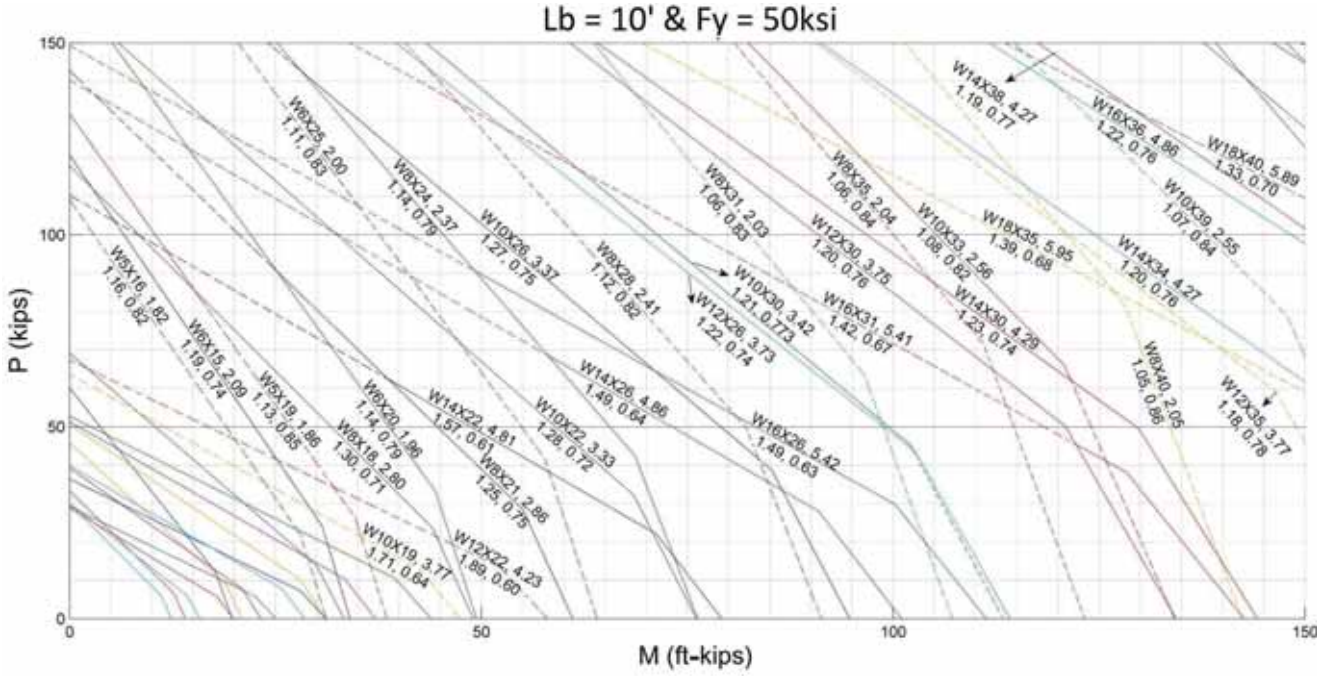


*Fig. 3. Proposed design aid (part 1).*

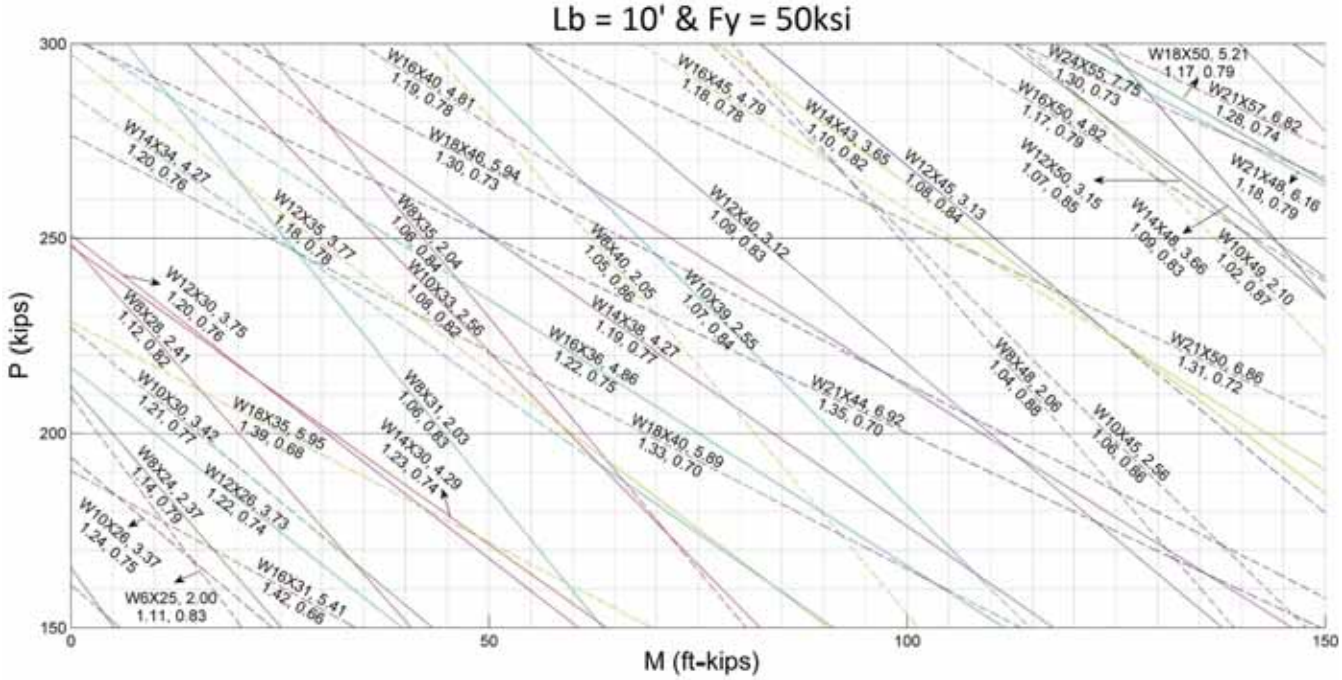


*Fig. 4. Proposed design aid (part 2).*

**Example 3.**

*Given:* $P_u = 400$ kips, $M_{ntx} = 600$ ft-kips, $C_b = 1.5$, $L_b = (KL)_y = 14$ ft. Select the lightest W-shape of ASTM A992 steel.

Compute $M'$ as follows:

$$M' = \frac{M}{C_b} = \frac{600}{1.5} = 400 \text{ ft-kips}$$

Then using Figure 5:

**Step 1.** Try W24×103 with $C_b = 1.22$

$$M' = \frac{600}{1.22} = 492 \text{ ft-kips} \rightarrow \text{N.G.}$$

**Step 2.** Try W30×99 with $C_b = 1.23$. This section will be acceptable with a $C_b = 1.22$. Because the curve is solid, it is the lightest shape.

**Example 4.**

*Given:* $P_u = 300$ kips, $M_{ntx} = 375$ ft-kips, $M_{nty} = 50$ ft-kips, $C_b = 1.5$, $L_b = (KL)_y = 14$ ft. Select the lightest W-shape of ASTM A992 steel.

From Figure 5, we have:

**Step 1.** $\frac{375}{1.5} + 50 = 300 \le M' \le 350$ and $r_b \le 2$ ∴ No answer

**Step 2.** $350 \le M' \le 400$ and $r_b \le 3$ ∴ No answer

**Step 3.** $400 \le M' \le 450$ and $r_b \le 4$

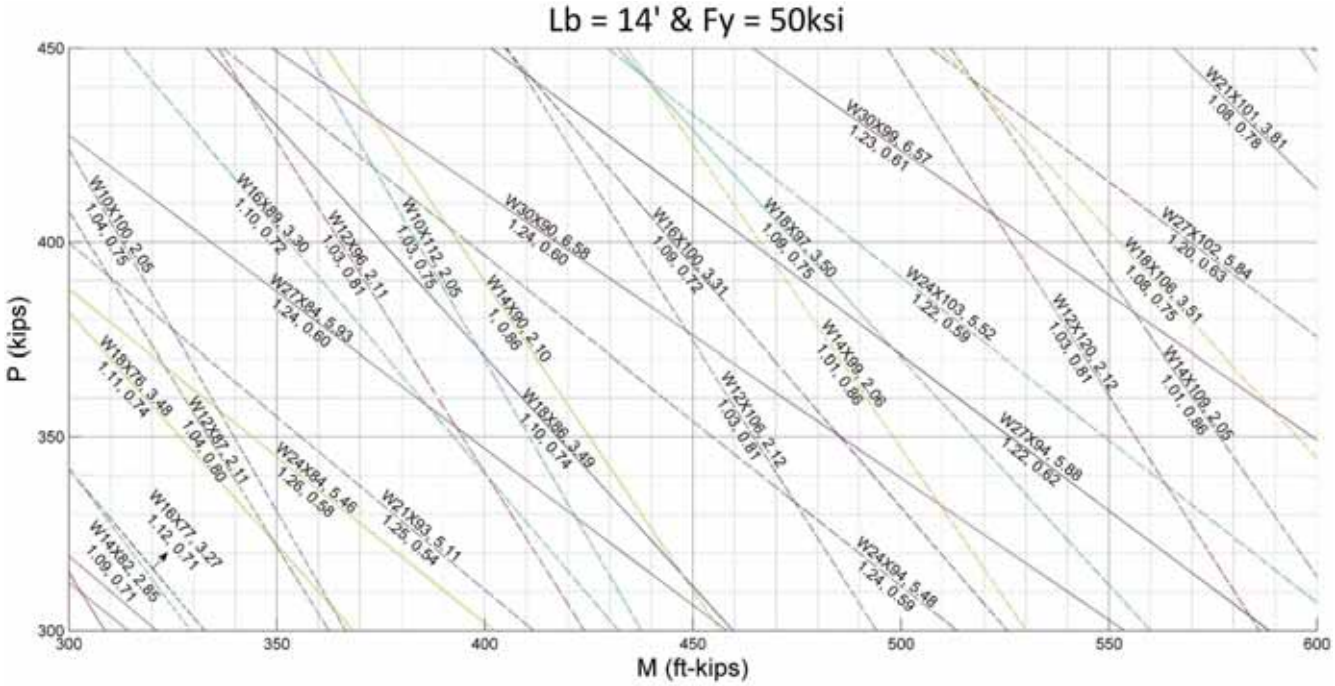


*Fig. 5. Proposed design aid (part 3).*

Try W12×96: $M' = \frac{375}{1.03} + (2.11)(50) = 470$ ft-kips $\rightarrow$ N.G.

Try W10×112: $M' = \frac{375}{1.03} + (2.05)(50) = 467$ ft-kips $\rightarrow$ N.G.

**Step 4.** $450 \le M' \le 500$ and $r_b \le 5$

W14×90 will not work because this section has the same $r_b$ but a smaller $C_b$ than the W12×96 has, so it has a lower capacity.

W18×86 will not work because of having a very large value for $r_b$.

Try W12×106: $r_b = 2.12$ and $C_b = 1.03$. Because it has the same values for $C_b$ and $r_b$ as a W12×96, no calculation is needed and it will work.

**Step 5.** $500 \le M' \le 550$ and $r_b \le 6$

Try W16×100: $M' = \frac{375}{1.09} + (3.31)(50) = 480$ ft-kips $\rightarrow$ Good

Try W14×99; $r_b = 2.06$ and $C_b = 1.01$

**Step 6.** $550 \le M' \le 600$ and $r_b \le 7$

Try W18×97: $M' = \frac{375}{1.09} + (3.5)(50) = 520 \rightarrow$ Good

Because the next solid curve with the same weight lighter than W18×97 is W27×94—which is not adequate—the next lighter shape with a solid curve is W30×99. Thus, W18×97 is the lightest shape.

## CONCLUSION

The AISC method is an accurate technique for determining the capacity of a section or to check the adequacy of a given section as a beam-column member. A design aid (Figures 3, 4 and 5) is proposed that leads to the minimum weight design for a beam-column with slightly less computational effort compared with the current method. It is important to remember that the least weight solution is not always the least cost solution; many other factors in the design and construction process must be considered as well. The proposed technique is simple, straightforward and covers the selection of beam-column members as well as the selection of individual beam or column members.

## ACKNOWLEDGMENT

This study was partially supported by the Office of the Associated Dean in Research, School of Engineering, Shiraz University.

## REFERENCES

AISC (1999), *LRFD Specification for Structural Steel Buildings*, American Institute of Steel Construction, Chicago, IL.

AISC (2001), *Load and Resistance Factor Design Manual of Steel Construction*, 3rd ed., American Institute of Steel Construction, Chicago, IL.

AISC (2010), *Specification for Structural Steel Buildings*, ANSI/AISC 360-10, American Institute of Steel Construction, Chicago, IL.

AISC (2011), *Steel Construction Manual*, 14th ed., American Institute of Steel Construction, Chicago, IL.

Aminmansour, A. (2000), "A New Approach for Design of Steel Beam-Columns," *Engineering Journal*, AISC, Vol. 37, No. 2, pp. 41–72.

Hosur, V. and Augustine, B. (2007), "Graphical Design Aid for Beam-Columns (LRFD)," *Engineering Journal*, AISC, Vol. 44, No. 2., pp. 147–180.

Keil, W.J. (2000), "LRFD Beam-Column Graphical Design Aid," *Engineering Journal*, AISC, Vol. 37, No. 3, pp. 99–119.

# Effective Weld Properties for Hollow Structural Section T-Connections under Branch In-Plane Bending

MATTHEW R. MCFADDEN and JEFFREY A. PACKER

## Abstract

The 2010 AISC *Specification for Structural Steel Buildings* has expanded the scope in Chapter K, "Design of HSS and Box Member Connections," to include a Section K4, "Welds of Plates and Branches to Rectangular HSS." An experimental program was undertaken to test various unreinforced HSS-to-HSS 90° T-connections subject to branch in-plane bending moment with the objective of determining the effectiveness of the welded joint. Twelve unique test specimens were designed to be weld-critical, and the results from the full-scale tests revealed that the current equation for the effective elastic section modulus for in-plane bending, $S_{ip}$, given in Table K4.1 of AISC 360-10, is very conservative. A modification to the current requirement that limits the effective width of the transverse weld elements is proposed, resulting in a safe but more economical weld design method for HSS-to-HSS T-connections subject to branch bending moment. By reanalyzing the data of prior weld-critical tests on HSS-to-HSS T- and X- (cross-) connections subject to branch axial loading, it is shown that the proposed new weld effective length recommendation is applicable to these connections as well. It is also concluded that the fillet weld directional strength enhancement factor, $(1.00 + 0.50\sin^{1.5}\theta)$, should not be used for strength calculations of welded joints to square and rectangular HSS, with the proposed revision, when the effective length method is used.

**Keywords:** hollow structural sections, welded joints, moment connections, gas-metal arc welding, effective weld properties, fillet welds, partial-joint-penetration flare-bevel-groove welds.

## INTRODUCTION

The design criteria for fillet welds have evolved over the years as more data have become available through experimental research. While often viewed as simplistic in nature, the way in which a fillet weld transfers the load through a connection can be complex, especially in semi-rigid connections between rectangular and square hollow structural sections (HSS). Because welding can only be performed around the outer perimeter of HSS walls and because the majority of connections between HSS are fillet-welded, the fillet welds are inherently eccentrically loaded, which causes secondary bending moments at the root.

With welded connections between HSS there are currently two design methods used for weld design (Packer, Sherman and Lecce, 2010):

1. The welds may be proportioned to develop the yield strength of the connected branch wall at all locations around the branch perimeter. This method will produce an upper limit on the required weld size and may be excessively conservative in some situations.
2. The welds may be designed as "fit-for-purpose" and proportioned to resist the applied forces in the branch. The highly nonuniform distribution of stress around the weld perimeter due to the relative flexibility of the connecting HSS face requires the use of effective weld lengths. This approach may potentially result in smaller weld sizes, thus providing a more economical design with improved aesthetics.

The design methods for fillet welds to develop the yield strength of the connected branch wall at all locations around the perimeter in various national and international codes, specifications and guidelines are reviewed and compared in McFadden, Sun and Packer (2013). In that paper, the equations were rearranged to solve for the minimum required effective weld throat ($t_w$) per unit length of the weld in terms of the branch wall thickness ($t_b$) for the simple case of an axially loaded HSS-to-HSS T-connection ($\theta = 90°$), using the equivalent of cold-formed HSS made to ASTM A500 Grade C (ASTM, 2010) with matching electrodes. That exercise demonstrated a considerable disparity in fillet weld design criteria.

Modern design methods based on data from full-scale tests of weld-critical connections between HSS performed at the University of Toronto (Frater and Packer, 1992a, 1992b; Packer and Cassidy, 1995) have led to the development and use of effective weld properties. These properties take into account the nonuniform distribution of normal stress and strain around the weld perimeter and exclude portions of the weld that are ineffective in resisting the applied loads.

Matthew R. McFadden, Project Engineer/Bridge Designer, MMM Group, Ottawa, ON, Canada. E-mail: matthew_mcfadden@outlook.com

Jeffrey A. Packer, Bahen/Tanenbaum Professor of Civil Engineering, University of Toronto, Toronto, ON, Canada (corresponding). E-mail: jeffrey.packer@utoronto.ca

The latest (third edition) of the International Institute of Welding (IIW) recommendations (IIW, 2012) requires that the design resistance of hollow section connections be based on failure modes that do not include weld failure, with the latter being avoided by satisfying either of the following criteria:

1. Welds are to be proportioned to achieve the capacity of the connected member walls.
2. Welds are to be proportioned as "fit-for-purpose" and to resist forces in the connected members, taking account of connection deformation/rotation capacity and considering weld effective lengths.

This document (IIW, 2012) thus specifically acknowledges the effective length concept for designing welds between HSS. The preceding two options for weld design are also adopted in an informative Annex to ISO 14346 (2013).

**American Codes and Specifications**

Specific design criteria for HSS connections (statically and cyclically loaded) are given in Clause 2, Design of Welded Connections, Part D, of AWS D1.1 (2010) and used with the applicable requirements of Part A. Those provisions may be used in conjunction with governing steel design specifications, such as AISC 360 (2010), to determine the strength of structural steel members or connections.

In Section K4 of AISC 360 (2010), a detailed design method considering effective weld properties for predominantly statically loaded HSS-to-HSS connections is given. The available strength of such connections incorporates the nonuniform load transfer around the perimeter of the weld due to differences in the relative flexibilities of the chord loaded normal to its surface and membrane stresses carried by the branch parallel to its surface. The nominal strengths of connections subject to branch axial load or bending are based on the limit state of shear rupture along the plane of the effective weld throat and are calculated as follows:

$$R_n \text{ or } P_n = F_{nw} t_w l_e \qquad \text{Spec. Eq. (K4-1)} \quad (1)$$

$$M_{n-ip} = F_{nw} S_{ip} \qquad \text{Spec. Eq. (K4-2)} \quad (2)$$

$$M_{n-op} = F_{nw} S_{op} \qquad \text{Spec. Eq. (K4-3)} \quad (3)$$

where the LRFD resistance factor, $\phi$, applied to the nominal strength values is equal to 0.75 and 0.80 for fillet welds and partial-joint-penetration (PJP) flare-bevel-groove welds, respectively.

The nominal stress of the weld metal, $F_{nw}$, for fillet welds and PJP groove welds, specified in Table J2.5 of AISC 360 (2010), is taken as 0.60 multiplied by the minimum tensile strength of the weld metal, $F_{EXX}$, for fillet welds subject to shear and PJP groove welds subject to tension normal to the weld axis. The use of a directional strength enhancement factor for fillet welds in HSS-to-HSS connections is currently not allowed when the effective length method is used (AISC, 2010; Packer et al., 2010).

The effective weld properties associated with Equations 1, 2 and 3 for T-, Y- and X- (cross-) connections (e.g., Figure 1a) under branch axial load or bending are specified in Table K4.1 of AISC 360 (2010) and summarized as follows:

Branch axial load:

$$l_e = \frac{2H_b}{\sin\theta} + 2b_{eoi} \qquad \text{Spec. Eq. (K4-5)} \quad (4)$$

Branch in-plane bending:

$$S_{ip} = \frac{t_w}{3}\left(\frac{H_b}{\sin\theta}\right)^2 + t_w b_{eoi}\left(\frac{H_b}{\sin\theta}\right) \qquad \text{Spec. Eq. (K4-6)} \quad (5)$$

Branch out-of-plane bending:

$$S_{op} = t_w\left(\frac{H_b}{\sin\theta}\right)B_b + \frac{t_w}{3}\left(B_b^2\right) - \frac{\left(t_w/3\right)\left(B_b - b_{eoi}\right)^3}{B_b} \qquad \text{Spec. Eq. (K4-7)} \quad (6)$$

where $b_{eoi}$ is equal to:

$$b_{eoi} = \frac{10}{B/t}\left(\frac{F_y t}{F_{yb} t_b}\right)B_b \le B_b \qquad \text{Spec. Eq. (K2-13)} \quad (7)$$

Also, for connections with $\beta > 0.85$ or $\theta > 50^\circ$, $b_{eoi}/2$ shall not exceed $2t$.

The weld effective length in Equation 4 was—for consistency—made equivalent to the branch wall effective lengths used in Section K2.3 of AISC 360 (2010) for the limit state of local yielding of the branch(es) due to uneven load distribution, which in turn is based on IIW (1989). The effective width of the individual weld element transverse to the chord, $b_{eoi}$, is illustrated in Figure 1b. This term was empirically derived on the basis of laboratory tests in the 1970s and 1980s (Davies and Packer, 1982). The effective elastic section modulus of welds for in-plane bending and out-of-plane bending, $S_{ip}$ (Equation 5) and $S_{op}$ (Equation 6), respectively, apply in the presence of the bending moments, $M_{ip}$ and $M_{op}$ (as shown in Figure 1). Equation 5 is derived from:

$$I_{ip} = 2 \times \frac{t_w}{12}\left(\frac{H_b}{\sin\theta}\right)^3 + 4t_w\left(\frac{b_{eoi}}{2}\right)\left(\frac{H_b}{2\sin\theta}\right)^2 \quad (8)$$

$$= \frac{t_w}{6}\left(\frac{H_b}{\sin\theta}\right)^3 + 4t_w\left(\frac{t_w b_{eoi}}{2}\right)\left(\frac{H_b}{\sin\theta}\right)^2$$

and substituted into:

$$S_{ip} = \frac{I_{ip}}{\left(H_b/2\sin\theta\right)} \quad (9)$$

In a similar manner, Equation 6 is derived from:

$$I_{op} = 2\times\left[t_w\left(\frac{H_b}{\sin\theta}\right)\left(\frac{B_b}{2}\right) + \frac{t_w}{12}\left(B_b^3\right) - \frac{t_w}{12}\left(B_b - b_{eoi}\right)^3\right]$$

$$= \frac{t_w}{2}\left(\frac{H_b}{\sin\theta}\right)\left(B_b^2\right) + \frac{t_w}{6}\left(B_b^3\right) - \frac{t_w}{6}\left(B_b - b_{eoi}\right)^3 \quad (10)$$

and substituted into:

$$S_{op} = \frac{I_{op}}{\left(B_b/2\right)} \quad (11)$$

While being based on informed knowledge of general HSS connection behavior, Equations 5 and 6 have not been substantiated by tests, and therefore are purely speculative.

## EXPERIMENTAL PROGRAM

An experimental program was performed at the University of Toronto to test various unreinforced HSS-to-HSS 90° T-connections subject to branch in-plane bending. The objective of the study was to investigate the effectiveness of the weld in resisting the forces at the ultimate limit state of weld rupture and verify or adjust the current effective weld properties postulated in Section K4 of AISC 360 (2010) for such connections. Details of the design procedure, fabrication process, test setup assembly and instrumentation are discussed herein.

### Design Procedure for Weld-Critical Connections

Twelve test specimens were designed to be weld-critical under the application of branch in-plane bending moments. Cold-formed HSS made to ASTM A500 Grade C (ASTM, 2010) were used for all branch and chord members in the experimental program. Their geometric configurations were selected based on available materials and key parameters that influence connection strength and behavior: branch-to-chord width ratio (β-ratio) and chord wall slenderness value. The outside dimensions of the chord remained constant (8 × 8 in.) for all test specimens to facilitate ease of setup and takedown in the testing rig. Nominal wall thicknesses of ¼, ⅜ and ½ inch were selected and correspond to chord wall slenderness values of 34, 23 and 17, respectively, when considering the design wall thickness (AISC, 2010). Outside dimensions of the branch members were 2 × 2, 4 × 4, 6 × 6 and 8 × 8 inches with β-ratios equal to 0.25, 0.50, 0.75 and 1.00, respectively. The combination of β-ratios and chord wall slenderness values gave a range of potential failure modes, including chord wall plastification, branch flexural failure and local yielding of the branches due to uneven load distribution. Experimental designation, chord and branch dimensions, key parameters, connection predicted failure modes and nominal LRFD connection flexural strengths for the individual test specimens are presented in Table 1.

Test specimens with $0.25 \le \beta \le 0.85$ are classified as

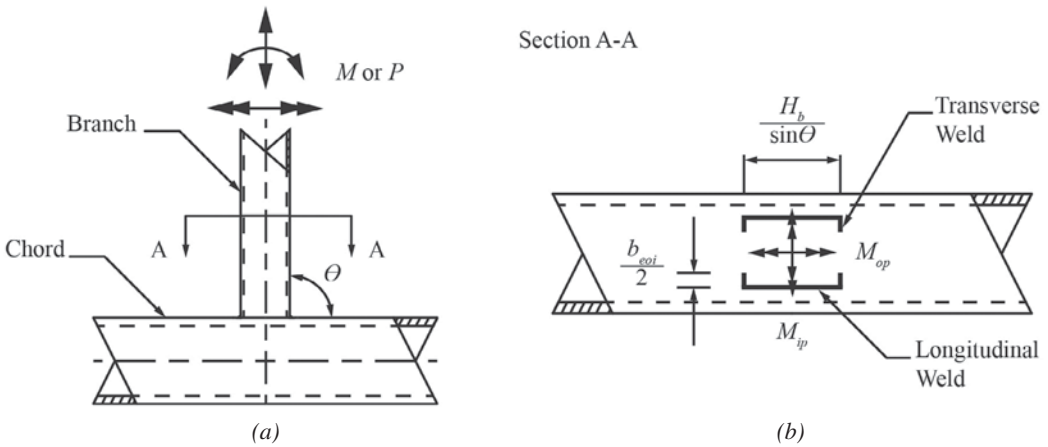


*Fig. 1. Weld effective length terminology for T-, Y-, and X- (cross-) connections under branch axial load or bending: (a) various load cases; (b) weld effective length dimensions.*

| Table 1. Test Specimen Member Sizes, Key Parameters, Predicted Failure Modes and Connection Nominal Design Strengths | | | | | | |
|---|---|---|---|---|---|---|
| Experimental Designation | Chord Designation (in.) | Branch Designation (in.) | Chord Wall Slenderness Value | β-Ratio | Connection Failure Mode† | LRFD Flexural Strength $\phi M_n$ (kip-ft) |
| T-0.25-34 | HSS 8×8×¼ | HSS 2×2×¼ | 34 | 0.25 | CW | 2.09 |
| T-0.25-23 | HSS 8×8×⅜ | HSS 2×2×¼ | 23 | 0.25 | BF | 3.62 |
| T-0.25-17 | HSS 8×8×½ | HSS 2×2×¼ | 17 | 0.25 | BF | 3.62 |
| T-0.50-34 | HSS 8×8×¼ | HSS 4×4×¼ | 34 | 0.50 | CW | 4.35 |
| T-0.50-23 | HSS 8×8×⅜ | HSS 4×4×¼ | 23 | 0.50 | CW | 9.79 |
| T-0.50-17 | HSS 8×8×½ | HSS 4×4×½ | 17 | 0.50 | CW | 17.4 |
| T-0.75-34 | HSS 8×8×¼ | HSS 6×6×¼ | 34 | 0.75 | CW | 10.4 |
| T-0.75-23 | HSS 8×8×⅜ | HSS 6×6×⅜ | 23 | 0.75 | CW | 23.3 |
| T-0.75-17 | HSS 8×8×½ | HSS 6×6×½ | 17 | 0.75 | CW | 41.4 |
| T-1.00-34 | HSS 8×8×¼ | HSS 8×8×¼ | 34 | 1.00 | BY | 39.4 |
| T-1.00-23 | HSS 8×8×⅜ | HSS 8×8×⅜ | 23 | 1.00 | BY | 66.5 |
| T-1.00-17 | HSS 8×8×½ | HSS 8×8×½ | 17 | 1.00 | BY | 99.1 |

† CW—chord wall plastification; BF—branch flexural failure; BY—local yielding of branch due to uneven load distribution

stepped connections, while those with $0.85 < \beta \leq 1.00$ are classified as matched connections. Their general configurations are depicted in Figures 2a and 2b. Stepped connections have a continuous fillet weld around the branch footprint, whereas matched connections have a fillet weld along the branch transverse walls and a PJP groove weld along the branch longitudinal walls. A transitional zone between the two types of welds exists at the branch corners.

Welds were designed to ensure that weld rupture preceded connection failure, whereby the predicted nominal flexural strength of the weld ($M_{n\text{-}ip}$) was less than the predicted LRFD flexural strength of the test specimen ($\phi M_n$). Weld sizes were initially selected based on standard sizes specified in AWS D1.1 (2010) satisfying the minimum requirements in Tables J2.3 and J2.4 of AISC 360 (2010) for PJP groove welds and fillet welds, respectively. Matching electrodes with a nominal tensile strength of 70 ksi were used for the calculations.

**Test Specimen Fabrication Process**

The welded joints were executed by an industrial robot modified to perform gas-metal arc welding (GMAW) at the Automation Division of Lincoln Electric's headquarters in Cleveland, Ohio. The welding equipment used throughout fabrication included a Fanuc ARC Mate 120iC 10L robotic arm, Fanuc system R-30iA power supply, Lincoln Electric PowerWave 455M/STT and 655 robotic welders, and an automatic wire feeder.

A 0.035-in.-diameter AWS ER70S-6 (SuperGlide S6) solid wire electrode with a nominal specified tensile strength of 70 ksi and a shielding gas mixture of 90% argon and 10% carbon dioxide supplied at a rate of 40 cubic feet per hour (CFH) was used to weld the test specimens. Welding process parameters recommended by the Lincoln Electric 2010 Welding Consumables Product Catalogue were used as a starting point, and adjusted throughout the fabrication

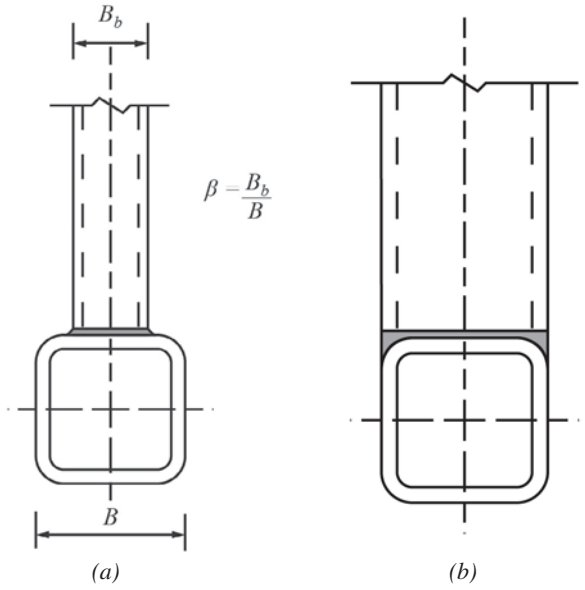


*Fig. 2. HSS-to-HSS T-connection classification: (a) side elevation of a stepped connection ($0.25 \leq \beta \leq 0.85$); (b) side elevation of a matched connection ($0.85 < \beta \leq 1.00$).*

process as necessary. To satisfy the qualification requirements of AWS D1.1 (2010) for prequalified welded joints, numerous trial specimens were created and macroetched before welding the actual test specimens. The macroetch specimens were used to calibrate the welding process parameters to achieve the desired weld size, profile, fusion with the base metal and root penetration for each joint.

Stepped connections were clamped to a level table and welded in the horizontal position. Matched connections were mounted to rotating chucks and welded in the flat position using coordinated motion. Root pass welds along the corner radii of the chord adjacent to the longitudinal PJP groove weld elements were required for the matched connections.

Once completed, the welded joints were inspected in accordance with the visual inspection acceptance criteria in Clause 6 of AWS D1.1 (2010). Discontinuities such as crack prohibition, undercut, porosity, weld profile and weld size were investigated. No discontinuities exceeding the allowable limits of the visual inspection acceptance criteria were observed.

**Test Setup and Instrumentation**

The test setup assembly is shown in Figure 3, wherein the vertical HSS branch is pulled laterally by the actuator (1) to create a bending moment in the branch and thus the connection and HSS chord. The testing arrangement was designed to minimize out-of-plane effects applied to the test specimen, to allow the branch member to deflect both horizontally and vertically without inducing restraint forces and to simply support the chord ends.

Unidirectional strain gages oriented along the longitudinal axis of the branch were installed at numerous locations around the branch perimeter to measure the nonuniform distribution of normal strain around its footprint, as well as to monitor out-of-plane effects during testing. The strain gages were placed approximately 9/16 in. above the vertical fillet weld toe to avoid the high strain region immediately adjacent to the toe caused by notch effects. Additional strain gages were placed at all four branch mid-wall locations in the constant stress region, which is located at least three times the branch width ($3B_b$) away from the connection

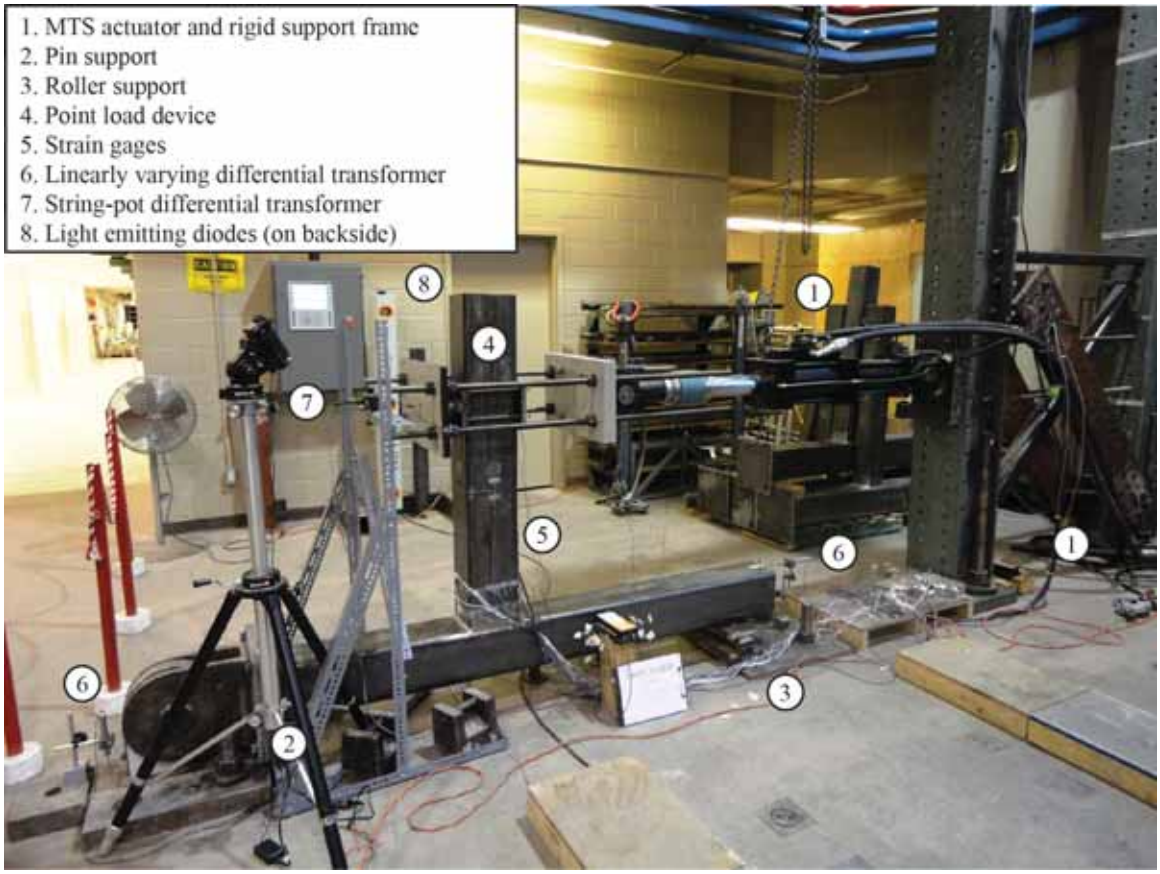


*Fig. 3. Elevation of the general test setup assembly for full-scale experiments.*

| Table 2. Average Measured Cross-Sectional Dimensions of HSS | | | | | |
|---|---|---|---|---|---|
| HSS Designation (in.) | Height and Width, *H* and *B* (in.) | Wall Thickness, *t* (in.) | Cross-Sectional Area, *A* (in.$^2$) | Outer Corner Radius (in.) | Inner Corner Radius (in.) |
| HSS 2×2×¼ | 2.01 | 0.227 | 1.52 | 0.482 | 0.248 |
| HSS 4×4×¼ | 4.02 | 0.225 | 3.34 | 0.492 | 0.282 |
| HSS 4×4×½ | 4.02 | 0.458 | 6.11 | 0.945 | 0.476 |
| HSS 6×6×¼ | 6.01 | 0.226 | 5.13 | 0.509 | 0.298 |
| HSS 6×6×⅜ | 6.00 | 0.342 | 7.48 | 0.772 | 0.416 |
| HSS 6×6×½ | 6.01 | 0.459 | 9.67 | 1.16 | 0.671 |
| HSS 8×8×¼ | 8.02 | 0.232 | 7.06 | 0.639 | 0.398 |
| HSS 8×8×⅜ | 7.99 | 0.344 | 10.1 | 0.939 | 0.588 |
| HSS 8×8×½ | 8.05 | 0.456 | 13.1 | 1.36 | 0.875 |

| Table 3. HSS Tensile Coupon Test Results | | | | | | |
|---|---|---|---|---|---|---|
| HSS Designation (in.) | $F_y$* (ksi) | $\varepsilon_y$ (× 10$^3$ με) | $F_u$ (ksi) | $\varepsilon_u$ (%) | $E$ (× 10$^3$ ksi) | $F_y/F_u$ |
| HSS 2×2×¼ | 59.3 | 2.27 | 67.5 | 21.3 | 26.2 | 0.879 |
| HSS 4×4×¼ | 62.1 | 1.99 | 76.2 | 27.3 | 31.1 | 0.815 |
| HSS 4×4×½ | 63.9 | 2.58 | 79.1 | 26.4 | 24.8 | 0.808 |
| HSS 6×6×¼ | 48.0 | 1.86 | 63.6 | 33.2 | 25.8 | 0.755 |
| HSS 6×6×⅜ | 50.7 | 1.94 | 61.5 | 33.9 | 26.2 | 0.824 |
| HSS 6×6×½ | 53.8 | 2.03 | 64.3 | 34.0 | 26.5 | 0.837 |
| HSS 8×8×¼ | 55.4 | 2.07 | 71.5 | 27.5 | 26.9 | 0.775 |
| HSS 8×8×⅜ | 57.1 | 2.24 | 73.9 | 32.3 | 25.5 | 0.773 |
| HSS 8×8×½ | 59.8 | 2.24 | 73.8 | 34.2 | 26.8 | 0.810 |
| * Determined by the 0.2% strain offset method. | | | | | | |

(Mehrotra and Govil, 1972). These were used to monitor out-of-plane effects during testing, which were observed to be insignificant.

To determine the branch deflection profile and chord wall deformation profiles throughout testing, a K610 optical camera was used to record the coordinates of strobing light-emitting diodes (LEDs). The LEDs were mounted to the test specimens and test setup assembly in various locations to record their *x*, *y* and *z* coordinates. The force components applied to the branch were used to calculate the in-plane moment, out-of-plane moment and torsion acting on the connection.

## EXPERIMENTAL RESULTS

### Geometric and Material Properties of HSS

All HSS cross-sectional dimensions were measured at multiple points. Cross-sections of each HSS used in the experimental program were saw-cut at least 12 in. away from the flame-cut ends of the parent tube and then machined normal to the longitudinal axis. They were scanned and traced using software with built-in measuring tools to determine the cross-sectional area, outside dimensions and outer/inner corner radii. Wall thicknesses were measured using a 1.0-in. Mitutoyo Digimatic Micrometer (accurate to ±0.00005 in.). The average geometric properties are given in Table 2.

The results from 27 individual tensile coupon (TC) tests are summarized in Table 3. Three TCs for each HSS used in the experimental program were tested in accordance with the standard methods for tension testing of metallic materials (ASTM, 2008). As required by ASTM A500 (ASTM, 2010), these TCs were saw-cut from the flat faces of the HSS not containing the seam weld and in the longitudinal direction. For each of the nine HSS sizes (Table 2), one TC was taken at the mid-width of the three HSS walls not containing the seam weld. The ductility of the material was

generally well beyond the minimum specified requirement (21% elongation).

**Geometric and Material Properties of As-Laid Welds**

The actual effective throat thickness of fillet-welded joints tested in the experimental program was measured after testing. Several macroetch specimens were prepared by cutting the connections normal to the longitudinal axis of the weld at numerous locations around the branch perimeter. The macroetch specimens were scanned and the horizontal/vertical leg sizes and effective weld throats were measured using software with built-in measuring tools. Average values of the effective weld throats for individual weld elements around the branch perimeter for each test specimen were used to calculate the LRFD and nominal flexural strengths of the welded joints using the equation for the effective elastic section modulus for in-plane bending (Equation 5). Because the design requirements of AISC 360 (2010) are based solely on the limit state of shear rupture along the plane of the effective weld throat, the measured values for the vertical and horizontal weld leg sizes are not presented in this paper.

Fillet weld effective throat measurements from the macroetch specimens were taken as the distance from the weld root to the outer surface at a 45° incline to the horizontal chord surface for uncracked and cracked sections, represented by red lines shown in Figure 4. The lengths of the red lines were averaged for the individual weld elements (identified as north, south, east and west) for each test specimen. An observation from the macroetch examinations of stepped connections was that the failure plane through the fillet welds of the stepped connections was consistently at an angle between 0° and 45° to the branch fusion face.

PJP flare-bevel-groove weld effective throats were measured from the macroetch specimens as the thickness of the thinner part joined ($t$, $t_b$) less the greatest perpendicular dimension from the base metal surface to the weld surface, $d$, as shown in Figure 5. This method is consistent with Section J2.1 of AISC 360 (2010) and AWS D1.1 (2010) for measuring complete joint penetration groove welds in T-connections without backing and welded from one side only. Because these PJP groove welds meet the qualification requirements of Clause 4.13 of AWS D1.1 (2010) for complete joint penetration butt joints in tubular connections, they may be measured as such.

The average effective weld throat thicknesses measured from the macroetch specimens for the individual weld elements of each test specimen are summarized in Table 4. A few of these are less than the minimum values in Tables J2.3 and J2.4 of AISC 360 (2010), after grinding, to ensure that weld fracture was the critical failure mode. Because all welds were sound and carefully controlled, the minimum weld size requirement would not affect the results. Those values were used—in combination with the geometric and material properties of the HSS, as well as the material properties of the as-laid weld metal—to calculate the predicted flexural capacities of the welded joints, which are used in the analyses performed in the following sections.

Three all-weld-metal TCs were created in accordance with Clause 4 of AWS D1.1 (2010). The TCs were extracted from welded test plates that were fabricated using the same electrode spool, equipment and fabrication processes (using the average welding process parameters) as those used to fabricate the welded joints tested in the experimental program. The welding process parameters for the TCs were 24-V arc voltage, 400-ipm (inches per minute) wire feed

*(a)* *(b)*

*Fig. 4. Example of fillet weld effective throat measurements from macroetch specimens: (a) fillet weld cross-section not cracked; (b) fully cracked fillet weld cross-section.*

speed, 15-ipm travel speed and a 90% argon/10% carbon dioxide shielding gas mixture supplied at a flow rate of 40 CFH. Every TC was tested in accordance with the standard methods for tension testing of metallic materials (ASTM, 2008), and the specified yield strength of the material was determined using the 0.2% offset method. The results from three all-weld-metal TC specimens are summarized in Table 5.

All of the measured material properties exceeded the minimum requirements for AWS ER70S-6 solid-wire electrodes. The average tensile strength of the as-laid weld metal was 26% larger than the nominal specified tensile strength of 70 ksi. This contributed to undesirable failure modes observed in two of the test specimens, whereby connection failure preceded weld failure.

**Results from Full-Scale Tests on Square HSS-to-HSS Moment T-Connections**

Twelve full-scale square HSS-to-HSS moment T-connections subject to branch in-plane bending were tested to failure in a quasi-static manner. Figure 6 summarizes the failure modes observed during the experimental program. Ten out of 12 test specimens failed by weld rupture. Two specimens (T-0.50-34 and T-0.50-17) failed by rupture of the chord face (or punching shear) on the tension side of the connection after extensive chord face plastification. These were tested early in the experimental program and indicated that the actual tensile strength of the weld metal was likely higher than the specified nominal strength (which was later confirmed).

A summary of the actual flexural strength (or ultimate moment) of the welded joints with the predicted nominal flexural strengths of the connections, calculated using the actual geometric and material properties of the HSS material and as-laid weld metal, is provided in Table 6. Every weld-critical test specimen failed at a moment considerably higher than the predicted nominal flexural strength of the connection. Table 6 also includes the measured initial elastic rotational stiffness of each connection and the corresponding connection rotation at failure. The moment versus connection rotation relationship was determined using the magnitude of force applied by the MTS actuator and coordinates from the LED targets measured throughout testing. Initial elastic rotational stiffness was determined from the slope of the linear-elastic region of the moment versus connection rotation relationships for each test specimen.

Figures 7 through 10 show the typical distribution of normal strain observed around the branch perimeter at three load levels: the actual, nominal and LRFD flexural strengths of the welded joint. The plots demonstrate that for a wide variety of connection geometric configurations, the distribution of normal strain around the branch perimeter adjacent to the welded joint in HSS-to-HSS moment T-connections is highly nonuniform.

At the nominal and LRFD strengths, strain distribution is nearly symmetric about the theoretical neutral axis, located at strain gage (SG)-5E for specimens with $\beta = 0.25$ and SG-7E for specimens with $0.25 > \beta \leq 1.00$, which is expected for connections subject to pure in-plane bending. The strains are largest at the branch corner which is typical of semi-rigid connections because of the flexible chord face and stiff branch corners, which attract more load. As expected, the magnitude of strain along the transverse faces (relative to the magnitude of strain at the corners) decreases as $\beta$ increases; hence, the effectiveness of the transverse

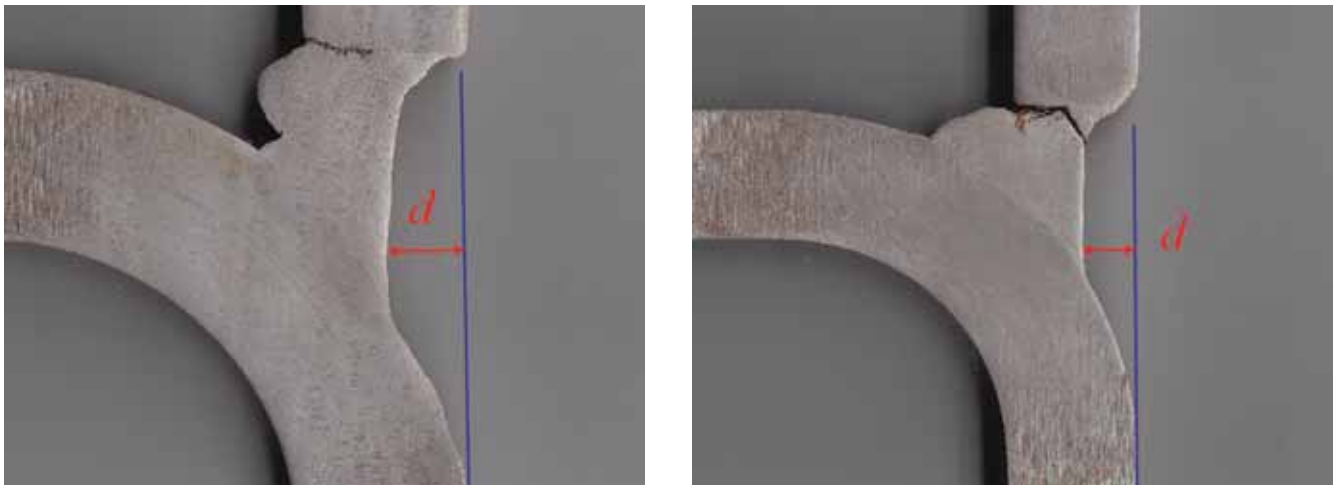


(a) (b)

*Fig. 5. Example of PJP groove weld effective throat measurements from macroetch specimens: (a) PJP groove weld cross-section not fully cracked; (b) fully cracked PJP groove weld cross-section.*

| Table 4. Average Effective Weld Throat Thickness Measured from Macroetch Specimens | | | | |
|---|---|---|---|---|
| **Specimen Designation** | **North Weld, Transverse (in.)** | **South Weld, Transverse (in.)** | **East Weld, Longitudinal (in.)** | **West Weld, Longitudinal (in.)** |
| T-0.25-34 | 0.102 | 0.097 | 0.089 | 0.088 |
| T-0.25-23 | 0.094 | 0.128 | 0.095 | 0.051 |
| T-0.25-17 | 0.090 | 0.101 | 0.092 | 0.094 |
| T-0.50-34 | 0.150 | 0.158 | 0.170 | 0.170 |
| T-0.50-23 | 0.154 | 0.133 | 0.168 | 0.180 |
| T-0.50-17 | 0.259 | 0.280 | 0.290 | 0.272 |
| T-0.75-34 | 0.112 | 0.087 | 0.068 | 0.134 |
| T-0.75-23 | 0.139 | 0.124 | 0.137 | 0.120 |
| T-0.75-17 | 0.237 | 0.200 | 0.158 | 0.277 |
| T-1.00-34 | 0.128 | 0.078 | **0.126** | **0.117** |
| T-1.00-23 | 0.180 | 0.232 | **0.204** | **0.208** |
| T-1.00-17 | 0.240 | 0.311 | **0.225** | **0.252** |

Note: Values in bold are PJP flare-bevel-groove welds.

| Table 5. All-Weld-Metal Tensile Coupon Material Test Results | | | | |
|---|---|---|---|---|
| **Coupon Designation** | **$F_{yw}$ (ksi)** | **$E$ ($\times 10^3$ ksi)** | **$F_{uw}$ (ksi)** | **$\varepsilon_u$ (%)** |
| [i] | 76.2 | 29.6 | 90.0 | 29.2 |
| [ii] | 75.7 | 31.6 | 86.9 | 28.3 |
| [iii] | 75.8 | 29.6 | 87.5 | 28.0 |
| Average | 75.9 | 30.3 | 88.1 | 28.5 |

| Table 6. Moment and Rotation Characteristics of the Tested Connections | | | | | | |
|---|---|---|---|---|---|---|
| **Specimen Designation** | **β-Ratio** | **Chord Wall Slenderness** | **Predicted Nominal Flexural Strength $M_{n-ip}$ (kip-ft)** | **Initial Elastic Rotational Stiffness of Connection (kip-ft/radian)** | **Connection Rotation at Failure ($\times 10^{-3}$ radians)** | **Actual Flexural Strength $M_u$ (kip-ft)** |
| T-0.25-34 | 0.25 | 34 | 1.02 | 33.1 | 368 | 4.11 |
| T-0.25-23 | 0.25 | 23 | 1.68 | 81.1 | 167 | 4.37 |
| T-0.25-17 | 0.25 | 17 | 2.10 | 194 | 46.3 | 4.82 |
| T-0.50-34* | 0.50 | 34 | 4.81 | N/A** | N/A** | 5.61 |
| T-0.50-23 | 0.50 | 23 | 7.62 | 343 | 195 | 15.2 |
| T-0.50-17* | 0.50 | 17 | 20.1 | 918 | 189 | 29.6 |
| T-0.75-34 | 0.75 | 34 | 7.79 | 534 | 77.8 | 14.4 |
| T-0.75-23 | 0.75 | 23 | 11.6 | 1,544 | 36.4 | 27.1 |
| T-0.75-17 | 0.75 | 17 | 22.1 | 3,148 | 40.2 | 52.2 |
| T-1.00-34 | 1.00 | 34 | 14.8 | 3,145 | 19.6 | 39.7 |
| T-1.00-23 | 1.00 | 23 | 29.3 | 5,296 | 21.8 | 64.7 |
| T-1.00-17 | 1.00 | 17 | 40.5 | 7,477 | 20.5 | 93.6 |

* Connection failure preceded weld rupture. Predicted nominal flexural strengths are those for the connection instead of the welded joint.
** Not available

weld element decreases. While it is evident that the transverse weld elements are less effective in resisting the applied loads, they still contribute to the flexural strength of the welded joint beyond the distance 2*t* from the longitudinal face of the branch and, hence, should not be neglected in weld resistance calculations.

At the ultimate moment, the distribution of strain is no longer symmetric about the theoretical neutral axis, indicating that plastic stress redistribution has taken place prior to failure. The magnitude of normal strain along the transverse weld elements indicates that a large portion of the weld perimeter is effective in resisting the applied loads.

*(a) T-0.25-34: weld rupture*

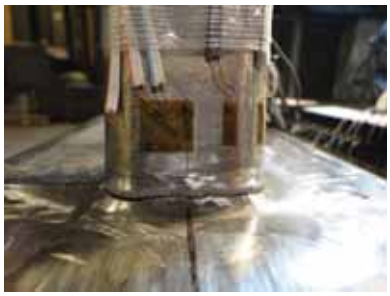

*(b) T-0.25-23: weld rupture*

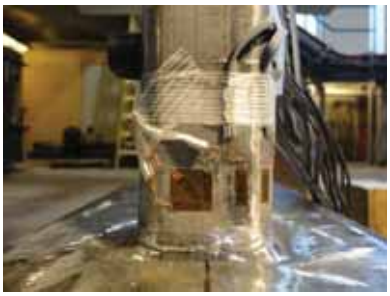

*(c) T-0.25-17: weld rupture*

*(d) T-0.50-34: chord face rupture*

*(e) T-0.50-23: weld rupture*

*(f) T-0.50-17: chord face rupture*

*(g) T-0.75-34: weld rupture*

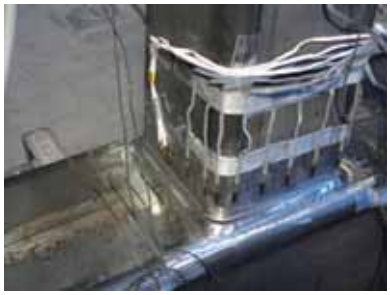

*(h) T-0.75-23: weld rupture*

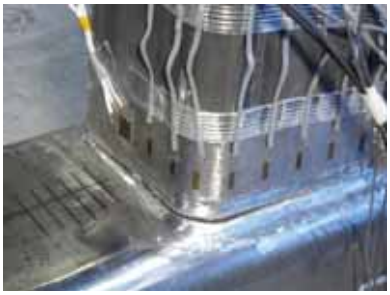

*(i) T-0.75-17: weld rupture*

*(j) T-1.00-34: weld rupture*

*(k) T-1.00-23: weld rupture*

*(l) T-1.00-17: weld rupture*

*Fig. 6. Failure modes of test specimens.*

## EVALUATION OF RESULTS

The objective of the experimental program was to verify or adjust the current effective elastic section modulus for in-plane bending defined by Equation 5 and postulated in Table K4.1 of AISC 360 (2010) for HSS-to-HSS moment T-connections. Because test specimens T-0.50-34 and T-0.50-17 failed by chord face rupture (considered a connection failure), they are not included in the analyses performed herein. The data from the successful tests are used to plot correlations between the actual and predicted flexural strengths of the welded joints using effective weld properties for the cases excluding and including the $(1.00 + 0.5 \sin^{1.5}\theta)$ fillet weld strength enhancement factor. Based on the analysis, a modification to the current effective weld properties is proposed.

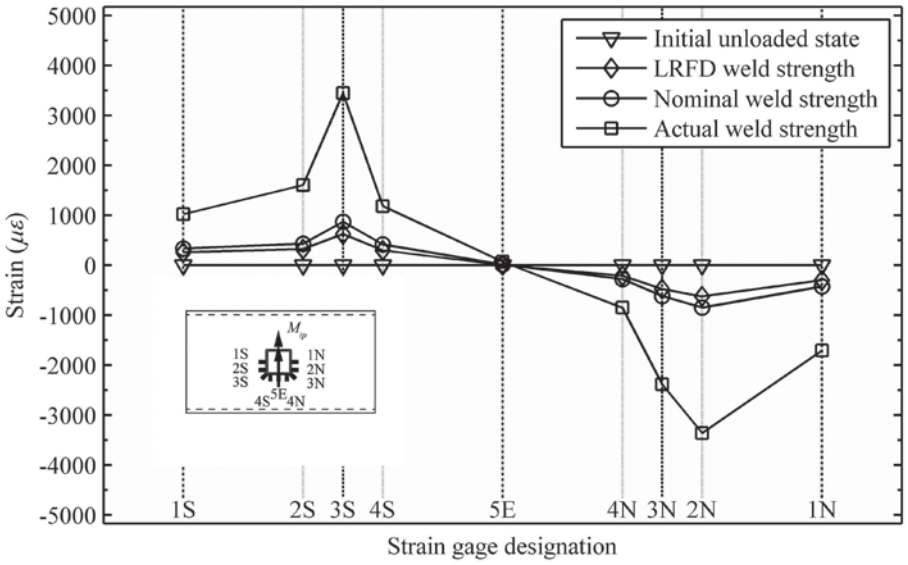


*Fig. 7. Typical distribution of normal strain around the branch perimeter for specimens with* $\beta = 0.25$.

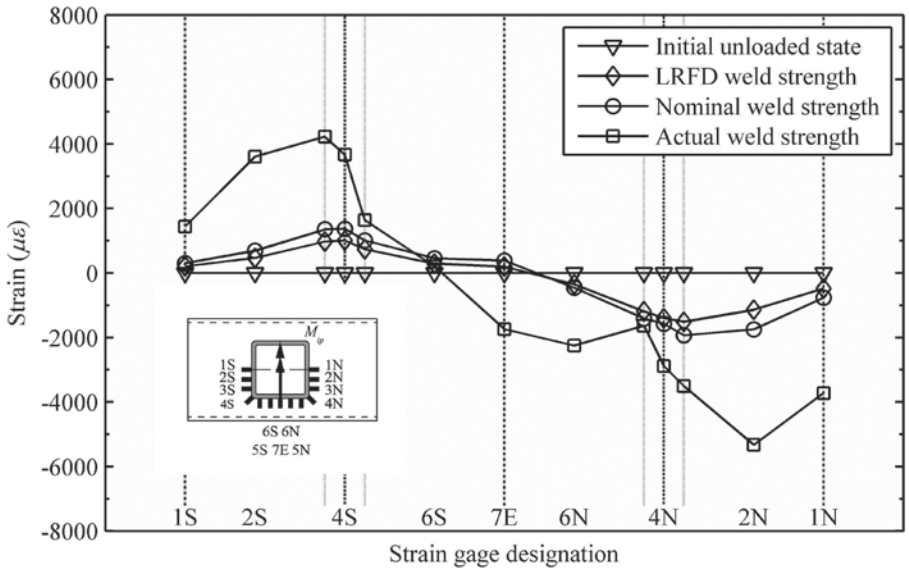


*Fig. 8. Typical distribution of normal strain around the branch perimeter for specimens with* $\beta = 0.50$.

**Evaluation of Current Effective Weld Properties**

In order to assess whether the safety margins are adequate or excessive, one can check to ensure that a minimum safety index of $\beta^+ = 4.0$ [as currently adopted by AISC 360 (2010) per Chapter B of the Specification Commentary] is achieved, using a simplified reliability analysis in which the resistance factor ($\phi$) is given by Equation 12 (Fisher et al., 1978; Ravindra and Galambos, 1978):

$$\phi = m_R \exp\left(-\alpha\beta^+ \text{COV}\right) \tag{12}$$

where $m_R$ is the mean of the ratio of actual element strength to nominal element strength, COV is the associated coefficient of variation and $\alpha$ is the coefficient of separation taken to be 0.55 (Ravindra & Galambos, 1978). Equation 12 neglects variations in material properties, geometric parameters and fabrication defects, relying solely on the so-called professional factor. In the absence of reliable statistical data related to welds, this is believed to be a conservative approach. Resistance factors of 0.75 and 0.80 are stipulated in Section K4 of AISC 360 (2010) to calculate the LRFD

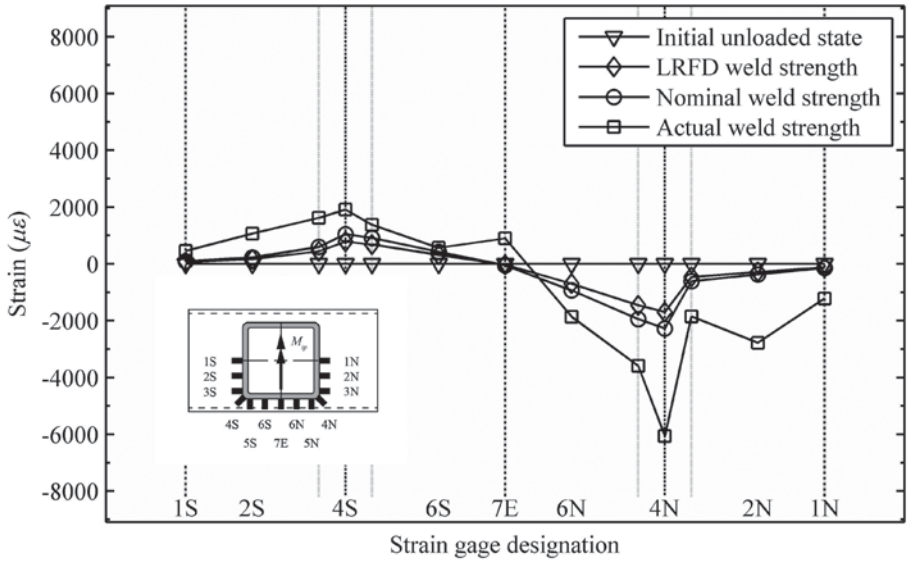


*Fig. 9. Typical distribution of normal strain around the branch perimeter for specimens with $\beta = 0.75$.*

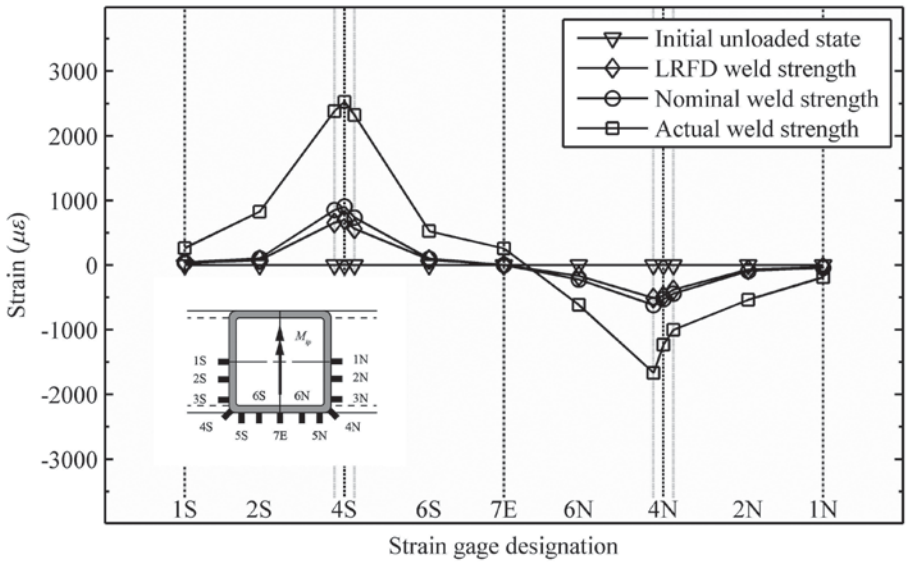


*Fig. 10. Typical distribution of normal strain around the branch perimeter for specimens with $\beta = 1.00$.*

| Table 7. Simplified Reliability Analysis of Square HSS-to-HSS Moment T-Connections | | |
|---|---|---|
| **Experimental Designation** | **Actual/Nominal Excluding $(1.00 + 0.5 \sin^{1.5}\theta)$ Factor** | **Actual/Nominal Including $(1.00 + 0.5 \sin^{1.5}\theta)$ Factor** |
| T-0.25-34 | 4.04 | 2.69 |
| T-0.25-23 | 2.59 | 1.73 |
| T-0.25-17 | 2.30 | 1.53 |
| T-0.50-23 | 2.00 | 1.34 |
| T-0.75-34 | 1.84 | 1.23 |
| T-0.75-23 | 2.34 | 1.56 |
| T-0.75-17 | 2.37 | 1.58 |
| T-1.00-34 | 2.68 | 2.41 |
| T-1.00-23 | 2.21 | 1.89 |
| T-1.00-17 | 2.31 | 1.89 |
| Mean | 2.47 | 1.78 |
| COV | 0.245 | 0.258 |
| $\phi$ | 1.44 | 1.01 |

design strength of fillet-welded joints and PJP groove welds, respectively.

The actual flexural strengths for each weld-critical connection are summarized in Table 6 with the predicted nominal flexural strengths, which were calculated using the measured geometric and material properties of the HSS and as-laid welds. Weld sizes for the individual weld elements were taken from Table 4, which is based on average measurements of the macroetch specimens.

The mean of the actual/predicted weld strengths, as well as the COV, are given in Table 7 and used, in combination with Equation 12, to calculate a resistance factor equal to 1.44. Because this is much larger than the 0.75 and 0.80 required for fillet welds and PJP groove welds, respectively, the current equation for the effective elastic section modulus for in-plane bending can be deemed very conservative.

The predicted nominal flexural strength was recalculated with the inclusion of the $(1.00 + 0.5 \sin^{1.5}\theta)$ factor applied to fillet weld elements. For test specimens with $0.25 > \beta \leq 0.75$, all four sides are fillet-welded and loaded normal ($\theta = 90°$) to the longitudinal axis of the weld; hence, the nominal flexural strength was increased by a factor of 1.5. For the matched connections, the factor was applied only to the transverse weld elements. A resistance factor equal to 1.01 was thus calculated (see Table 7). The correlations excluding and including the $(1.00 + 0.5 \sin^{1.5}\theta)$ factor are plotted in Figures 11 and 12, respectively.

Because $\phi$ is still larger than the resistance factors for fillet welds and PJP groove welds, the $(1.00 + 0.5 \sin^{1.5}\theta)$ factor can be applied safely with the current equation for the effective elastic section modulus for in-plane bending for HSS-to-HSS moment T-connections. Although it may be safe for such connections, it was proven to be unsafe when applied to axially loaded T- and cross- (or X-) connections between HSS (McFadden et al., 2013). Thus, for consistency, it would not be practical to apply the $(1.00 + 0.5 \sin^{1.5}\theta)$ factor to some types of HSS connections under specific loads and not to others.

If the requirements of the Canadian Standards Association (CSA) S16 (2009) are evaluated, an identical result to AISC 360 (2010) is obtained. Although they have different resistance factors for fillet welds [equal to 0.67 and 0.75 for CSA S16 (2009) and AISC 360 (2010), respectively], the equations come out identical as shown.

For CSA S16 (2009):

$$\phi M_{n-ip} = 0.67\phi_w \left(F_{EXX} S_{ip}\right) \tag{13}$$
$$\phi M_{n-ip} = 0.67\left(0.67\right)\left(F_{EXX} S_{ip}\right)$$
$$\phi M_{n-ip} = 0.45\left(F_{EXX} S_{ip}\right)$$

For AISC 360 (2010):

$$\phi M_{n-ip} = \phi\left(F_{nw} S_{ip}\right) \tag{14}$$
$$\phi M_{n-ip} = 0.75\left(0.60 \times F_{EXX} S_{ip}\right)$$
$$\phi M_{n-ip} = 0.45\left(F_{EXX} S_{ip}\right)$$

Because $\phi$ is much larger than 0.67, the equation for the effective elastic section modulus for in-plane bending may be deemed very conservative for CSA S16 (2009) too.

**Evaluation of Modified Effective Weld Properties**

The branch strain distribution plots show that the transverse weld elements are effective in resisting the applied loads beyond the limit of two times the chord wall thickness ($2t$), and a more reasonable limit appears to be $B_b/4$. Thus, the requirement in Section K4 of AISC 360 (2010):

When $\beta > 0.85$ or $\theta > 50^\circ$, $b_{eoi}/2$ shall not exceed $2t$

could be modified to:

When $\beta > 0.85$ or $\theta > 50^\circ$, $b_{eoi}/2$ shall not exceed $B_b/4$

This modification to the requirement limiting the value of $b_{eoi}$ increases the effective length of the transverse weld

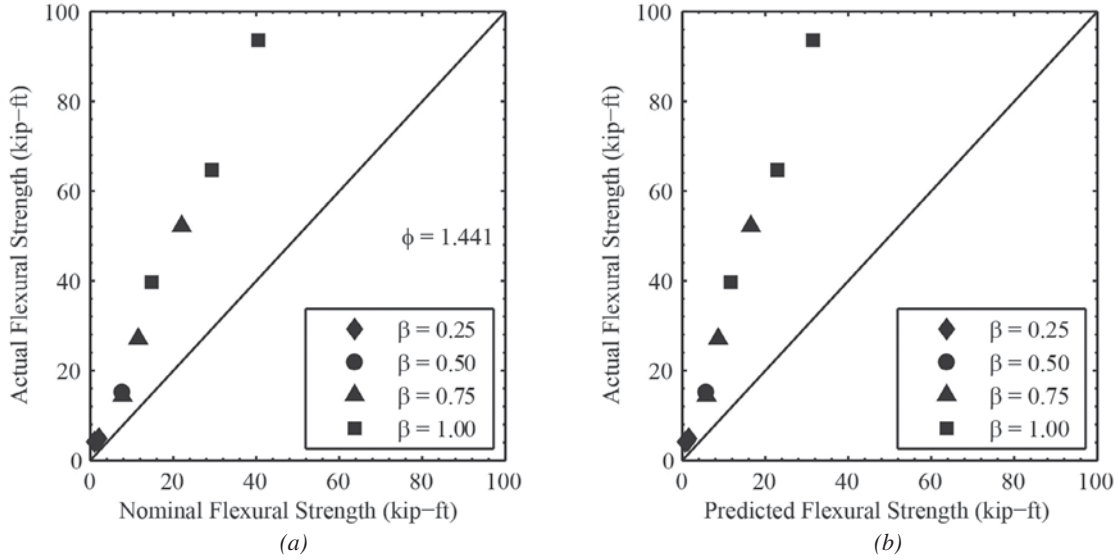


*Fig. 11. Correlation with test results for square HSS-to-HSS moment T-connections and excluding the $(1.00 + 0.50 \sin^{1.5}\theta)$ term: (a) actual strength vs. predicted nominal strength ($M_{n\text{-}ip}$); (b) actual strength vs. predicted LRFD strength ($\phi M_{n\text{-}ip}$).*

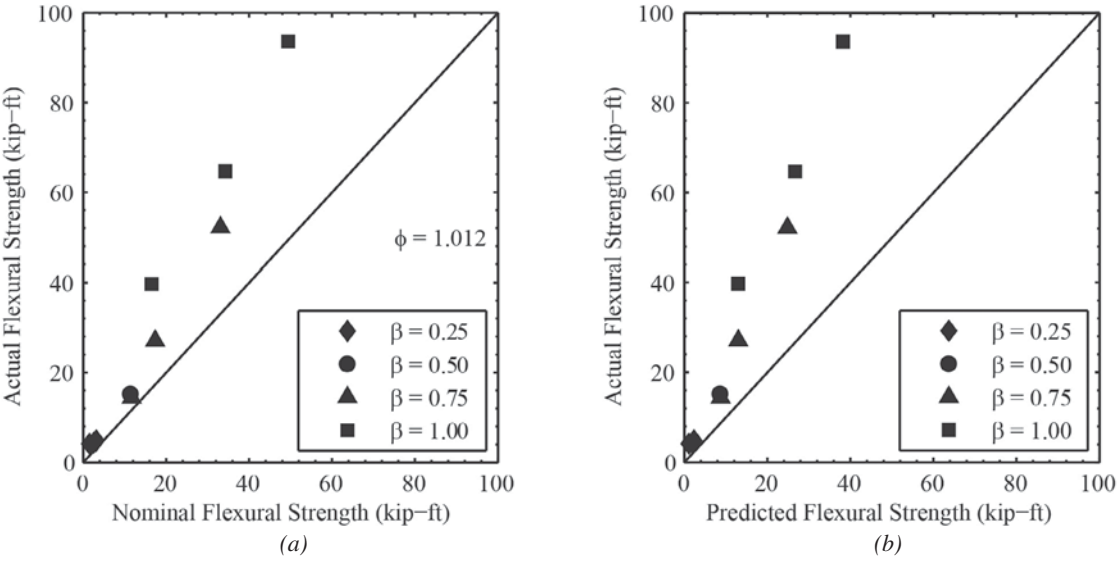


*Fig. 12. Correlation with test results for square HSS-to-HSS moment T-connections and including the $(1.00 + 0.50 \sin^{1.5}\theta)$ term: (a) actual strength vs. predicted nominal strength ($M_{n\text{-}ip}$); (b) actual strength vs. predicted LRFD strength ($\phi M_{n\text{-}ip}$).*

| Table 8. Actual versus Predicted Nominal Flexural Strength Using the $b_{eoi}$ Modification and Excluding the $(1.00 + 0.5 \sin^{1.5}\theta)$ Factor | | | |
|---|---|---|---|
| **Experimental Designation** | **Actual Flexural Strength $M_u$ (kip-ft)** | **Predicted Nominal Flexural Strength $M_{n-ip}$ (kip-ft)** | **Actual/Nominal** |
| T-0.25-34 | 4.11 | 1.02 | 4.04 |
| T-0.25-23 | 4.37 | 1.43 | 3.06 |
| T-0.25-17 | 4.82 | 1.41 | 3.43 |
| T-0.50-23 | 15.2 | 9.22 | 1.65 |
| T-0.75-34 | 14.4 | 10.8 | 1.34 |
| T-0.75-23 | 27.1 | 17.0 | 1.60 |
| T-0.75-17 | 52.2 | 28.9 | 1.81 |
| T-1.00-34 | 39.7 | 19.9 | 2.00 |
| T-1.00-23 | 64.7 | 44.2 | 1.46 |
| T-1.00-17 | 93.6 | 62.0 | 1.51 |
| | | Mean | 2.19 |
| | | COV | 0.437 |
| | | $\phi$ | 0.836 |

elements, which ultimately leads to an increased predicted flexural strength. An exception is for small HSS branch member sizes, such as for HSS 2×2×¼, where this modified requirement actually decreases the effective length of the transverse welds. This results in an even more conservative approach (which was shown in the previous section to already be very conservative).

The correlations in Table 7 and Figure 11 have been recalculated with the $b_{eoi}$ modification, excluding the $(1.00 + 0.5 \sin^{1.5}\theta)$ factor, and the results are summarized in Table 8 and plotted in Figure 13. As shown, the modification provides a resistance factor equal to 0.836, which is larger than those for fillet welds and PJP groove welds; hence, the modified requirement can be deemed adequately conservative for such connections for AISC 360 (2010) and CSA S16 (2009).

The proposed $b_{eoi}$ modification is also potentially applicable to the equations for the effective length under branch axial load (Equation 4) and the effective elastic section modulus for out-of-plane bending (Equation 6). While there are no available test data on weld-critical connections between square/rectangular HSS loaded by branch out-of-plane bending, the data from weld-critical axially loaded T- and X- (or cross-) connection tests performed at the University of Toronto (Packer and Cassidy, 1995) can be reanalyzed using the modified requirement to investigate whether it remains a conservative assumption. Performing a simplified reliability analysis on the data gives a mean value of the actual/predicted strengths equal to 1.11 and a COV equal to 0.141 for a calculated resistance factor, $\phi$, equal to 0.820. Because this is larger than 0.75, which is required for fillet welds, the modified requirements to the effective weld properties in Table K4.1 (AISC, 2010) proposed in this section may also be deemed adequately conservative for axially loaded HSS-to-HSS T- and X- (or cross-) connections. Figure 14 shows the correlation with the test results from that study (Packer and Cassidy, 1995).

The correlations including the fillet weld directional strength enhancement factor are plotted in Figures 15 and 16 for 90° square HSS-to-HSS moment T-connections (this study) and axially loaded HSS-to-HSS T- and X- (or cross-) connections (Packer and Cassidy, 1995), respectively. Because each produces a resistance factor, $\phi$, considerably less than 0.75, the fillet weld directional strength enhancement factor equal to $(1.00 + 0.5 \sin^{1.5}\theta)$ should not be used for such connections in combination with the modified requirement proposed herein to the Table K4.1 (AISC, 2010) effective weld properties.

## CONCLUSIONS AND RECOMMENDATIONS

Based on the results from this experimental program, which consisted of 12 full-scale tests on square HSS-to-HSS moment T-connections designed to be weld-critical, and on the reanalysis of data from previous experimental programs consisting of full-scale tests on weld-critical connections between HSS (Packer and Cassidy, 1995), the following conclusions and recommendations are made:

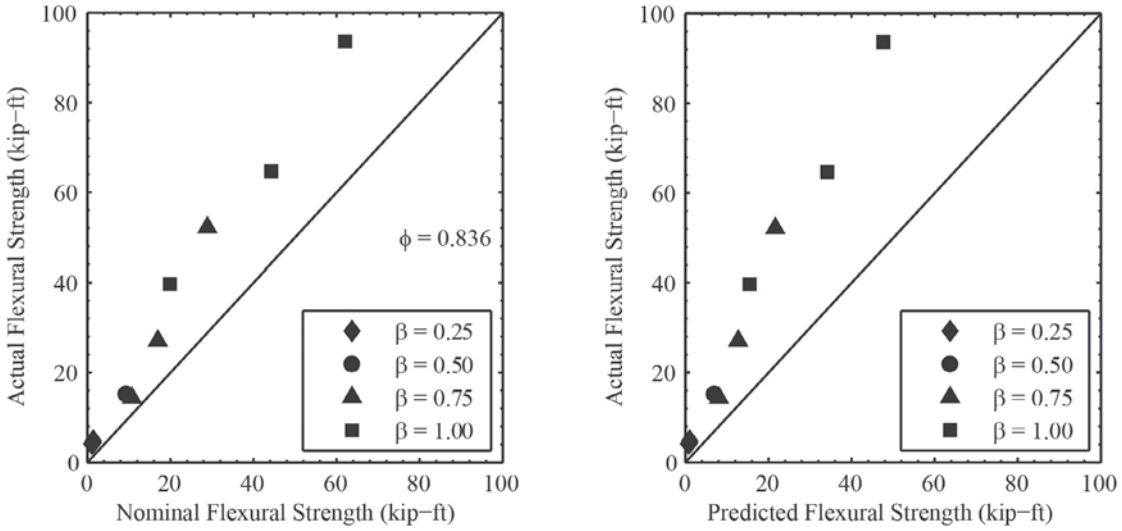


*Fig. 13. Correlation with test results for square HSS-to-HSS moment T-connections using the modification to AISC 360 (2010) and excluding the $(1.00 + 0.5 \sin^{1.5}\theta)$ factor: (a) actual strength vs. predicted nominal strength ($M_{n-ip}$); (b) actual strength vs. predicted LRFD strength ($\phi M_{n-ip}$).*

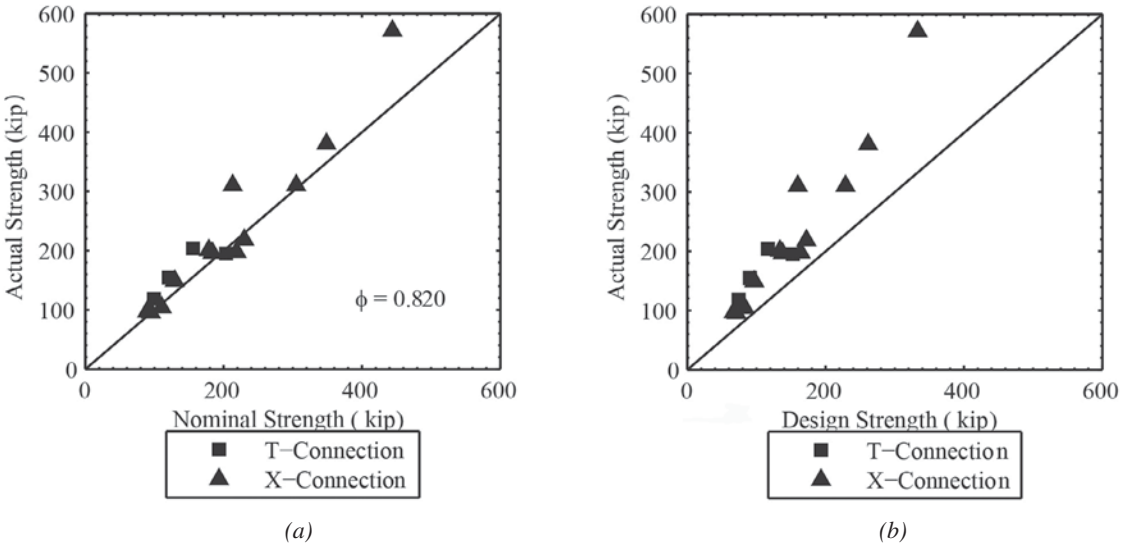


*Fig. 14. Correlation with test results for HSS-to-HSS axially-loaded T- and X-connections (Packer and Cassidy, 1995) using the modification to AISC 360 (2010) and excluding the $(1.00 + 0.5 \sin^{1.5}\theta)$ factor: (a) actual strength vs. predicted nominal strength ($R_n$); (b) actual strength vs. predicted LRFD strength ($\phi R_n$).*

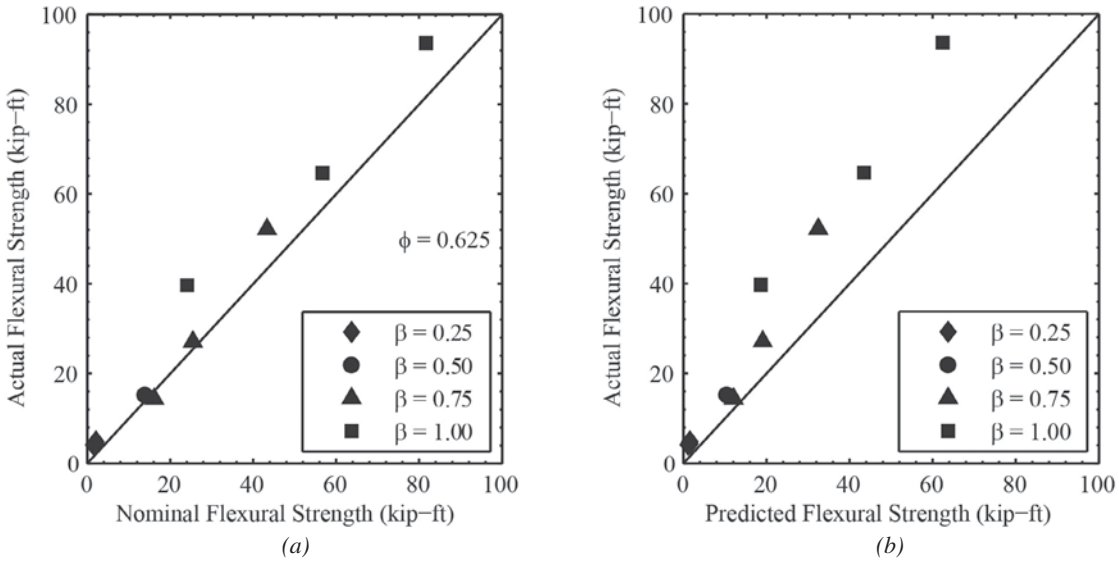


*Fig. 15. Correlation with test results for square HSS-to-HSS moment T-connections using the modification to AISC 360 (2010) and including the ($1.00 + 0.5 \sin^{1.5}\theta$) factor: (a) actual strength vs. predicted nominal strength ($M_{n-ip}$); (b) actual strength vs. predicted LRFD strength ($\phi M_{n-ip}$).*

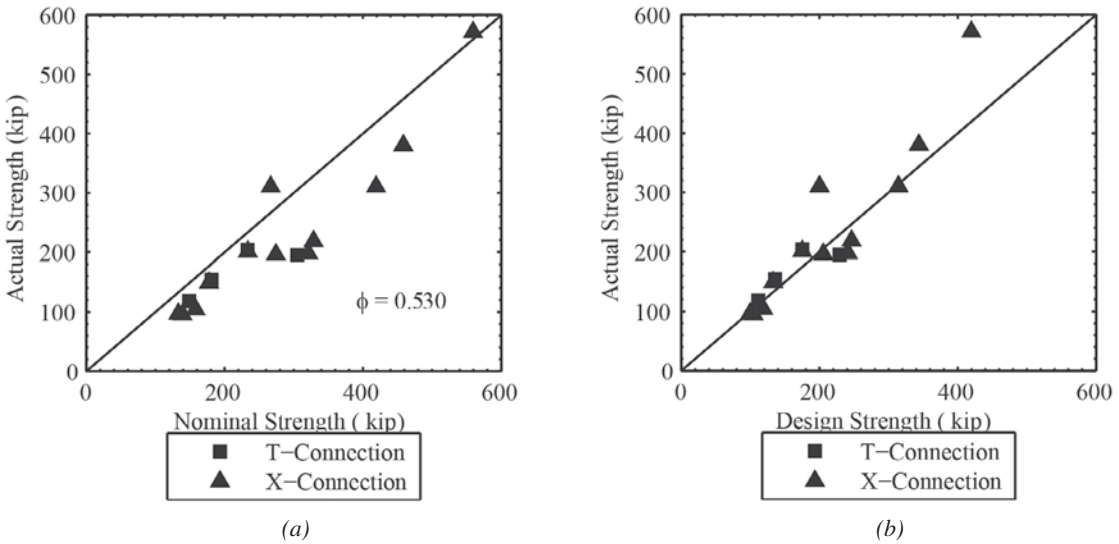


*Fig. 16. Correlation with test results for HSS-to-HSS axially-loaded T- and X-connections (Packer and Cassidy, 1995) using the modification to the AISC 360 (2010) and including the ($1.00 + 0.5 \sin^{1.5}\theta$) factor: (a) actual strength vs. predicted nominal strength ($R_n$); (b) actual strength vs. predicted LRFD strength ($\phi R_n$).*

- The $(1.00 + 0.50 \sin^{1.5}\theta)$ factor (or fillet weld directional strength enhancement factor) should not be universally applied to all connections between HSS, when the effective length method is used, because it may result in an unsafe design. This may be because connections with HSS are inherently eccentrically loaded (because welding can only be performed on one side of the branch wall) and secondary effects create additional tension at the fillet weld roots.
- Macroetch specimens of the failed welds showed that the angle of the failure plane through the weld, for stepped connections that are fillet-welded all-around the branch perimeter, is between 0 and 45° to the branch fusion face.
- The distribution of normal strain around the branch perimeter adjacent to the welded joint in a HSS-to-HSS T-connection subject to branch in-plane bending is highly nonuniform.
- As the β-ratio for HSS-to-HSS moment T-connections decreases, the effective length of the weld element along the transverse walls of the branch increases (and vice versa).
- The current equation for the effective elastic section modulus for in-plane bending specified in Table K4.1 of AISC 360 (2010) is very conservative and can be considered a lower bound, safe design approach.
- Modifying the requirement that limits the effective width, $b_{eoi}$, in Table K4.1 (AISC, 2010) from:

  When $\beta > 0.85$ or $\theta > 50^\circ$, $b_{eoi}/2$ shall not exceed $2t$

  to:

  When $\beta > 0.85$ or $\theta > 50^\circ$, $b_{eoi}/2$ shall not exceed $B_b/4$

  increases the predicted strength of welded joints in square HSS-to-HSS moment T-connections subject to branch bending. Adopting this modification is still conservative (Figure 13) and generally provides a more economical design approach, within the parameter range of $t_b \le t$ studied. Furthermore, if the same modification ($b_{eoi}/2 \le B_b/4$) is extended to previous weld-critical tests on HSS-to-HSS T- and X- (or cross-) connections (Packer and Cassidy, 1995), subject to branch axial loading, then reanalysis of those test results shows that the proposed effective length modification is also acceptable for those connections (Figure 14).


## ACKNOWLEDGMENTS

The authors are grateful for the financial support of the American Institute of Steel Construction and the advice of the AISC project steering committee, to Lincoln Electric for fabrication of test specimens, to Atlas Tube for donation of the HSS members, to the laboratory staff at the University of Toronto Structural Testing Facility and to Mr. V. Kan and Mr. T. Pereira (summer research students) for laboratory assistance.


## SYMBOLS

| | |
|---|---|
| $A$ | Cross-sectional area of HSS, in.$^2$ |
| $B$ | Overall width of HSS chord, measured normal to the plane of the connection, in. |
| $B_b$ | Overall width of HSS branch, measured normal to the plane of the connection, in. |
| COV | Coefficient of variation |
| $E$ | Young's modulus, ksi |
| $F_{EXX}$ | Filler metal classification strength, ksi |
| $F_{nw}$ | Nominal stress of weld metal, ksi |
| $F_u$ | Ultimate tensile strength of HSS, ksi |
| $F_{uw}$ | Ultimate tensile strength of weld metal, ksi |
| $F_y$ | Yield stress of HSS, ksi |
| $F_{yb}$ | Yield stress of HSS branch, ksi |
| $F_{yw}$ | Yield stress of weld metal, ksi |
| GMAW | Gas-metal arc welding |
| $H$ | Overall height of HSS chord, measured in the plane of the connection, in. |
| $H_b$ | Overall height of HSS branch member, measured in the plane of the connection, in. |
| $I_{ip}$ | Moment of inertia for in-plane bending, in.$^4$ |
| $I_{op}$ | Moment of inertia for out-of-plane bending, in.$^4$ |
| $M_{ip}$ | Applied in-plane bending moment, kip-in. |
| $M_{op}$ | Applied out-of-plane bending moment, kip-in. |
| $M_{n\text{-}ip}$ | Nominal flexural strength of weld for in-plane bending (AISC, 2010), kip-in. or kip-ft. |
| $M_{n\text{-}op}$ | Nominal flexural strength of weld for out-of-plane bending (AISC, 2010), kip-in. or kip-ft. |
| $M_u$ | Ultimate flexural strength for in-plane bending, kip-in. or kip-ft. |

$P$ Applied force, kip

$P_n$ Nominal axial strength, kip

$R_n$ Nominal strength of HSS member, ksi

SG Strain gage

$S_{ip}$ Effective elastic section modulus of weld for in-plane bending (AISC, 2010), in.$^3$

$S_{op}$ Effective elastic section modulus of weld for out-of-plane bending (AISC, 2010), in.$^3$

$b_{eoi}$ Effective width of the branch face welded to the chord, in.

$d$ Greatest perpendicular dimension measured from a line flush to the base metal surface to the weld surface, in.

$l_e$ Effective weld length of groove and fillet welds for HSS, in.

$m_R$ Mean of the ratio (actual element strength/nominal element strength)

$t$ Wall thickness of HSS chord member, in.

$t_b$ Wall thickness of HSS branch member, in.

$t_w$ Effective weld throat around the perimeter of the branch, in.

$\alpha$ Coefficient of separation (taken equal to 0.55)

$\beta$ Width ratio; the ratio of overall branch width to chord width for HSS

$\beta^+$ Safety index (taken equal to 4.00)

$\varepsilon_u$ Elongation at rupture, ultimate strain, in./in.

$\varepsilon_y$ Strain at material yield point, in./in.

$\phi$ Resistance factor (associated with the LRFD design method)

$\phi_w$ Resistance factor for welded joints according to CSA (2009) equal to 0.67

$\theta$ Included angle between the branch and chord, degrees; angle of loading measured from the weld longitudinal axis, degrees

## REFERENCES


AISC (2010), ANSI/AISC 360-10, *Specification for Structural Steel Buildings*, American Institute of Steel Construction, Chicago, IL.

ASTM (2008), E8/E8M-08, *Standard Test Methods for Tension Testing of Metallic Materials*, American Society for Testing Materials, West Conshohocken, PA.

ASTM (2010), ASTM A500/A500M-10, *Standard Specification for Cold-Formed Welded and Seamless Carbon Steel Structural Tubing in Rounds and Shapes*, American Society for Testing Materials, West Conshohocken, PA.

AWS (2010), ANSI/AWS D1.1/D1.1M:2010, *Structural Welding Code—Steel, 22*, American Welding Society, Miami, FL.

CSA (2009), CSA S16-09. *Design of Steel Structures*, Canadian Standards Association, Toronto, ON, Canada.

Davies, G. and Packer, J.A. (1982), "Predicting the Strength of Branch Plate—RHS Connections for Punching Shear," *Canadian Journal of Civil Engineering,* Vol. 9, No. 3, pp. 458–467.

Fisher, J.W., Galambos, T. V., Kulak, G.L. and Ravindra, M.K. (1978), "Load and Resistance Factor Design Criteria for Connectors," *Journal of the Structural Division,* ASCE*,* Vol. 104, No. 9, pp. 1427–1441.

Frater, G.S. and Packer, J.A. (1992a), "Weldment Design for RHS Truss Connections, I: Applications," *Journal of Structural Engineering*, ASCE, Vol. 118, No. 10, pp. 2784–2803.

Frater, G.S. and Packer, J.A. (1992b), "Weldment Design for RHS Truss Connections, II: Experimentation," *Journal of Structural Engineering*, ASCE, Vol. 118, No. 10, pp. 2804–2820.

IIW (1989), Doc. XV-701-89, *Design Recommendations for Hollow Section Joints—Predominantly Statically Loaded,* 2nd ed., International Institute of Welding, Paris, France.

IIW (2012), Doc. XV-1402-12, *Static Design Procedure for Welded Hollow Section Joints—Predominantly Statically Loaded,* 3rd ed., International Institute of Welding, Paris, France.

ISO (2013), ISO 14346:2013(E), *Static Design Procedure for Welded Hollow-Section Joints—Recommendations*, International Standards Organization, Geneva, Switzerland.

McFadden, M.R., Sun, M. and Packer, J.A. (2013), "Weld Design and Fabrication for RHS Connections," *Steel Construction,* Vol. 6, No. 1, pp. 5–10.

Mehrotra, B.L. and Govil, A.K. (1972), "Shear Lag Analaysis of Rectangular Full-Width Tube Connections," *Journal of the Structural Division,* ASCE, Vol. 98, No. ST1, pp. 287–305.

Packer, J.A. and Cassidy, C.E. (1995), "Effective Weld Length for HSS T, Y, and X Connections," *Journal of Structural Engineering,* ASCE, Vol. 121, No. 10, pp. 1402–1408.

Packer, J.A., Sherman, D.R. and Lecce, M. (2010), *Steel Design Guide 24: Hollow Structural Section Connections,* American Institute of Steel Construction, Chicago, IL.

Ravindra, M.K. and Galambos, T.V. (1978), "Load and Resistance Factor Design for Steel," *Journal of the Structural Division,* ASCE, Vo. 104, No. 9, pp. 1337–1353.

# Ten Years of Studies on the State of the Art

REIDAR BJORHOVDE

## INTRODUCTION

This issue of "Current Steel Structures Research" for the *Engineering Journal* focuses on the entire 10 years of reporting on steel structures research around the world. The first paper appeared in the journal in the first issue of 2005 (Vol. 42, No. 1). The current paper is number 36 in the series; it will be the final contribution from the current Research Editor.

The collaboration and active support of the highly competent staff of AISC has been essential—most importantly, the efficient and knowledgeable efforts of Keith Grubb, the Editor of the *Engineering Journal*. At the start of the effort, your Research Editor established a support group that would prove to be a critical feature of the information gathering. This was the International Steel Structures Research Advisors (ISSRA), and the members were invaluable in an effort that was very complex and could easily have turned out to be impossible. The members and their affiliations are provided in a separate section of this paper.

Research is conducted in many universities around the world, along with governmental and private industry research laboratories and other institutions that continue to contribute significantly to the state of the art. Although levels of funding vary greatly, the fact of the matter is that our knowledge has continued to expand and to reach high levels of performance.

Originally, the data collection effort was to focus entirely on other countries, with no information coming from current U.S. projects. It was quickly decided to incorporate American projects as well, considering the magnitude and importance of the U.S. research and construction communities.

Quality universities of all sizes have researched hundreds of issues, producing results that have advanced our knowledge by orders of magnitude. Equally important is that design standards and codes have allowed new theories and approaches to enter into design and construction practice.

Reidar Bjorhovde, Dr.-Ing., Ph.D., P.E., P.Eng., Research Editor of the AISC *Engineering Journal,* Tucson, AZ. Email: rbj@bjorhovde.com

As is typical of many engineering research projects, many are multiyear and multipartner efforts—some are also multicountry efforts. The outcomes of the projects focus on industry and professional needs and the incorporation of results within educational systems. Implementing the results into the legal framework of the myriad codes and standards that govern the work of the engineering profession has been difficult but ultimately successful. Significant credit is due the researchers and their colleagues in practice, as well as their willingness to share their findings across national borders. The entire enterprise is indeed a global undertaking.

## INTERNATIONAL STEEL STRUCTURES RESEARCH ADVISORS (ISSRA)

The members of the ISSRA group were specifically selected because of their continuing research work and involvement for many years. Each was selected to cover research efforts in a specific country or region. In addition, your Research Editor continually reviewed international research reports and surveys and contacted key individuals to incorporate additional projects that may have been overlooked. The ISSRA group consisted of the following individuals, shown with their home institutions and the countries or regions they were asked to cover:

- Carlos Aguirre, Technical University Federico Santa Maria, Valparaíso, Chile (*Chile, Colombia and Argentina*)
- Sergio M. Alcocer, Institute of Engineering, National Autonomous University of Mexico (UNAM), Mexico City, Mexico (*Mexico*)
- Eduardo Bayo, University of Navarra, Pamplona, Spain (*Spain*)
- Darko Beg, University of Ljubljana, Ljubljana, Slovenia (*Slovenia, Croatia and Greece*)
- Frans S. K. Bijlaard, Delft University of Technology, Delft, The Netherlands (*The Netherlands*)
- Mark Bradford, University of New South Wales, Sydney, NSW, Australia (*Australia*)

- Dinar R. Z. Camotim, Technical University of Lisbon, Lisbon, Portugal (*Portugal and Brazil*)
- S. L. Chan, Polytechnic University of Hong Kong, Hong Kong, China (*China and Hong Kong*)
- Hennie de Clercq, Southern African Institute of Steel Construction (SAISC), Johannesburg, South Africa (*South Africa*)
- G. Charles Clifton, University of Auckland, Auckland, New Zealand (*New Zealand*)
- André Colson, National University of Science and Technology of Strasbourg, Strasbourg, France, and the French National Construction Association (FNTP), Paris, France (*France*)
- Dan Dubina, Polytechnic University of Timisoara, Timisoara, Romania (*Romania and Bulgaria*)
- Jostein Hellesland, University of Oslo, Oslo, Norway (*Norway, Sweden and Denmark*)
- Miklos Ivanyi, Budapest University of Technology, Budapest, Hungary (*Hungary and Russia*)
- Jean-Pierre Jaspart and René Maquoi, University of Liège, Liège, Belgium (*Belgium and Luxembourg*)
- Jouko Kouhi, Finnish Constructional Steel Association, Helsinki, Finland (*Finland*)
- Sand-Dae Kim, RIST, Korea University, and Hyo-Nam Cho, Nanyang University, Seoul, Korea (*Korea*)
- Yoshihiro Kimura, Nagasaki University, Nagasaki, Japan, and Masayoshi Nakashima, Kyoto University, Kyoto, Japan (*Japan*)
- Ulrike Kuhlmann, University of Stuttgart, Stuttgart, Germany (*Germany and Austria*)
- Guo-Qiang Li, Tongji University, Shanghai, China (*China*)
- Richard Liew, National University of Singapore, Singapore (*Singapore and Malaysia*)
- David H. McKinnon and Michael I. Gilmor, Canadian Institute of Steel Construction (CISC), Toronto, Ontario, Canada (*Canada*)
- David B. Moore, British Constructional Steel Association (BCSA), London, England (*United Kingdom and Ireland*)
- Alain Nussbaumer and Manfred Hirt, ÉPFL, Lausanne, Switzerland (*Switzerland*)
- Thomas Schlafly, American Institute of Steel Construction (AISC), Chicago, Illinois, United States (*United States*)
- Luis S. da Silva, University of Coimbra, Coimbra, Portugal (*Portugal and Brazil*)
- K. C. Tsai, National Taiwan University, Taipei, Taiwan (*Taiwan*)
- František Wald, Czech Technical University, Prague, Czech Republic (*Czech Republic and Slovakia*)
- Riccardo Zandonini, University of Trento, Trento, Italy (*Italy*)

**Locations of Research Projects**

Table 1 identifies the countries where research projects have been reported, along with the number of projects for each.

Because many of the projects within the European Union (EU) are multinational efforts, the lead research institution and its country have been used in the tabulation; simply adding the numbers for each of the EU member countries would have given a distorted picture. On the other hand, the aggressive funding model that is used for the EU countries expresses a gratifying emphasis on the importance of research, which goes hand in hand with the European emphasis on education at all levels.

It is also interesting to note the large number of projects in the United States and Canada, for a total of 74. Although the funding mechanisms and levels of support are very different in the two countries (e.g., professors are paid for 12 months in Canada, as opposed to the 9 that is common in the United States), they have similarly aggressive attitudes toward conducting research and publishing papers and reports.

**Research Project Subjects**

It is sometimes difficult to identify a single primary goal for a project because typical studies may involve material choice, material performance, frames, members, connections, stability and many other subjects. Also, for the last 30 to 40 years in the United States, studies focusing on the response characteristics for seismic conditions and the mitigation of the accompanying problems have been extremely important. That broad subject is now probably the single most important area for structural engineering, not in the least because so many additional areas have been identified as vulnerable to seismic events. In North America alone, what used to be an issue for primarily the West Coast is now a consideration for most of the continent.

The ductility and energy absorption capacity of steel and steel-framed buildings and bridges have placed steel in the forefront of practical solutions for seismic structural

| Table 1. Geographic Distribution of Research Projects | | | | | |
|---|---|---|---|---|---|
| Country | Number of Projects Reported | Country | Number of Projects Reported | Country | Number of Projects Reported |
| Argentina | 1 | Germany | 32 | Portugal | 18 |
| Australia | 7 | Greece | 5 | Romania | 6 |
| Austria | 1 | Hong Kong | 6 | Singapore | 11 |
| Belgium | 20 | Hungary | 2 | Slovenia | 11 |
| Brazil | 3 | Italy | 13 | South Africa | 3 |
| Canada | 34 | Japan | 19 | Spain | 6 |
| Chile | 7 | Korea | 4 | Switzerland | 8 |
| China | 19 | Lithuania | 1 | Sweden | 12 |
| Czech Republic | 6 | The Netherlands | 10 | Taiwan | 4 |
| Denmark | 1 | New Zealand | 5 | United Kingdom | 21 |
| Finland | 2 | Norway | 2 | United States | 40 |
| France | 14 | Poland | 1 | | |

concerns. But even more knowledge is needed, and the labor of researchers and code writers continues to be complex, demanding and—above all—expensive.

Table 2 provides an overview of research topics during the past 10 years. The primary emphases of the projects are generally clear, but it must be understood that what may have started as a secondary focus was, in some cases, expanded to become the primary direction of subsequent studies. Such evolution is a common and, generally, very fortunate occurrence for improving the state of the art. However, so-called scope creep is an ever-present source of frustration to graduate student researchers and their advisors. Academic research is a complex proposition, and practical, "business-focused" solutions to every research problem are elusive. Nonetheless, researchers in the United States, Canada and many other locales appreciate the involvement of industry and their emphasis on practical needs. Engineering research is really *applied* research, aiming at solutions that can be used. There is no greater satisfaction for engineering researchers than to have their solutions used in actual practice and to have relevant criteria adopted in a national specification or standard. It is the ultimate acknowledgment and recognition by their peers.

Table 2 concentrates on primary research topics, which by necessity have to be somewhat broad. Many of these topics apply to building structures; many cover a range of efforts that apply to all types of structures.

### Topics Reported in the "Current Research" Papers

In the following section of the paper, the research topics that have been discussed in the individual papers are identified, including the volume and issue number of the relevant *Engineering Journal*. Readers are encouraged to review journal issues of interest to determine specific topics, the researchers and their institution(s). Publication references are also given for most of the projects, although it was quite common that the status of the relevant project had not advanced sufficiently to have produced papers or reports in the public domain. One or more years later, it is likely that a web search might provide the relevant publication data, and readers are encouraged to seek such information.

**Paper No. 1—Vol. 42, No. 1, 2005**

Simple beam connections in combined shear and tension
Influence of weld imperfections on earthquake performance
Influence of column web stiffening on seismic behavior
Seismic performance of buckling-restrained brace-to-gusset plate connections
Ductility and moment redistribution requirements for high-strength beams with bolted connections
Applicability of high- and ultra-high-strength steels for civil engineering structures
Lateral-torsional buckling of composite beams during the building construction stages
Composite action and confinement effects in tubular composite columns
Structural behavior of horizontal shear studs
Composite beam and slab panel fire design procedure
Simulation-based design of slender structures
Seismic retrofitting of framed structures using steel braces
Pseudo-dynamic testing of a full-scale 3-story, 3-bay buckling restrained composite frame
Competitive steel and composite bridges by innovative steel-plated structures

| Table 2. Research Topic Distribution | | |
|---|---|---|
| **General Subject** | **Brief Description** | **Number of Projects** |
| Materials | Material properties and testing for same | 17 |
| Bolts and welds | Installation, fabrication, construction | 13 |
| Members | 2D and 3D, static and dynamic, seismic, limit states, elastic and inelastic | 38 |
| Connections | Bolted, welded, 2D and 3D, limit states | 43 |
| Connections, seismic | Bolted, welded, rotation capacity, energy absorption, limit states | 24 |
| Frames | Including stability, seismic and fire effects, limit states | 71 |
| Composite construction | Members, connections, stability, seismic and fire effects, limit states | 30 |
| Fabrication and construction | All aspects | 6 |
| Bridges | All aspects of design, fabrication and construction, limit states, fatigue and fracture | 28 |
| Special structures | Mill buildings, warehouses, towers, cranes, load effects, fatigue and fracture, limit states | 48 |

Composite bridge research program (MIKTI) of France
Rehabilitation of fatigue-damaged orthotropic steel bridge decks

**Paper No. 2—Vol. 42, No. 2, 2005**
Analysis and behavior of beams curved in plane
Shear resistance of longitudinally stiffened panels
Understanding the behavior of U-section steel sheet piles
Integrated blast and fire analysis of steel-framed structures
Validation of English portal frame practice for use in continental Europe
Rotation capacity of moment connections
Design of simple beam connections in steel buildings
Bolted links for eccentrically braced steel frames
Static and cyclic behavior of connections in steel and composite structures
Connection design for steel buildings at risk for terror attack
Behavior and strength of composite columns subjected to fire
Load-carrying capacity of anchor plates with welded studs
Improvement of fatigue life of welded structural components
Effective use of high-strength steels in welded structures subjected to fatigue loading
Design of a new type of orthotropic plate
Design of composite bridges with twin steel girders
Optimization of a symmetric welded I-section

**Paper No. 3—Vol. 42, No. 3, 2005**
Characteristics and behavior of plasma-cut welded H-shaped steel columns
Design of steel and composite cellular beams subjected to fire
Failure of floor slabs under extreme loading
Behavior and design of steel structures under fire
Reinforcing of blast walls using energy absorbing impact barriers
Progressive collapse of tall buildings
Seismic performance of steel frames by using simplified methods
Glued connections and members for structural steel applications
Effect of a midspan diaphragm on the dynamic behavior of a composite railroad bridge

**Paper No. 4—Vol. 42, No. 4, 2005**
Improved weathering steels for bridge applications
Extra-high-strength steel plasticity and modeling
Shallow composite beams with web openings as connectors
Socket-type footings for composite columns
Improved modeling and assessment of lattice towers
Behavior and strength of scaffolding systems
Strengthening reinforced concrete columns by encased steel shapes
Buckling-restrained braced frames with backup moment frames
Performance of steel plate shear wall frames with low-yield steel
Hysteretic performance of shear panel dampers
Patch load resistance of longitudinally stiffened girder webs
Fatigue tests for welded joints with ultra-thick plates

**Paper No. 5—Vol. 43, No. 1, 2006**
High-strength bolted connections in high-strength steels
Bolted connections made with high-strength steel S690
Behavior of beam-to-beam and beam-to-column end-plate connections under fire conditions
Use of plasma cutting in the preparation of bolt holes
Design of cast iron columns, including tension fracture capacity

Cracking in galvanized steel elements
Effective width of composite girders with reduced height for the calculation of deflections
Overhead traveling crane support structures
Storage racks in seismic areas
Competitive steel and composite bridges through improved steel plated structures

**Paper No. 6—Vol. 43, No. 2, 2006**
Fatigue behavior of welded circular hollow section connections
Fatigue behavior of cast steel nodes in tubular bridges
Probabilistic study of fatigue in post-weld treated tubular bridge structures
Earthquake protection of historical buildings by reversible mixed technologies
Large cyclic deformation capacity of steel members
Robust structures by joint ductility
Passive control design through tuning of structural properties of elastoplastic damping devices
Capacity of semi-compact steel shapes
Deformation-based approach to determine the minimum degree of partial shear connection in composite beams
Decision-making tools for steel structures engineering

**Paper No. 7—Vol. 43, No. 3, 2006**
Beam-to-column connections with beams of unequal height
Design of extended shear tabs
Evaluation of the plastic rotation capacity of beam-to-column connections
Experimental behavior of standardized end-plate connections under arbitrary cyclic loads
Moment-rotation characteristics of slender portal frame connections
Making bolt holes in the fabrication of structural steel
Partially encased composite columns with high performance concrete
Semi-analytical buckling strength analysis of stiffened plates
Analysis and design of rehabilitated built-up hybrid composite members
Use of stainless steel for welded bridges in aggressive environments

**Paper No. 8—Vol. 43, No. 4, 2006**
High-strength steel moment connections
Contact splices for columns
Strength and stiffness requirements for column splices
Hybrid experiments of large-scale steel braced frames and steel shear walls
Reduced beam section connections with built-up box columns
Composite action through adhesive shear connection
Cost estimation, optimization and competitiveness of composite floor systems
Connections by adherence for steel-concrete composite bridge structures
Shear connections in composite girders with corrugated steel webs

**Paper No. 9—Vol. 44, No. 1, 2007**
Robustness of common steel connections in fire
Performance-based fire engineering design of steel and composite structures
Performance-based design for the fire situation
Testing and numerical modeling of welded joints for very high strength steel
Reliability of semi-rigid (PR) beam-to-column welded joints
Structural behavior of anchor plates
Self-centering steel moment-resistant frames

**Paper No. 10—Vol. 44, No. 2, 2007**
Cyclic testing and analysis of steel columns subjected to high axial loads and rotation demand
Evaluation of cumulative plastic deformation capacity for buckling-restrained braces in frames
Seismic behavior and response modification factors of structural steel systems
Seismic design of buckling-restrained braced frames (BRBFs)
Strength and ductility of welded high-strength steel connections
Robustness in structural steel framing systems
Robustness test for a steel-concrete composite floor
Renovation techniques for fatigue cracked orthotropic steel bridge decks

**Paper No. 11—Vol. 44, No. 3, 2007**
Analytical studies of the behavior of welded T-stub moment connections
Large web openings for service integration in composite floors
Elasto-plastic collapse deflection analysis of three-dimensional steel frames
Experimental evaluation of steel and composite shear walls
High-strength frames in seismically resistant building structures
Behavior of restrained beams and beam-to-column connections
Behavior of composite beams under fire conditions
Economic and durable design of composite bridges with integral abutments
High-strength steel tower for wind turbines

**Paper No. 12—Vol. 44, No. 4, 2007**
Tests on bolted shear connections in high-strength steel
Development of a hysteretic model with pinching for steel connections
Estimation of cyclic characteristics for thin web plates after shear buckling

System behavior factors for composite and mixed structural systems
Practical design methods for steel and composite frames with semi-rigid connections

**Paper No. 13—Vol. 45, No. 1, 2008**
Residual stresses in hot-rolled shapes of S460 steel
Influence of the Bauschinger effect on deflections of cambered beams
Equivalent moment distribution factors for lateral-torsional buckling
Controlled rocking of steel-framed buildings with replaceable energy dissipating fuses
Software for design of plate structures against plate buckling

**Paper No. 14—Vol. 45, No. 2, 2008**
Three-dimensional behavior of semi-rigid connections
Behavior of longitudinal double plates-to-RHS connections
Welded steel beam design using particle swarm analysis
Modeling of micro- and macro-structural size effects for fatigue of welded tubular structures
Advanced engineering for orthotropic bridge decks and surfacing solutions
Ponding of roof structures

**Paper No. 15—Vol. 45, No. 3, 2008**
Special concentrically braced frames (SCBFs)
Energy dissipation characteristics of semi-rigid connections
Cross-sectional stability of hot-rolled shapes
Behavior and strength of steel columns with partial damage of the fire-retardant coating
Composite beams with precast hollowcore slabs
Hybrid steel plate girders
Design of stainless steel plate girders for shear

**Paper No. 16—Vol. 45, No. 4, 2008**
Behavior and strength of link-to-column connections in eccentrically braced frames
Use of cast steel connectors for bracing connections in special concentrically braced frames
Minimizing the strength of bracing connections
Block shear evaluation for members with uncommon failure paths
Testing of shear lugs for column bases
Punching shear resistance of tension bolts
Three-dimensional web-based semi-rigid steel frame analysis with graphical interface
Monitoring of crane girders in actual structures
Cold-formed stainless steel hollow structural sections

**Paper No. 17—Vol. 46, No. 1, 2009**
Sustainability of steel structures
Seismic design and analysis of rectangular concrete-filled steel tube members and frames
Market opportunities for innovative fastening solutions for steel structures
Size effects in the fatigue behavior of tubular bridge connections
A methodology for an integral life cycle analysis of bridges in view of sustainability
Load rating of curved composite steel I-girder bridges through load testing with heavy trucks

**Paper No. 18—Vol. 46, No. 2, 2009**
Static and seismic behavior of steel and composite bolted end-plate beam-to-column connections
Behavior of slip-critical connections with fillers
Applications of connections using cast structural steel elements
Design of composite steel-concrete systems for multistory building construction
Structural performance of steel-concrete-steel sandwich composite structures
Innovative solutions for beam connections in small and medium span composite bridges

**Paper No. 19—Vol. 46, No. 3, 2009**
Robustness of seismically resistant multistory frames with accidental column loss scenarios
Robustness of parking garages against localized fire
Robust structures for joint ductility
Uplift criteria for unanchored circular tanks subjected to seismic loads
Geometric nonlinear analysis of slender structures
Seismic response of cold-formed steel structural systems in special bolted moment frames
Application of optimization techniques to assess effects of imperfections

**Paper No. 20—Vol. 46, No. 4, 2009**
Performance of dual-steel connections of high-strength components under monotonic and cyclic loading
Performance-based approaches for high-strength tubular columns and connections subjected to seismic and fire loads
Design and integrity assessment of high-strength tubular structures for extreme loads
Imperfections for global analysis of frames: EC3 drawbacks and energy-based procedures
Extension of service life of existing and new welded steel structures

**Paper No. 21—Vol. 47, No. 1, 2010**
Slender thin-walled box columns
Behavior of composite beams with deep trapezoidal slabs containing headed stud shear connectors
Buckling of slender composite concrete-filled steel columns
Strength and behavior of steel storage racks
Stability of girders using U-frames
Use of adhesives to strengthen steel structures

**Paper No. 22—Vol. 47, No. 2, 2010**

Development of improved welded moment connections for earthquake-resistant design

Seismic behavior of reduced beam section moment connections to deep columns

Horizontally curved tubular flange girders

Damage-free, seismic-resistant, self-centering, concentric braced frames

Steel plate shear walls with partially encased composite columns

Repair of fatigue cracks in steel structures

Crack propagation in tubular joints under compressive loading

Bending-shear interaction in plate girders

**Paper No. 23—Vol. 47, No. 3, 2010**

Progressive collapse of steel and composite building structures

Behavior of semi-rigid (PR) wide-flange beam-to-tubular column connections

Structural use of stainless steel

Structural steel elliptical hollow sections

The continuous strength method for structural steel design

Application of cast nodes and very high strength steel in the offshore industry

Fatigue strength of hybrid truss girders

Development of an improved design method for cold-formed stainless steel members

**Paper No. 24—Vol. 47, No. 4, 2010**

Development of distributed hybrid testing techniques and their application in collapse simulation of steel moment frames

Performance and retrofit of steel beam-to-column connections of high-rise buildings

Friction resistance developed between the steel base plate and the mortar surface

Slit-wall system serving as a structural damping mechanism and as a condition assessment device for the structure

Response control of steel structures using dampers

Structural behavior of beam-column subassemblies with damper connections

Stability conditions of buckling-restrained braced frames

Buckling and post-buckling behavior of steel members

Evaluation of the ultimate earthquake resistance of moment frames

Identification of displacement-induced fatigue using a wireless sensor network

Effect of compressive residual stress to improve the fatigue strength under variable stress conditions

Seismic response of steel structures with tubular bracing members

**Paper No. 25—Vol. 48, No. 1, 2011**

Steel-precast concrete composite girders with nonconventional shear connectors

Predicting the effect of post-weld treatment applied under load

Full-scale testing of Gerber frames

Behavior and design of steel single-angle beam columns

Strengthening of steel beams under load

Structural performance of HSS steel frame assemblies with moment connections in fire

**Paper No. 26—Vol. 48, No. 2, 2011**

Performance of concrete-filled steel tubular beam-to-column connections

Performance of high-strength steel structures

Analysis and design of high-strength steel fabricated columns

Fatigue performance of welded H-beam with corrugated web

Construction process analysis of large and complex spatial steel structure

Behavior, strength and construction of cold-formed steel structures

Direct analysis for structures in steel, composite and reinforced concrete construction

Modeling of long-span composite beams with high-performance materials and deformable shear connectors

Enhancing the performance of steel structures with fiber-reinforced polymers

**Paper No. 27—Vol. 48, No. 3, 2011**

Economical and safe design of steel joints subjected to natural fires

Robustness of car parking garages against localized fires

Sustainable steel and composite bridges in the built environment

High-strength steel towers for wind turbines

Detection of cracks in steel components by means of ultrasound excited thermography

Adhesive bonded cast steel—structural steel connections

Optimization of supporting structures for offshore wind energy converters

High-strength steel in seismic-resistant building frames

Displacement-based seismic design of steel structures

Laboratories' university network of seismic engineering

**Paper No. 28—Vol. 48, No. 4, 2011**

Second-order effects in steel frames with locally buckled members

Direct strength method of design of simple and complex thin-walled shapes for combined actions

Drive-in racks subject to impact loads

Long-term behavior of composite steel-concrete members and its effect on their ultimate response

Ultra-high-strength concrete-filled columns for high-rise construction
Fatigue behavior of tubular connections fabricated with enhanced partial joint penetration welds
Lightweight composite sandwich panels subjected to extreme loads
Residual stress in high-strength steel joints
Experimental and numerical studies on steel beam-to-column connections subjected to sudden column removal scenario
Fatigue study of partially overlapped circular hollow section K-joints

**Paper No. 29—Vol. 49, No. 1, 2012**
Design of connections to composite columns for improved fire robustness
Modeling of membrane action of floor slabs exposed to fire
Composite beams with high ribbed concrete deck
Performance of small-diameter headed stud shear connectors
Composite beams with high-performance concrete and high-strength steel
Development of innovative steel-glass structures for architectural and structural applications
Behavior and strength of bolted connections in bearing
Longitudinally stiffened plate girders subjected to moment and shear interaction
Intermediate transverse stiffeners in plate girders
Flame straightening of structural steel elements
Self-centering sliding hinge joint
Effects of floor slab resistance on the inelastic behavior of chevron-type eccentrically braced frames

**Paper No. 30—Vol. 49, No. 2, 2012**
Flexural and lateral-torsional buckling of steel frames by a general second-order approach
Assessment of structures with welding discontinuities
Toughness requirements for plastic design with structural steel
Composite bridges with integral abutments
Development of innovative steel-glass structures for architectural and structural applications
Cold-formed steel construction
Performance of steel-concrete composite structures
Behavior of steel and composite structures under fire conditions
Double split tee moment connections

**Paper No. 31—Vol. 49, No. 3, 2012**
Analysis of thin-walled steel structures using generalized beam theory (GBT)
Distortional mode interaction in cold-formed steel columns
Energy-absorbing fuses for seismic-resistant steel frames
Steel-concrete composite truss bridges
Steel-concrete composite cable-stayed bridges
Bolted and screwed connections under ambient and elevated temperatures

**Paper No. 32—Vol. 49, No. 4, 2012**
Design of beam to composite column connections for improved fire robustness
Progressive collapse modeling of steel-framed structure in fire
Dynamic behavior of steel connections with high strain rate and noncyclic dynamic loading
Making the case for design for deconstruction
High steel towers for wind turbines—projects 1 and 2
Optimization of frames for effective assembly
Stability of industrial steel pallet racks
Base plate connections for rack structures
Structural robustness of composite frames

**Paper No. 33—Vol. 50, No. 2, 2013**
Improved structural systems for performance-based earthquake engineering
Assessment of gravity framing contributions to system behavior
Development of collapse-prevention systems
Hybrid frame systems
Effect of defects on the seismic behavior of steel moment connections
Super-high-strength tension bolts
Ring-shaped steel plate shear walls
Self-centering beams for resilient earthquake resistance
Seismic moment connections for deep beams with slender webs
Testing of long and very slender composite tubular columns in high strength steel and concrete
Seismic composite systems for high performance
Broad evaluation of common approaches to composite system strength and serviceability
Steel beam deflections and stresses during lifting
Capacity prediction of open-web steel joists partially braced by a standing seam roof
Limit state design of metal building wall and roof system
Strength prediction of steel columns and beams with holes
Highway bridge fire hazard assessment
Fracture critical system analysis
Design and fabrication standards to eliminate fracture critical concerns for steel members traditionally classified as fracture critical

**Paper No. 34—Vol. 50, No. 4, 2013**
HSS under impulsive loading
Welding of HSS
Elliptical hollow section connections
Cast steel connectors
Self-centering energy dissipative braces for the protection of structures against extreme loading

Eccentrically braced steel frames with replaceable yielding links
Base rocking steel frames with higher mode control mechanisms
Hybrid (analytical-experimental) simulation method
Ductile fuses for HSS and I-shaped braces
Seismic response of X-braced frames
Slotted gusset plate connections for slotted HSS brace connections

**Paper No. 35—Vol. 51, No. 2, 2014**
Collapse prevention of low ductility concentrically braced frames
Shaking table testing of advanced seismic force resisting systems
Future experimental research on column buckling under seismic demand
Innovative connection solutions
Fabrication of connections
Experimental and numerical studies
Connection design
Grouped shear connection

**Paper No. 36 –Vol. 51, No. 4, 2014**
Survey of 10 years of "current steel structures research"

## SUMMARY

After 10 years of examining steel structure research around the world, it is clear that innovative and practical developments continue to take place. All aspects of steel construction benefit—not the least because there is an efficient mechanism for review and practical adoption into design specification and standards. While change may not occur as fast as some engineers would like, the importance of carefully developed criteria with attention to the needs of practice and industry is paramount.

My thanks to everyone who assisted in this effort.

*Reidar Bjorhovde*
*Tucson, Arizona*
*June 20, 2014*

# GUIDE FOR AUTHORS

**SCOPE:** The ENGINEERING JOURNAL is dedicated to the improvement and advancement of steel construction. Its pages are open to all who wish to report on new developments or techniques in steel design, research, the design and/or construction of new projects, steel fabrication methods, or new products of significance to the uses of steel in construction. Only original papers should be submitted.

**GENERAL:** Papers intended for publication may be submitted by mail to the Editor, Keith Grubb, ENGINEERING JOURNAL, AMERICAN INSTITUTE OF STEEL CONSTRUCTION, One East Wacker Drive, Suite 700, Chicago, IL, 60601, or by email to grubb@aisc.org.

The articles published in the *Engineering Journal* undergo peer review before publication for (1) originality of contribution; (2) technical value to the steel construction community; (3) proper credit to others working in the same area; (4) prior publication of the material; and (5) justification of the conclusion based on the report.

All papers within the scope outlined above will be reviewed by engineers selected from among AISC, industry, design firms, and universities. The standard review process includes outside review by an average of three reviewers, who are experts in their respective technical area, and volunteers in the program. Papers not accepted will not be returned to the author. Published papers become the property of the American Institute of Steel Construction and are protected by appropriate copyrights. No proofs will be sent to authors. Each author receives three copies of the issue in which his contribution appears.

**MANUSCRIPT PREPARATION:** Manuscripts must be provided in Microsoft Word format. Include a PDF with your submittal. View our complete author guidelines at **www.aisc.org/ej**.

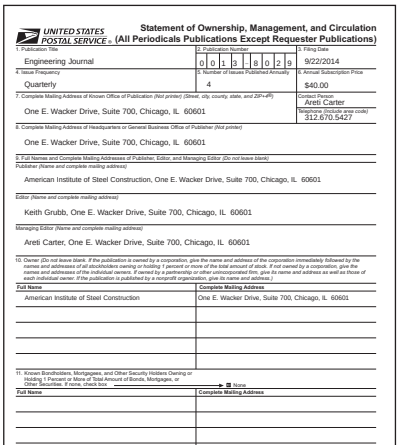

UNITED STATES POSTAL SERVICE

**Statement of Ownership, Management, and Circulation (All Periodicals Publications Except Requester Publications)**

| 1. Publication Title | 2. Publication Number | 3. Filing Date |
|---|---|---|
| Engineering Journal | 0 0 1 3 - 8 0 2 9 | 9/22/2014 |
| 4. Issue Frequency | 5. Number of Issues Published Annually | 6. Annual Subscription Price |
| Quarterly | 4 | $40.00 |

7. Complete Mailing Address of Known Office of Publication (*Not printer*) (*Street, city, county, state, and ZIP+4®*): One E. Wacker Drive, Suite 700, Chicago, IL 60601 — Contact Person: Areti Carter; Telephone (Include area code): 312.670.5427

8. Complete Mailing Address of Headquarters or General Business Office of Publisher (*Not printer*): One E. Wacker Drive, Suite 700, Chicago, IL 60601

9. Full Names and Complete Mailing Addresses of Publisher, Editor, and Managing Editor (*Do not leave blank*)

Publisher (*Name and complete mailing address*): American Institute of Steel Construction, One E. Wacker Drive, Suite 700, Chicago, IL 60601

Editor (*Name and complete mailing address*): Keith Grubb, One E. Wacker Drive, Suite 700, Chicago, IL 60601

Managing Editor (*Name and complete mailing address*): Areti Carter, One E. Wacker Drive, Suite 700, Chicago, IL 60601

10. Owner (*Do not leave blank. If the publication is owned by a corporation, give the name and address of the corporation immediately followed by the names and addresses of all stockholders owning or holding 1 percent or more of the total amount of stock. If not owned by a corporation, give the names and addresses of the individual owners. If owned by a partnership or other unincorporated firm, give its name and address as well as those of each individual owner. If the publication is published by a nonprofit organization, give its name and address.*)

| Full Name | Complete Mailing Address |
|---|---|
| American Institute of Steel Construction | One E. Wacker Drive, Suite 700, Chicago, IL 60601 |

11. Known Bondholders, Mortgagees, and Other Security Holders Owning or Holding 1 Percent or More of Total Amount of Bonds, Mortgages, or Other Securities. If none, check box → ☒ None

| Full Name | Complete Mailing Address |
|---|---|

12. Tax Status (*For completion by nonprofit organizations authorized to mail at nonprofit rates*) (*Check one*)
The purpose, function, and nonprofit status of this organization and the exempt status for federal income tax purposes:
☒ Has Not Changed During Preceding 12 Months
☐ Has Changed During Preceding 12 Months (*Publisher must submit explanation of change with this statement*)

PS Form **3526**, September 2007 (*Page 1 of 3 (Instructions Page 3)*) PSN 7530-01-000-9931 **PRIVACY NOTICE**: See our privacy policy on www.usps.com

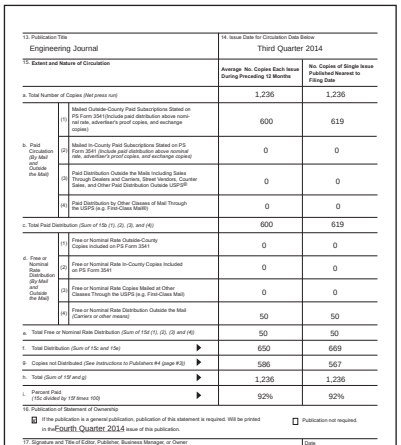

| 13. Publication Title | 14. Issue Date for Circulation Data Below |
|---|---|
| Engineering Journal | Third Quarter 2014 |

| 15. Extent and Nature of Circulation | | | Average No. Copies Each Issue During Preceding 12 Months | No. Copies of Single Issue Published Nearest to Filing Date |
|---|---|---|---|---|
| a. Total Number of Copies (*Net press run*) | | | 1,236 | 1,236 |
| b. Paid Circulation (By Mail and Outside the Mail) | (1) | Mailed Outside-County Paid Subscriptions Stated on PS Form 3541(Include paid distribution above nominal rate, advertiser's proof copies, and exchange copies) | 600 | 619 |
| | (2) | Mailed In-County Paid Subscriptions Stated on PS Form 3541 (*Include paid distribution above nominal rate, advertiser's proof copies, and exchange copies*) | 0 | 0 |
| | (3) | Paid Distribution Outside the Mails Including Sales Through Dealers and Carriers, Street Vendors, Counter Sales, and Other Paid Distribution Outside USPS® | 0 | 0 |
| | (4) | Paid Distribution by Other Classes of Mail Through the USPS (e.g. First-Class Mail®) | 0 | 0 |
| c. Total Paid Distribution (*Sum of 15b (1), (2), (3), and (4)*) | | | 600 | 619 |
| d. Free or Nominal Rate Distribution (By Mail and Outside the Mail) | (1) | Free or Nominal Rate Outside-County Copies included on PS Form 3541 | 0 | 0 |
| | (2) | Free or Nominal Rate In-County Copies Included on PS Form 3541 | 0 | 0 |
| | (3) | Free or Nominal Rate Copies Mailed at Other Classes Through the USPS (e.g. First-Class Mail) | 0 | 0 |
| | (4) | Free or Nominal Rate Distribution Outside the Mail (*Carriers or other means*) | 50 | 50 |
| e. Total Free or Nominal Rate Distribution (*Sum of 15d (1), (2), (3) and (4)*) | | | 50 | 50 |
| f. Total Distribution (*Sum of 15c and 15e*) | | | 650 | 669 |
| g. Copies not Distributed (*See Instructions to Publishers #4 (page #3)*) | | | 586 | 567 |
| h. Total (*Sum of 15f and g*) | | | 1,236 | 1,236 |
| i. Percent Paid (*15c divided by 15f times 100*) | | | 92% | 92% |

16. Publication of Statement of Ownership
☒ If the publication is a general publication, publication of this statement is required. Will be printed in the Fourth Quarter 2014 issue of this publication. ☐ Publication not required.

17. Signature and Title of Editor, Publisher, Business Manager, or Owner — Date: 9/22/2014

I certify that all information furnished on this form is true and complete. I understand that anyone who furnishes false or misleading information on this form or who omits material or information requested on the form may be subject to criminal sanctions (including fines and imprisonment) and/or civil sanctions (including civil penalties).

PS Form **3526**, September 2007 (*Page 2 of 3*)


There's always a solution in steel.

ENGINEERING JOURNAL
American Institute of Steel Construction
One East Wacker Drive, Suite 700
Chicago, IL 60601

312.670.2400 www.aisc.org